ISSN 2413-5577

№ 3 Июль – Сентябрь 2024

Экологическая безопасность прибрежной и шельфовой зон моря

Ecological Safety of Coastal and Shelf Zones of Sea

No. 3 July – September 2024

ecological-safety.ru

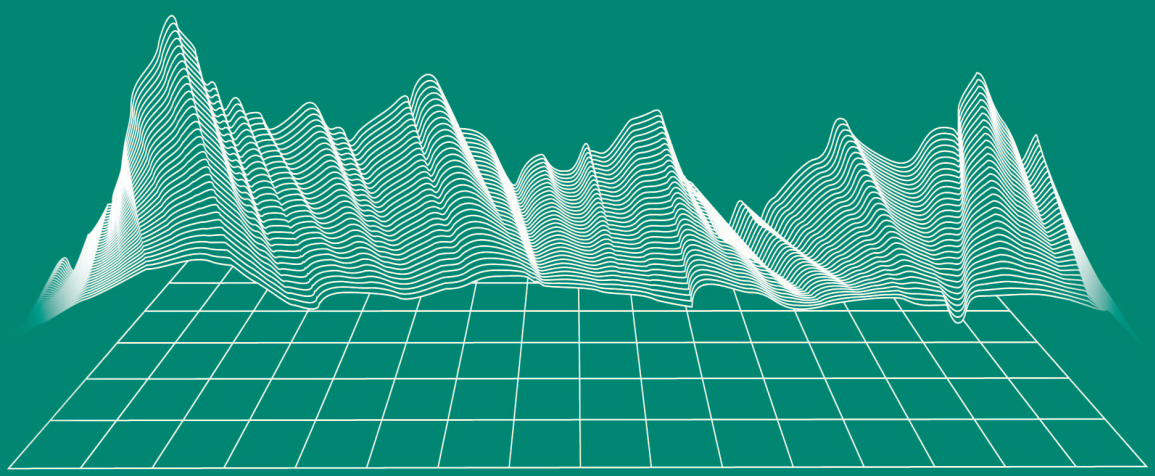

ISSN 2413-5577
No. 3, 2024
July – September

Publication frequency:
Quarterly
16+

ECOLOGICAL SAFETY OF COASTAL AND SHELF ZONES OF SEA

Scientific and theoretical peer reviewed journal

FOUNDER AND PUBLISHER:
Federal State Budget Scientific Institution
Federal Research Centre
"Marine Hydrophysical Institute of RAS"

The Journal publishes original research results, review articles (at the editorial board's request) and brief reports.

The Journal aims at publication of results of original scientific research concerning the state and interaction of geospheres (atmosphere, lithosphere, hydrosphere, and biosphere) within coastal and shelf areas of seas and oceans, methods and means of study thereof, ecological state of these areas under anthropogenic load as well as environmental protection issues.

The Journal's editorial board sees its mission as scientific, educational and regulatory work to preserve the ecological balance and restore the resource potential of coastal and shelf areas believing that despite the geographical limitations of the areas under study, the processes taking place within them have a significant impact on the waters of the seas and oceans and economic activity.

The Journal publishes original research materials, results of research performed by national and foreign scientific institutions in the coastal and shelf zones of seas and oceans, review articles (at the editorial board's request) and brief reports on the following major topics:
- Scientific basis for complex use of shelf natural resources
- Marine environment state and variability
- Coastal area state and variability; coast protection structures
- Monitoring and estimates of possible effects of anthropogenic activities
- Development and implementation of new marine environment control and monitoring technologies

The outcome of the research is information on the status, variability and possible effects of anthropogenic activities in the coastal and shelf marine areas, as well as the means to perform calculations and to provide information for making decisions on the implementation of activities in the coastal zone.

e-mail: ecology-safety@mhi-ras.ru

website: http://ecological-safety.ru

Founder, Publisher and Editorial Office address:
2, Kapitanskaya St.,
Sevastopol, 299011, Russia

Phone, fax: + 7 (8692) 54-57-16

РЕДАКЦИОННАЯ КОЛЛЕГИЯ

CONTENTS

No. 3. 2024 July – September, 2024

СОДЕРЖАНИЕ

№ 3. 2024 Июль – Сентябрь, 2024

Original article

The Recurrence of Winter Invasions of Cold Air over the Black Sea

V. V. Efimov *, O. I. Komarovskaya

Marine Hydrophysical Institute of RAS, Sevastopol, Russia
* *e-mail: vefim38@mail.ru*

Abstract
Invasions of cold air masses into the atmosphere over the Black Sea in winter cause the intensive cooling of the surface water layer and contribute to the formation and development of a cold intermediate layer. Although such invasions are relatively rare, they regularly recur in winter. The article studies characteristics of the probability of cold invasions into the atmosphere of the Black Sea region. The article studies series of daily wind data, as well as data on sensible and latent heat fluxes and sea temperature in winter at various points in the west and east of the northern and central parts of the Black Sea. The cases of cold air masses invasion characterized by strong northerly winds were highlighted. The article considered statistical parameters of the winds in points characteristic of the north-westerly, northerly and north-easterly winds in the open central part of the sea and points in the coastal north-western and north-eastern regions. Wind roses and graphs of cumulative distributions were constructed for the offshore points which allowed determining the periods of recurrence of strong northerly winds in winter. A direct dependence of the magnitude of heat fluxes from the sea surface on the northerly wind speed in winter was revealed. It is shown that cold invasion led to seawater cooling as illustrated by the decrease in seawater temperature at the surface and at 50 m depth in 2012.

Keywords: Black Sea, cold invasions, northerly wind, recurrence period, heat fluxes, sea water temperature

Acknowledgements: The study was carried out under state assignment no. FNNN-2024-0014 “Fundamental studies of interaction processes in the sea–air system that form the physical state variability of the marine environment at various spatial and temporal scales”.

For citation: Efimov, V.V. and Komarovskaya, O.I., 2024. The Recurrence of Winter Invasions of Cold Air over the Black Sea. *Ecological Safety of Coastal and Shelf Zones of Sea*, (3), pp. 6–15.

Повторяемость зимних вторжений холодного воздуха над Черным морем

В. В. Ефимов *, О. И. Комаровская

Морской гидрофизический институт РАН, Севастополь, Россия
** e-mail: vefim38@mail.ru*

Аннотация
Вторжения холодных воздушных масс в атмосферу над Черным морем зимой являются причиной интенсивного выхолаживания поверхностного слоя вод и способствуют формированию и развитию холодного промежуточного слоя. Хотя такие вторжения относительно редки, в зимние периоды они регулярно повторяются. Статья посвящена исследованию характеристик вероятности холодных вторжений в атмосферу Черноморского региона. Исследованы ряды суточных ветровых данных, а также данных о потоках явного и скрытого тепла и температуре моря зимой в различных точках на западе и востоке северной и центральной частей Черного моря. Выделены случаи вторжения холодных масс воздуха, характеризующиеся сильными ветрами северного направления. Рассмотрены статистические параметры ветров в характерных для ветра северо-западного, северного и северо-восточного направления точках в открытой центральной части моря и в прибрежной северо-западной и северо-восточной областях. Для морских точек построены розы ветров и графики кумулятивных распределений, позволившие определить периоды повторяемости сильных ветров северного направления в зимний период. Выявлена прямая зависимость величины потоков тепла с поверхности моря от скорости северного ветра в зимний период. Показано охлаждение морской воды как результат холодного вторжения для случая 2012 г. на примере полей понижения температуры моря на поверхности и на глубине 50 м.

Ключевые слова: Черное море, холодные вторжения, северный ветер, период повторяемости, потоки тепла, температура морской воды

Благодарности: работа выполнена в рамках государственного задания по теме № FNNN-2024-0014 «Фундаментальные исследования процессов взаимодействия в системе океан-атмосфера, формирующих изменчивость физического состояния морской среды на различных пространственно-временных масштабах».

Для цитирования: *Ефимов В. В., Комаровская О. И.* Повторяемость зимних вторжений холодного воздуха над Черным морем // Экологическая безопасность прибрежной и шельфовой зон моря. 2024. № 3. С. 6–15. EDN URLGZH.

Introduction

The cooling of the Black Sea surface in winter is most intense when cold air masses invade across the northern boundary of the sea (1–5). While rare, cold air invasions into the atmosphere over the Black Sea are a recurrent phenomenon in winter. In the southern and especially the south-eastern part of the sea, such invasions are less pronounced and less intense.

Typically, the cases of invasion of cold air masses correspond to the passage of a cold atmospheric front across the northern boundary of the sea. They are accompanied by an increase in surface wind speed up to 10–15 m/s and a decrease in air temperature down to –5...–10°C. As a result, intense convection and clouding

develop in the cold boundary layer of the atmosphere above the relatively warm sea, the temperature of which in winter is in the range of 5–9 °C. A distinctive clouding pattern is observed in satellite snapshots, manifesting as cellular or roller structures [2]. Fig. 1 shows an illustrative example of such a snapshot.

In response to such events, the Black Sea exhibits lowering of the surface layer temperature, development of strong wind waves and wind currents and significant deepening of the upper quasi-homogeneous sea layer. Such an important feature of the vertical thermohaline structure of the sea as a cold intermediate layer (CIL) is formed. The water temperature minimum at depths of 50–70 m is believed to be formed in the open sea regions as a result of deep penetrating convection under conditions of large fluxes of sensible and latent heat from the sea surface [4, 6]. Advective transport of cold water from the shallow north-western region by the coastal western currents and further southwards by the Rim Current system is considered to be the second, less important cause of CIL formation [4, 8–11].

The characteristics and mechanisms of formation of the sea response to cold air mass invasion episodes require further study. The purpose of this work is to statistically assess the recurrence of such phenomena.

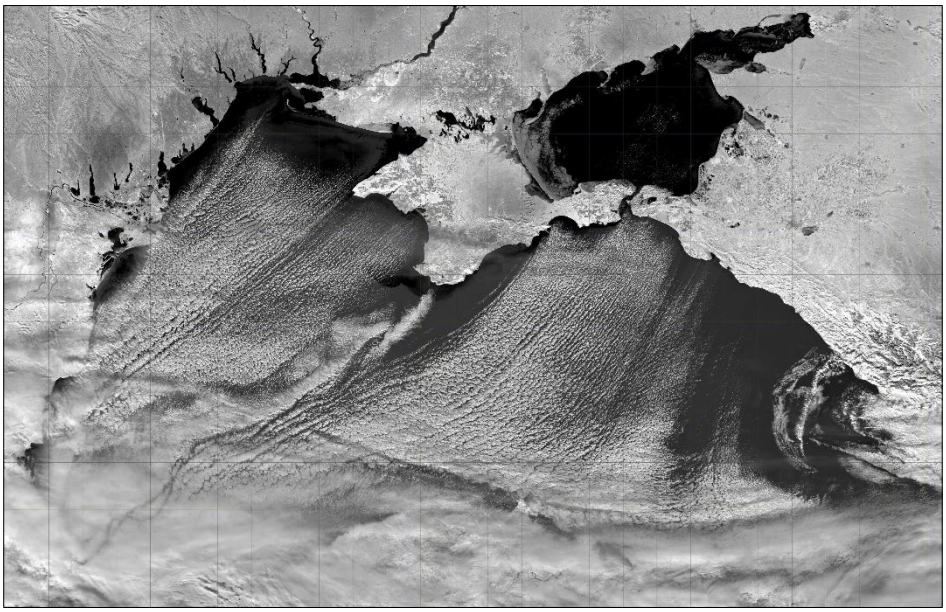

Fig. 1. A satellite image of clouding during the invasion of cold air on 9 February 2012 (http://rapidfire.sci.gsfc.nasa.gov/imagery/subsets/)

Data and methods of study

To assess the characteristics of the probability of cold air invasion into the Black Sea region atmosphere, ERA5 reanalysis data (spatial resolution 0.25° × 0.25°) on wind speed at 10 m height and heat fluxes at the sea surface were used [12], as well as Copernicus climate reanalysis data (resolution about 10 km) on water temperature and surface wind speed [1)].

When identifying cases of cold air mass invasion, the northerly wind direction with a wind speed of at least 5 m/s at a height of 10 m was taken as a defining feature. Wind directions from strictly north-westerly to strictly north-easterly, i. e. inclusive of all angles within the selected range of 90°, were considered to be northerly.

Data series of the winter period (January and February) with a time interval of 1 day at selected points separately in the north-west and north-east of the Black Sea region were studied. These two points were selected taking into account the characteristic features of the Black Sea meteorological regime during the winter period. The data at the north-western point describe the invasions of cold air, which is formed at the south-eastern periphery of the anticyclone with the centre north-west of the Crimea [13], into the atmosphere of the northern boundary of the sea. The second point was selected due to its relevance to the phenomenon of cold north-eastern air invasion, which has been identified as a factor responsible for the development of the Novorossiysk Bora [2]. The choice of two winter months is related to the more general objective of studying the mechanism of deep cooling of the Black Sea, which is maximally developed in the second half of the winter period of the year [9, 11].

Our choice of criteria for determining the invasion of cold air masses is certainly quite arbitrary. Concurrently, an initial examination of synoptic data indicates that the predominant cooling of the sea takes place at north-easterly winds.

Obtained results and discussion

To determine the frequency of northerly winds, wind speed series were examined at points on the Black Sea northern coast at coordinates (46.7° N; 31° E) and (44.9° N; 38° E). The data set encompasses the winter months (January and February) between the years 1940 and 2022 (83 years), with a time interval of 1 day. The series comprises 4918 values pertaining to wind speed components. At the western point, 1727 instances of northerly winds were identified, 685 of which exhibited wind speeds of at least 5 m/s, with a maximum speed of approximately 14.3 m/s and an average speed of approximately 6.5 m/s. At the eastern point, 1009 instances of northerly winds were identified, with 117 days exhibiting wind speeds of at least 5 m/s. The maximum recorded wind speed was 9.6 m/s, while the average speed was approximately 6.1 m/s.

The picture undergoes a notable transformation over the sea, where we examined the series of daily wind data for January and February over a 44-year period (1980–2023) at two sea points in the north-west (45.5° N; 31.5° E) and north-east (44° N; 37° E), situated in the almost central region of the sea. The series comprised

[1)] E.U. Copernicus Marine Service Information: Global Ocean Physics Reanalysis. https://doi.org/10.48670/moi-00021

2607 values. At the western sea point, 870 instances of northerly winds were identified, of which 680 exhibited wind speeds of at least 5 m/s, with a maximum of 15.7 m/s and an average speed of 8.5 m/s. At the eastern point, 877 instances of northerly winds were identified, of which 623 exhibited wind speeds of at least 5 m/s, with a maximum of 19.4 m/s and an average speed of 8.4 m/s.

Fig. 2 shows wind roses constructed according to these wind data.

The wind roses display a notable discrepancy in their shapes. At the eastern point, there is a markedly higher prevalence of north-easterly winds, with speeds exceeding 6 m/s. Furthermore, both eastern and western points exhibit a minimal presence of westerly and easterly winds, with relatively weak winds constituting the predominant contribution. It should be noted that the distributions of surface wind speeds are considered, given that these are significantly dependent on the features of the atmospheric boundary layer, including orography and temperature contrasts between sea and land in coastal regions [14]. The discrepancy in the wind roses observed at two points over the sea situated approximately 600 km apart can be attributed primarily to the influence of boundary effects such as the impact of the elevated Crimean and Caucasus Mountains.

Generalized Extreme Value (GEV) distribution was used to assess important probabilistic characteristics such as return values and recurrence periods (i. e. values occurring once in a certain time period, the so-called recurrence period for a given return value)

$$F(x, \mu, \sigma, \xi) = e^{-\left[1+\xi\left(\frac{x-\mu}{\sigma}\right)\right]^{-1/\xi}},$$

where μ is position parameter; σ and ξ are scale and shape parameters, respectively.

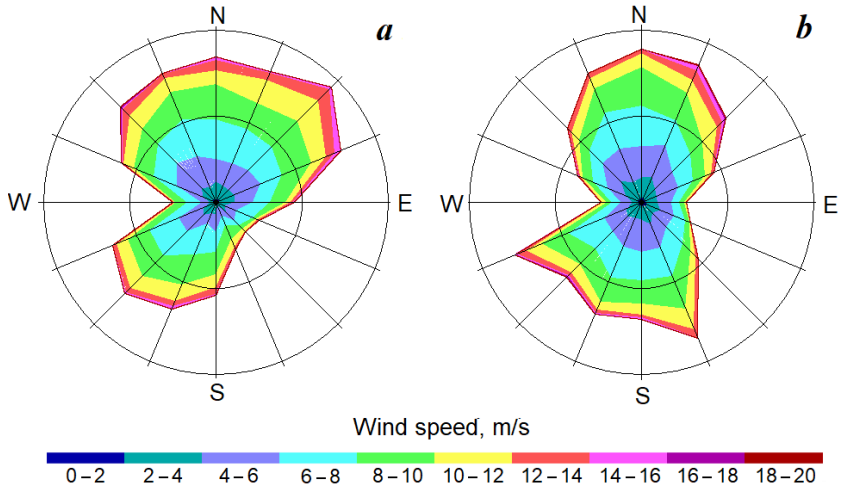

Fig. 2. Wind roses for offshore points in the west (*a*) and east (*b*)

Return values and recurrence periods are related by the following relationship

$$F = (1 - 1/T(U)),$$

where F is probability density estimation (percentile) for the return value of estimated quantity U and its expectation time (recurrence period) T.

The GEV distribution enables the approximation of the so-called tails of the cumulative distribution functions for values exceeding a selected threshold value.

Fig. 3 shows cumulative distributions of northerly wind speed values at sea points in logarithmic coordinates from the threshold value of 6 m/s. The plots exhibit a slight elevation in wind speed probability within the range of approximately 12 m/s at the western point. Notably, the eastern point exhibited exceptionally high wind speeds, though the discrepancy was minimal. It is noteworthy that this eastern region of the sea is the location where strong wind phenomena, namely the Novorossiysk Bora, are observed during the winter season.

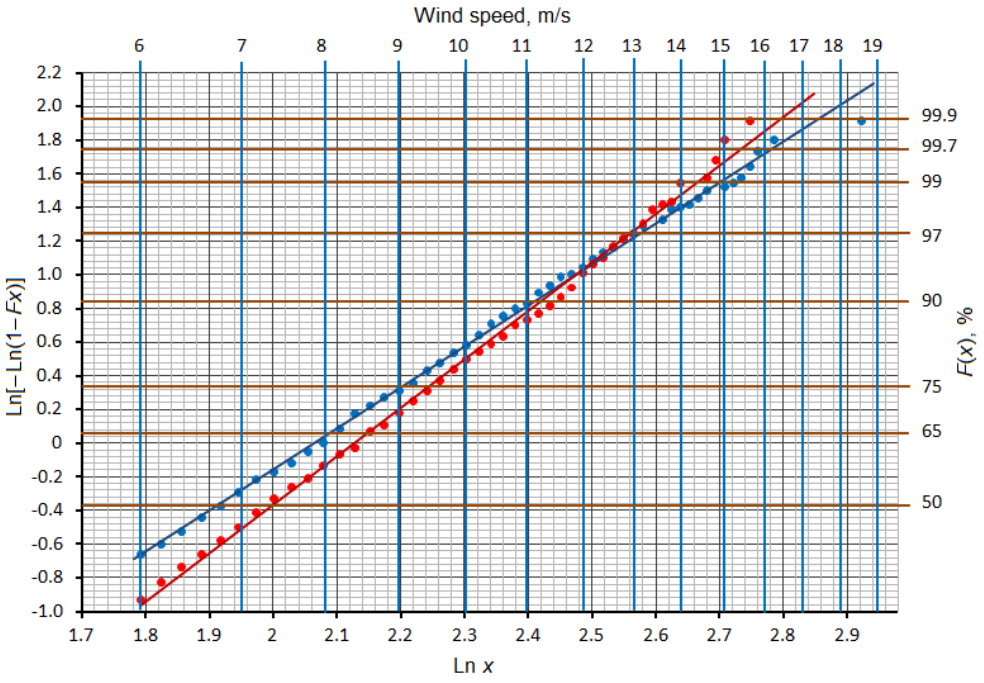

Fig. 3. Cumulative distribution functions of wind speed values in logarithmic coordinates at offshore points in the north-west and north-east of the Black Sea. The blue dots are 44° N, 37° E; the red dots are 45.5° N, 31.5° E

Recurrence periods T (days) for the series of daily values of northerly wind speed at offshore points for January–February in 1980–2023

U, m/s	45.5° N, 31.5° E	44° N, 37° E
8	7.2	8.4
9	10.2	11.9
10	15.8	17.7
11	26.6	28.3
12	49.6	48.2
13	102.7	87.7
14	238	171
15	623	359

An important characteristic of wind speed anomaly is the recurrence period, which represents the expectation time for a particular extreme value. Approximations of this distributions allowed us to obtain estimates for the recurrence periods of high wind speeds. Estimates of the recurrence periods T for the return highest values of northerly wind speed at a height of 10 m U at these sea points are given in the Table.

The results indicate that episodes of cold air invasion with speeds exceeding 8 m/s have an average recurrence period of approximately 8 days. It can be observed that higher wind speeds exhibit a longer recurrence period. Episodes of cold air invasion with speeds exceeding 14 m/s recur infrequently in the eastern part of the sea, with a recurrence period of approximately 5.5 months. This interval encompasses the winter periods of January and February. At the western point, the recurrence period is even less frequent, occurring once every 8 months (approximately once every 4 years).

A direct dependence of the sensible and latent heat fluxes from the sea surface on the northerly wind speed value was revealed, and a linear relation between them was obtained: $H = 37.9\,U$, where H is total heat flux; U is wind speed.

Given the rather high correlation between wind speed and total heat flux (approximation reliability $R \sim 0.5$), the main attention was paid to the response of sea temperature to wind speed perturbations.

Episodes of cold invasions, despite their short duration (usually not more than 2–3 days), have a noticeable impact on the temperature decrease in a sufficiently deep water layer. The case of the cold invasion on 8–9 February 2012 was selected according to the data of the Copernicus climate reanalysis using the above criteria.

As can be seen from Fig. 4, the temperature decrease spread in the upper layer up to 50 m depth. At the same time, the distribution of the sea surface temperature decrease is spatially much more homogeneous compared to the temperature decrease field at a depth of 50 m. Generally speaking, the physical mechanism of deep penetrating cooling in the winter period manifested in the inhomogeneities of the temperature field requires a separate consideration.

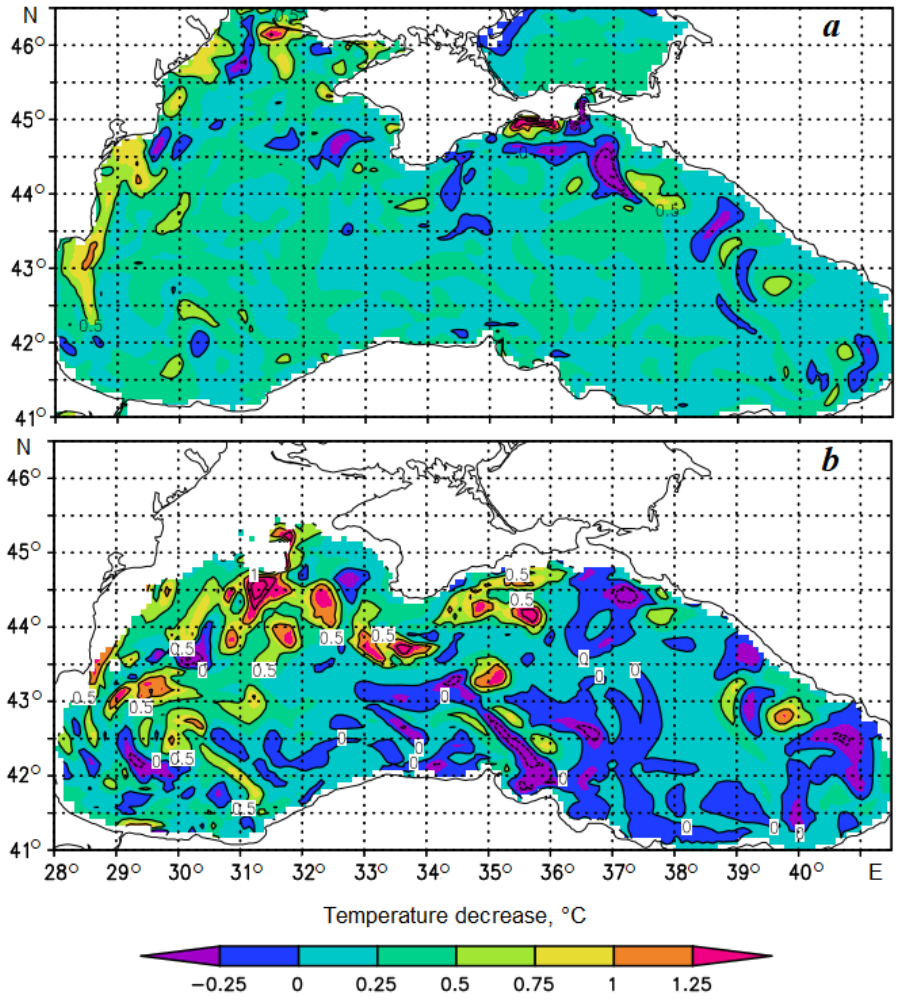

Fig. 4. Decrease of the Black Sea water temperature at the surface (*a*) and at a depth of 50 m (*b*) during two days of the cold air invasion of 10 February 2012

Conclusion

The invasion of cold air across the northern, north-western and north-eastern boundaries of the Black Sea in winter, usually accompanied by increased wind speeds and decreased temperature values, can be classified as an extreme meteorological phenomenon that requires further investigation. The ERA5 reanalysis and Copernicus climate reanalysis data sets with increased spatial resolution were used for their study.

Two points were selected, situated in the eastern and western regions of the northern Black Sea basin, in close proximity to the centre. The distribution functions of extreme wind speed values were constructed for each location.

The recurrence periods of high wind speeds during the winter invasion of cold air from the north were estimated.

It is shown that the cases of invasions with significant increases in wind speed and decreases in air temperature are relatively rare events. However, they lead to a noticeable decrease in sea temperature from the surface down to depths of 40–50 m. As an example of a cold invasion case on 8–9 February 2012, data on changes in sea temperature at the surface and at a depth of 50 m for two-day period are presented.

A more detailed analysis of the physical mechanisms of the Black Sea response to episodes of cold air invasions, highlighted using the derived estimates, based on the WRF-NEMO coupled atmosphere-sea model is beyond the scope of this paper and will be presented later.

References

1. Simonov, A.I. and Altman, E.N., 1991. [*Hydrometeorology and Hydrochemistry of Seas of the USSR. Vol. 4. The Black Sea. Iss. 1. Hydrometeorological Conditions*]. Saint Petersburg: Gidrometeoizdat, 429 p. (in Russian).
2. Efimov, V.V., Komarovskaya, O.I. and Bayankina, T.M., 2019. Temporal Characteristics and Synoptic Conditions of Extreme Bora Formation in Novorossiysk. *Physical Oceanography*, 26(5), pp. 361–373. https://doi.org/10.22449/1573-160X-2019-5-361-373
3. Efimov, V.V. and Yarovaya, D.A., 2014. Numerical Simulation of Air Convention in the Atmosphere During the Invasion of Cold Air over the Black Sea. *Izvestiya, Atmospheric and Oceanic Physics*, 50(6), pp. 610–620. https://doi.org/10.1134/S0001433814060073
4. *Овчинников И. М., Попов Ю. И.* Особенности формирования холодного промежуточного слоя в Черном море при экстремальных зимних условиях // Труды ГОИН. 1990. Вып. 190. С. 132–151.
5. Iarovaia, D.A. and Efimov, V.V., 2021. Development of Cold Sea Surface Temperature Anomalies in the Black Sea. *Izvestiya, Atmospheric and Oceanic Physics*, 57(4), pp. 413–424. https://doi.org/10.1134/S0001433821040228
6. Kolesnikov, A.G., 1953. [Annual Variation of Temperature, Stability and Vertical Turbulent Heat Exchange in the Open Black Sea]. *Trudy Morskogo Gidrofizicheskogo Instituta AN SSSR*, 3, pp. 3–13 (in Russian).
7. Ivanov, V.A. and Belokopytov, V.N., 2013. *Oceanography of the Black Sea*. Sevastopol: ECOSI-Gidrofizika, 210 p.
8. Korotaev, G.K., Knysh, V.V. and Kubryakov, A.I., 2014. Study of Formation Process of Cold Intermediate Layer Based in Reanalysis of Black Sea Hydrophysical Fields for 1971–1993. *Izvestiya*, *Atmospheric and Oceanic Physics*, 50(1), pp. 41–56. https://doi.org/10.1134/S0001433813060108
9. Kuklev, S.B., Zatsepin, A.G. and Podymov, O.I., 2019. Formation of the Cold Intermediate Layer in the Shelf-Slope Northeastern Part Zone of the Black Sea. *Journal of Oceanological Research*, 47(3), pp. 58–71. https://doi.org/10.29006/1564-2291.JOR-2019.47(3).5 (in Russian).
10. Belokopytov, V.N., 2011. Interannual Variations of the Renewal of Waters of the Cold Intermediate Layer in the Black Sea for the Last Decades. *Physical Oceanography*, 20(5), pp. 347–355. https://doi.org/10.1007/s11110-011-9090-x
11. Stanev, E.V., Peneva, E. and Chtirkova, B., 2019. Climate Change and Regional Ocean Water Mass Disappearance: Case of the Black Sea. *Journal of Geophysical Research: Oceans*, 124(7), pp. 4803–4819. https://doi.org/10.1029/2019JC015076

12. Hersbach, H., Bell, B., Berrisford, P., Hirahara, S., Horányi, A., Muñoz-Sabater, J., Nicolas, J., Peubey, C., Radu, R. [et al.], 2020. The ERA5 global reanalysis. *Quarterly Journal of the Royal Meteorological Society*, 146(730), pp. 1999–2049. https://doi.org/10.1002/qj.3803
13. Efimov, V.V., Savchenko, A.O. and Anisimov, A.E., 2014. Features of the Black Sea-Atmosphere Heat Exchange in Autumn-Winter Period. *Morskoy Gidrofizicheskiy Zhurnal*, (6), pp. 71–81 (in Russian).
14. Efimov, V.V. and Anisimov, A.E., 2011. Climatic Parameters of Wind-Field Variability in the Black Sea Region: Numerical Reanalysis of Regional Atmospheric Circulation. *Izvestiya, Atmospheric and Oceanic Physics*, 47(3), pp. 350–361. https://doi.org/10.1134/S0001433811030030

Submitted 8.02.2024; accepted after review 6.03.2024;
revised 17.06.2024; published 25.09.2024

About the authors:

Vladimir V. Efimov, Head of Atmosphere and Ocean Interaction Department, Marine Hydrophysical Institute of RAS (2 Kapitanskaya St., Sevastopol, 299011, Russian Federation), Dr.Sci. (Phys.-Math.), Professor, **ORCID ID: 0000-0002-4262-9902, ResearcherID: P-2063-2017, Scopus Author ID: 7202138991**, *vefim38@mhi-ras.ru*

Olga I. Komarovskaya, Research Associate, Marine Hydrophysical Institute of RAS (2 Kapitanskaya St., Sevastopol, 299011, Russian Federation), **ORCID ID: 0000-0003-1415-1283, ResearcherID: G-1814-2019, Scopus Author ID: 6504262996**, *komarovskaya@mhi-ras.ru*

Contribution of the authors:

Vladimir V. Efimov – problem statement, article text preparation

Olga I. Komarovskaya – calculations, preparation of graphic materials, text editing

All the authors have read and approved the final manuscript.

Original article

Multiscale Eddies Dynamics in the Pacific Ocean Adjacent to the Kamchatka Peninsula and the Northern Kuril Islands

A. V. Zimin [1] *, **D. A. Romanenkov** [1], **A. A. Konik** [1], **O. A. Atadzhanova** [1, 2], **E. I. Svergun** [1], **A. I. Varkentin** [1, 3], **O. B. Tepnin** [1, 3]

[1] *Shirshov Institute of Oceanology of RAS, Moscow, Russia*

[2] *Marine Hydrophysical Institute of RAS, Sevastopol, Russia*

[3] *Kamchatka Branch of VNIRO, Petropavlovsk-Kamchatsky, Russia*

* *e-mail: zimin2@mail.ru*

Abstract

The Pacific Ocean shelf and continental slope off the Kamchatka Peninsula and the Northern Kuril Islands are the area of spawning and early stages of life for some commercial fish species. However, it remains a poorly studied area with a limited set of observational data. In this paper, we perform a comprehensive analysis of heterogeneous satellite observations and global tidal model results over March–August 2015–2021. The work aims to obtain new information on the spatial and temporal variability of the characteristics of different-scale eddy structures and to assess the influence of tidal dynamics on some features of this variability. The following open data archives and atlases are used: Mesoscale Eddy Trajectory Atlas Product Meta3.2 DT, Terra, Aqua/MODIS and VIIRS/Suomi NPP (ocean surface temperature, chlorophyll a), Sentinel-1A/B radar images, NASA SMAP wind, AVISO absolute dynamic topography, TPXO9 tidal currents, CMEMS GLORYS12v1 currents. The paper uses the analysis results to assess the interannual and seasonal variability of the incidence and characteristics of mesoscale and submesoscale eddies and its relation to variations in the East Kamchatka Current and wind regime. The contribution of the tide to the eddy dynamics is shown. As an example, we consider the case of manifestation of small eddies at the periphery of the mesoscale anticyclonic eddy in Avacha Bay. It is shown that the interaction of this anticyclonic structure with tidal currents can serve as an independent mechanism of submesoscale eddy generation. This finding can be extended to the entire study region, which appears to be important for understanding the factors affecting the survival of commercial fishes at early life stages.

Keywords: eddy, altimetry, radar, optical range, mesoscale eddies, submesoscale eddies, tide, currents, vorticity, pollock, Pacific Ocean

Acknowledgements: This work has been supported by the grants of the Russian Science Foundation № 23-17-00174, https://rscf.ru/project/23-17-00174/

For citation: Zimin, A.V., Romanenkov, D.A., Konik, A.A., Atadzhanova, O.A., Svergun, E.I., Varkentin, A.I. and Tepnin, O.B., 2024. Multiscale Eddies Dynamics in the Pacific Ocean Adjacent to the Kamchatka Peninsula and the Northern Kuril Islands. *Ecological Safety of Coastal and Shelf Zones of Sea*, (3), pp. 16–35.

Разномасштабная вихревая динамика на акватории Тихого океана, прилегающей к полуострову Камчатка и северным Курильским островам

А. В. Зимин [1] *, **Д. А. Романенков** [1], **А. А. Коник** [1], **О. А. Атаджанова** [1, 2], **Е. И. Свергун** [1], **А. В. Варкентин** [1, 3], **О. Б. Тепнин** [1, 3]

[1] *Институт океанологии им. П.П. Ширшова РАН, Москва, Россия*

[2] *Морской гидрофизический институт РАН, Севастополь, Россия*

[3] *Камчатский филиал ФГНБУ «ВНИРО», Петропавловск-Камчатский, Россия*

* *e-mail: zimin2@mail.ru*

Аннотация

Акватория шельфа и материкового склона Камчатского полуострова и северных Курильских островов со стороны Тихого океана является областью нереста и обитания некоторых видов промысловых рыб на ранних стадиях развития. Однако она остается недостаточно изученным районом океана с ограниченным набором данных наблюдений. Выполнен комплексный анализ разнородных спутниковых наблюдений и результатов расчетов по глобальной приливной модели за март – август 2015–2021 гг. Цель работы – получение новых сведений о пространственно-временной изменчивости характеристик разномасштабных вихревых структур и оценка влияния приливной динамики на некоторые особенности этой изменчивости. Используются следующие открытые архивы данных и атласы: *Mesoscale Eddy Trajectory Atlas Product Meta*3.2 *DT*, *MODIS-Terra*/*Aqua* и *VIIRS-Suomi NPP* (температура поверхности океана, концентрация хлорофилла *a*), радиолокационные изображения *Sentinel*-1*A*/*B*, ветер *NASA SMAP*, абсолютная динамическая топография *AVISO*, приливные течения *TPXO*9, течения *CMEMS GLORYS*12*v*1. По результатам анализа оценены межгодовая и сезонная изменчивость частоты встречаемости и характеристик мезомасштабных и субмезомасштабных вихрей и ее связь с вариациями Восточно-Камчатского течения и ветрового режима. Показан вклад прилива в вихревую динамику. В качестве примера рассмотрен случай проявления малых вихрей на периферии мезомасштабного антициклонического вихря в Авачинском заливе. Установлено, что взаимодействие антициклонической структуры с приливными течениями может служить самостоятельным механизмом генерации субмезомасштабных вихрей. Этот вывод может быть распространен для всего региона исследования, что представляется важным в понимании факторов, влияющих на выживание промысловых рыб на ранних стадиях развития.

Ключевые слова: вихрь, альтиметрия, спутниковая радиолокация, оптический диапазон, мезомасштабные вихри, субмезомасштабные вихри, прилив, течения, завихренность, минтай, Тихий океан

Благодарности: исследование выполнено за счет гранта Российского научного фонда № 23-17-00174, https://rscf.ru/project/23-17-00174/.

Для цитирования: Разномасштабная вихревая динамика на акватории Тихого океана, прилегающей к полуострову Камчатка и северным Курильским островам / А. В. Зимин [и др.] // Экологическая безопасность прибрежной и шельфовой зон моря. 2024. № 3. С. 16–35. EDN VPBEOU.

Introduction

The shelf and continental slope area of the Kamchatka Peninsula and the Northern Kuril Islands on the Pacific Ocean side represents an area of mass spawning and habitation of pollock (*Gadus chalcogrammus* Pallas) of the East Kamchatka population in the early stages of development. The pollock spawning in the region under consideration begins in March and ends in June [1]. Two types of spawning are identified: deepwater and shelf [2–4]. The first type is characteristic of areas with depths of 500–600 m, occurring in the tops of deepwater submarine canyons that extend into the shelves of Avacha and Kronotsky Gulfs. The second type is observed in areas with depths of 50–170 m and is mainly characteristic of the southeastern tip of Kamchatka and the Northern Kuril Islands [1]. Juvenile fish aggregations are concentrated in spawning areas and are abundant in the southern parts of the gulfs and shallow waters of the southeastern coast of Kamchatka [5]. Following hatching, the larvae ascend to the subsurface [2], where they must undergo development in the shelf zone in order to survive throughout the life cycle, from larvae to juveniles to fingerlings [6, 7]. Consequently, the study of distinctive characteristics of local water dynamics represents a priority task in elucidating the mechanisms influencing the yield of generations of East Kamchatka pollock.

The cold East Kamchatka Current and the associated eddy structures exert a considerable influence on the variability of the hydrological structure of the waters of the region under consideration [8, 9]. On average, the prevailing direction of water transport in the near-surface layer of the shelf and the continental slope of the peninsula is southwesterly. During the pollock spawning season, the current velocity varies from 5 to 45 cm/s [10]. At the same time, mesoscale eddies move relatively fast (with a velocity of ~ 4–5 cm/s), predominantly moving in the same direction [11]. Mesoscale structures of predominantly anticyclonic type, with a diameter of 70–150 km, are clearly discernible in the infrared and visible ranges and according to satellite altimeter data [12, 13]. The formation of these structures is attributed to the instability of the main current flow, with the generation areas influenced by the specific characteristics of the bottom topography and coastline, including the presence of extensive bays and capes along the oceanic coastline of the peninsula. Notable bays include Avacha Gulf, which is a primary pollock spawning ground [3], and is predominantly characterised by background anticyclonic circulation [14, 15] due to the influence of bottom relief and shoreline heterogeneities. Mesoscale eddies, determined from a variety of data sources, are often observed in the gulf, affecting the variability of water mass characteristics and the mixing of biologically productive coastal and oceanic waters [10, 16]. In particular, such formations may provide nutrients to the subsurface ocean and determine the level of phytoplankton development.

Note that at the periphery of mesoscale structures, according to satellite radar observations in the bays of the Kamchatka Peninsula, groups of eddy structures with sizes predominantly up to 5 km are recorded [17, 18]. Eddies of such sizes are classified as submesoscale, with the upper boundary of this category determined by the characteristic value of the internal Rossby radius. In the Pacific Ocean waters adjacent to the Kamchatka Peninsula and the Northern Kurils, the value of the baroclinic Rossby radius has been observed to vary from 4 to 15 km [19]. However, no systematic generalisation of data on the frequency of occurrence of small (submesoscale) eddies and the peculiarities of their generation has been made for this region. Submesoscale eddies are widespread in the World Ocean as a whole [20] and can play a significant role in the intensification of mixing, horizontal and vertical transport of heat and matter in local water areas [21]. The mechanisms responsible for the generation of small eddies are quite diverse [22] and include baroclinic-barotropic instability in the region of currents and frontal zones; topographic effects during the flow around seamounts, islands, and peninsulas; spatially inhomogeneous wind effects; interaction of larger eddies and their dissipation; water exchange through straits; and tidal dynamics. The role of these processes in the development of submesoscale water dynamics in the study area has yet to be evaluated. However, the importance of tidal processes, particularly those occurring in a spring-neap cycle, has been highlighted by [23] for the Northern Kuril Islands. It can be assumed that the intensive tidal dynamics observed in the water area under consideration, as evidenced in the Arctic seas [21, 24], can be a key factor on scales ranging from hundreds of metres to tens of kilometres and time intervals spanning minutes to days, corresponding to the submesoscale interval of hydrological field variability. Accordingly, the role of tides in shaping the features of submesoscale dynamics, which may have a significant impact on pollock survival at early developmental stages in the gulfs of the Kamchatka Peninsula and the adjacent waters of the Northern Kuril Islands, remains an open question. This motivates the present study.

The objective of this study is to obtain new data on the spatial and temporal variability of the characteristics of multiscale eddy structures and to assess the influence of tidal dynamics on some of its features in the Pacific Ocean waters adjacent to the Kamchatka Peninsula and the Northern Kurils from March to August (during the spawning period and early stages of pollock development). This will be achieved by generalising multi-year satellite data archives with the use of model calculations of tidal currents.

Materials and methods

The analysis of mesoscale eddies in the region adjacent to the Kamchatka Peninsula and the Northern Kurils (Fig. 1) for the period from March to August 2015–2021 was based on daily information on the rotation type, centre position, and radius of each eddy. The data were obtained from the Mesoscale Eddy Trajectory Atlas Product Meta3.2 DT archive [1)], which is based on daily mean absolute

[1)] Available at: https://doi.org/10.24400/527896/a01-2022.005.YYMMDD [Accessed: 25 August 2024]

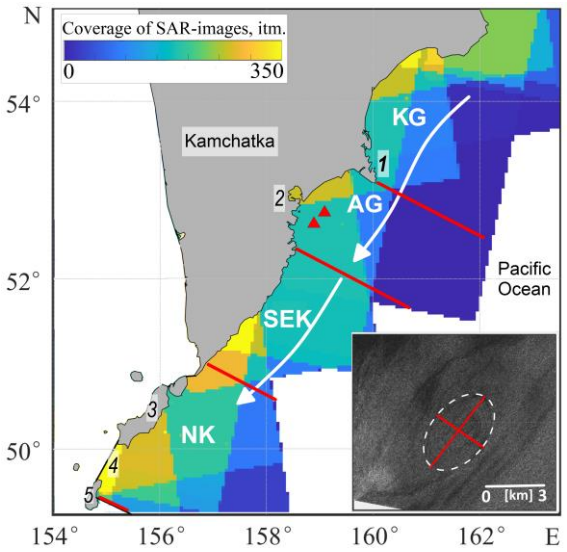

Fig. 1. Coverage of SAR images between March and August for 2015–2021: KG – Kronotsky Gulf; AG – Avacha Gulf; SEK – south-eastern Kamchatka; NK – northern Kuril Islands. *1* – Cape Shipunsky, *2* – Avacha Bay, *3* – Paramushir Island, *4* – Fourth Kuril Strait, *5* – Onekotan Island. The triangles indicate the Northern and Southern deepwater canyons in the Avacha Gulf. The white arrows show the main flow of the East Kamchatka Current. The inset shows an example of the manifestation of a cyclonic eddy structure on a SAR-image on 16 July 2016 at 19:57 UTC+0. The dashed line denotes the eddy boundary, the red lines are its large and small diameters

dynamic topography fields of the AVISO product with a spatial resolution of 0.25° × 0.25° in latitude and longitude.

Furthermore, instantaneous satellite fields of ocean surface temperature (OST) and chlorophyll a concentration from MODIS-Aqua, MODIS-Terra, VIIRS-Suomi NPP of L2 processing level with ~1 km resolution were additionally used (URL: https://oceancolor.gsfc.nasa.gov). A total of 3,160 fields were used for the days when mesoscale eddy manifestations were documented. The data that had quality indices of 0 (excellent) and 1 (good) based on the Near-infrared (NIR) algorithm evaluation [25] were selected. The fields were interpolated onto a grid corresponding to the fields of the absolute dynamic topography of the AVISO product. Subsequently, the temperature and chlorophyll a concentration at the centre and outer boundary of the mesoscale eddy, along with the horizontal gradient between them, were estimated.

A multi-year archive of Sentinel-1A/B high-resolution radar images (SAR) in C-band and Interferometric Wide (IW) imaging modes with a resolution of 20 m and a swath width of 250 km was used as initial data for recording surface manifestations of submesoscale eddies (URL: https://search.asf.alaska.edu/).

A total of 1,405 images covering the study region for the period from March to August 2015–2021 were analysed. The SAR coverage map of the region is presented in Fig. 1. Extreme irregularity in coverage can be evident, but in each of the selected areas, coverage varies from 50–100 SAR images over deepwater areas to 300–350 SAR images in coastal areas. The mean number of images per area is approximately 170.

As surface manifestations of submesoscale eddies, structures formed by thin dark or, conversely, bright light bands twisted into spirals or arcs were recorded on the SAR images (Fig. 1 inset). The structures observed in the images were predominantly the result of the film mechanism, while eddies caused by ice and shear waves were noted on fewer occasions [26]. As in previous studies [24, 27], eddies were detected visually from the manifestations described above, and their characteristics were determined based on the characteristics of the inscribed ellipse. The following characteristics we ere identified: centre coordinates, diameter (calculated as the mean between the large and small diameters) and type of rotation. The counterclockwise spiral was taken as a manifestation of the eddy with the cyclonic type of rotation and the clockwise spiral – with the anticyclonic type of rotation.

The analysis employed monthly average NASA SMAP [2)] (Soil Moisture Active Passive) scatterometer data with a spatial resolution of 0.25° in latitude and longitude for the period March to August 2015–2021. These data were used to examine the characteristics of the drive wind.

Surface currents were estimated using monthly mean zonal and meridional component data from the GLOBAL OCEAN PHYSICS REANALYSIS product [3)] (CMEMS GLORYS12v1) for 0–10 m horizons for March–August 2015–2021. Additionally, geostrophic currents from the AVISO altimetry product were used (URL: https://doi.org/10.48670/moi-00148). The background relative vorticity was calculated according to the method described in [28].

The characteristics of tidal currents were estimated from TPXO9 atlas data [29] at a resolution of 1/30° in latitude and longitude. Using TMD software (URL: https://github.com/EarthAndSpaceResearch/TMD_Matlab_Toolbox_v2.5) for selected points in the four sub-areas shown in Fig. 1, the total tide was precalculated for the eight main harmonic components (*M*2, *S*2, *N*2, *K*2, *K*1, *O*1, *P*1, *Q*1) for the entire study period. Secondary (nonlinear and long-period) harmonics were not taken into account, since special attention was paid to the variability of the characteristics of currents within a spring-quadrature cycle equal to half a lunar month. In order to obtain the results of the tidal current calculations for each of the four sub-areas shown in Figure 1, the data was taken from a single point, which was located above the sub-area signature. The tidal current field for the Avacha Gulf on 26.06.2018 was calculated using a 1/30° grid.

[2)] Available at: https://podaac.jpl.nasa.gov [Accessed: 25 August 2024].

[3)] Available at: https://doi.org/10.48670/moi-00021

Results

Mesoscale eddies. In the Pacific Ocean water area adjacent to the Kamchatka Peninsula and the Northern Kurils, 351 manifestations of mesoscale eddies with an average diameter of 90 km were recorded from March to August 2015–2021. Among the structures, the predominance of anticyclonic eddies (211) over cyclonic eddies (140) was noted, with the diameters of cyclones being on average larger than those of anticyclones.

Figure 2, *a* illustrates the spatial distribution of the trajectories of motion of mesoscale eddies over the specified period. The majority of eddies exhibiting both types of rotation (117 in total) were observed in the vicinity of the Kronotsky Gulf, whereas the greatest number of anticyclonic eddies (60 in total) were noted in the Avacha Gulf. The trajectories are presented in Fig. 2, *b*. It should be noted that only the characteristics of eddies falling within the areas of satisfactory coverage of the water area by SAR images were taken into account in the statistical analysis (see Fig. 1). However, due to the inherent limitations of altimetric measurements, the eddies in the immediate vicinity of the shoreline were not detected.

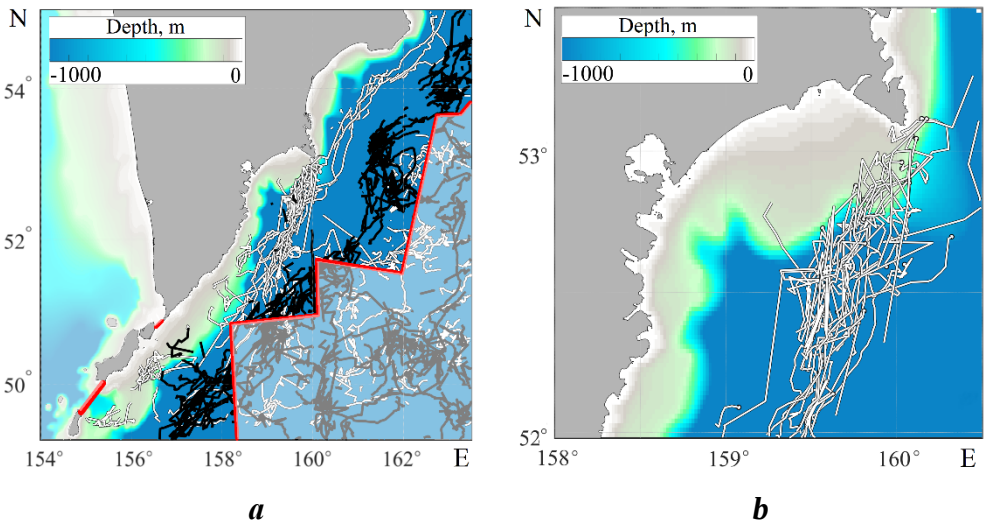

Fig. 2. Trajectories of mesoscale eddy movement in the areas adjacent to the Kamchatka Peninsula and the Kuril Islands from March to August 2015–2021 (*a*): the black lines indicate the cyclonic structure trajectories; the white lines indicate the anticyclonic structure trajectories. The red broken line limits the coastal area corresponding to the zone of satisfactory coverage of SAR images; tracks of anticyclonic mesoscale eddies near the Avacha Gulf (*b*)

In the study area, most of the mesoscale eddies move in a southwesterly direction, being formed as a result of the baroclinic instability [30] and interaction of the main flow of the East Kamchatka Current with bottom topography and large-scale irregularities of the coastline [9]. The known asymmetry in the distribution of cyclones and anticyclones relative to the current jet is confirmed [9]. Anticyclonic eddy structures tend to move closer to the coast and have an average lifetime of 21 days, while cyclonic structures tend to be more seaward and have a longer lifetime of 25 days. The main places of anticyclonic eddy formation are Kronotsky and Avacha gulfs, and less frequently these eddies occur in the shelf areas near the southern ends of capes jutting out into the sea, near Onekotan Island and the Fourth Kuril Strait. Intense eddy motion in these areas can influence the position and structure of cold and warm intermediate layers [31] and shape the distribution of abiotic environmental factors that determine the development of pollock eggs and larvae [3, 5].

On average, about 50 mesoscale eddy structures (Fig. 3, *a*) with a diameter of 90 km are observed in the study area from March to August each year. The interannual variability of their number does not exceed ±20 % and their mean diameter ±10 %. The year 2021 is anomalous in terms of the number of eddies. That year, the Kamchatka Current, especially in the spring months, deflected significantly to the southeast of the coast, forming a strong anticyclonic ring after passing Cape Shipunsky at the crossing of Avacha Gulf [10]. In 2016 and 2017, when the number of eddy structures was higher than the average, the East Kamchatka Current was pushed towards the coast and its velocity was above or close to the multi-year average.

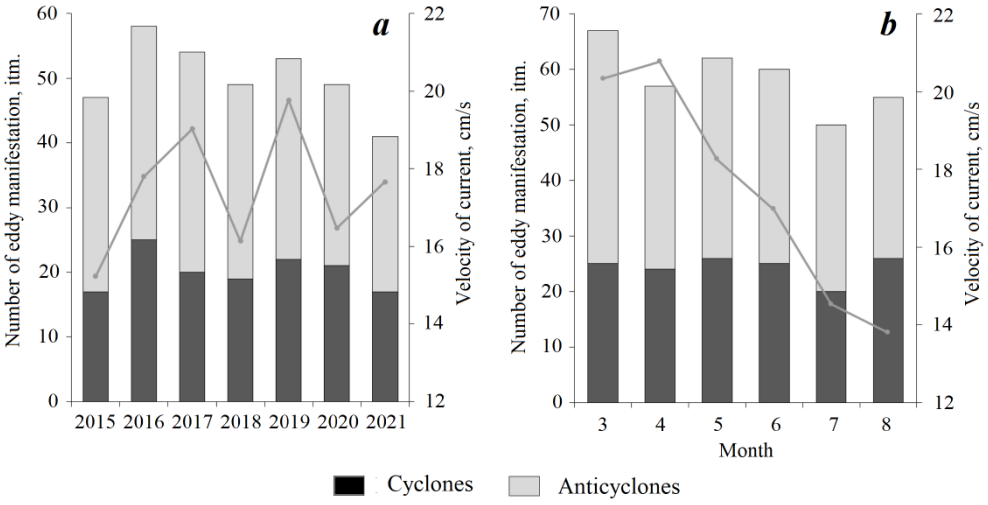

F i g . 3 . Distribution of the number of mesoscale eddies and average velocity of currents (gray line) in the upper layer based on CMEMS reanalysis data by years (*a*) and months (*b*)

Analysis of the intra-annual variability showed (Fig. 3, *b*) that the maximum number of eddy structures (65) was recorded in March and the minimum (50) in July. The observed maximum of manifestations is probably related to the weakening of the East Kamchatka Current due to rearrangement of atmospheric processes determined by the shift in the position of the Aleutian minimum [32, 33]. This is also confirmed by the seasonal change in surface current velocity from 21 cm/s in April to 14 cm/s in August, as observed in the CMEMS GLORYS12v1 reanalysis data. There are no significant seasonal trends in the variability of mean eddy diameters (diameters vary from 87 to 95 km for different months).

A generalisation of the OST data showed that the mean core temperature of mesoscale anticyclones was 5.8 °C and that of cyclonic anticyclones – 6.7 °C. This distribution is probably related to the peculiarities of the formation of mesoscale structures. Anticyclones, formed mainly in the bays of the Kamchatka Peninsula, trap and retain cold and dispersed shelf waters [11, 34]. Cyclones formed at the eastern edge of boundary currents, to which the East Kamchatka Current belongs, trap and transport warm and saline water [35]. The calculated mean annual temperature gradient between the centre and the periphery was 1.2 °C per 0.25° for anticyclones and 0.7 °C per 0.25° for cyclones. The maximum surface temperature gradient associated with eddies reaches 5 °C per 0.25°. These gradient values are quite significant and similar to estimates for frontal zones of climatic origin [36]. In addition, the outer boundary of mesoscale anticyclonic eddies tends to exhibit significant

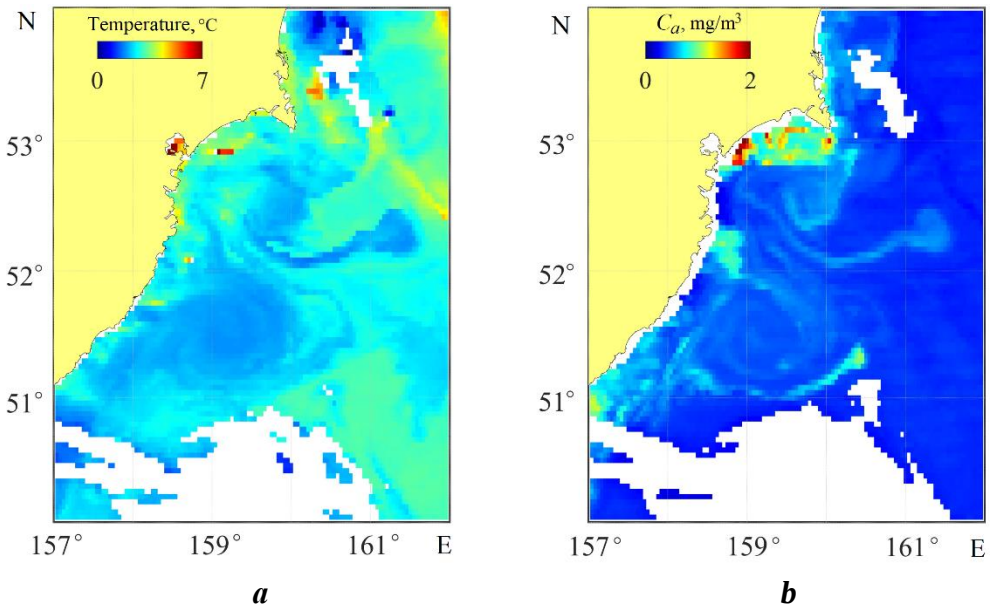

F i g . 4 . Manifestations of anticyclonic structures in fields of sea surface temperature (*a*) and chlorophyll a (*b*) according to MODIS spectroradiometer data from the Aqua satellite on April 26, 2017

gradients in chlorophyll a concentration (Fig. 4, *b*), averaging about 1.5 mg/m^3 per 0.25°, potentially making them areas of rich food resources favourable for pollock survival during early developmental stages [16].

Submesoscale eddies. In the study area during the warm period from 2015 to 2021, 559 surface manifestations of small (submesoscale) eddy structures were recorded, with diameters ranging from 300 m to 22.5 km, with a mean value of 3.4 km. In general, eddy structures are distributed over the whole area (Fig. 5, *a*), but they are mainly concentrated in the shelf zone and its coastal part. The most frequent manifestations are observed near the shores of the Kronotsky Gulf and near Avacha Bay (more than in every fifth to sixth SAR image), and also southeast of Paramushir Island (more than in every ninth to tenth SAR image). The dominance of eddies of the cyclonic type (428) over eddies of the anticyclonic type (131) can be seen. The mean diameter of eddies of both types was almost identical – 3.6 km for cyclones and 3.4 km for anticyclones.

Cyclonic eddy manifestations were most common at 2 to 4 km (Fig. 5, *b*) – about 40 % of all cyclones, and anticyclonic eddy manifestations – up to 2 km – about 30 % of all anticyclones. At the same time, almost 3/4 of all eddy manifestations had a diameter of up to 4 km, which corresponds to the minimum Rossby radius in the area [19]. In general, eddies of this diameter were found predominantly over the shelf or continental slope; large submesoscale eddies with a diameter of 10 km or more (about 5 %) were always found only over deep water.

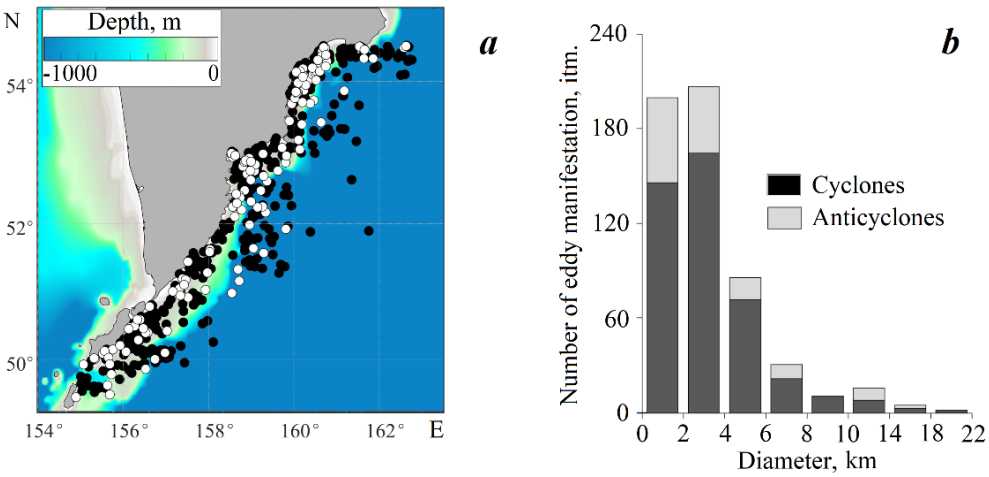

Fig. 5. Spatial distribution of centers of surface submesoscale eddy manifestations between March and August 2015–2021 (the black and white points indicate cyclonic and anticyclonic eddies, respectively) (*a*); the number of eddies depending on the diameter and type of rotation (*b*)

In 2015–2016, there were not many manifestations of submesoscale eddy structures (less than 10 % of the total number) due to low image availability in the area (Fig. 6, *a*). In 2017 and 2020, almost the same number of manifestations was recorded. As a rule, eddies were recorded on the shelf, most frequently in the Kronotsky Gulf in 2017, in the Avacha Gulf and near Paramushir Island in 2020. In 2018, eddies were most often observed in the form of groups. The maximum number of small eddies was observed in 2019 – 28 % of the total number. They were almost evenly distributed over the shelf, except for the area near Paramushir Island. In 2021, despite good data availability, few submesoscale eddies were detected. It is worth noting that the number of mesoscale eddy structures recorded this year is at an absolute minimum.

Regarding the description of the intra-annual variability of submesoscale activity, it should be noted that the monthly data availability for the period under consideration ranged from 221 to 240 SAR images. The minimum number of small eddies was recorded in March (Fig. 6, *b*). They were observed only as single eddies. In April, compared to March, the number of manifestations increased and they were more frequent in the shelf areas, especially in the Kronotsky Gulf. In May, the number of eddies increased, with the greatest increase recorded in the Avacha Gulf and near Paramushir Island. In June, almost 30 % of the total number of eddies were recorded. They were mainly recorded in groups. In July, the number of eddies decreased and they were mainly recorded in the Avacha Gulf.

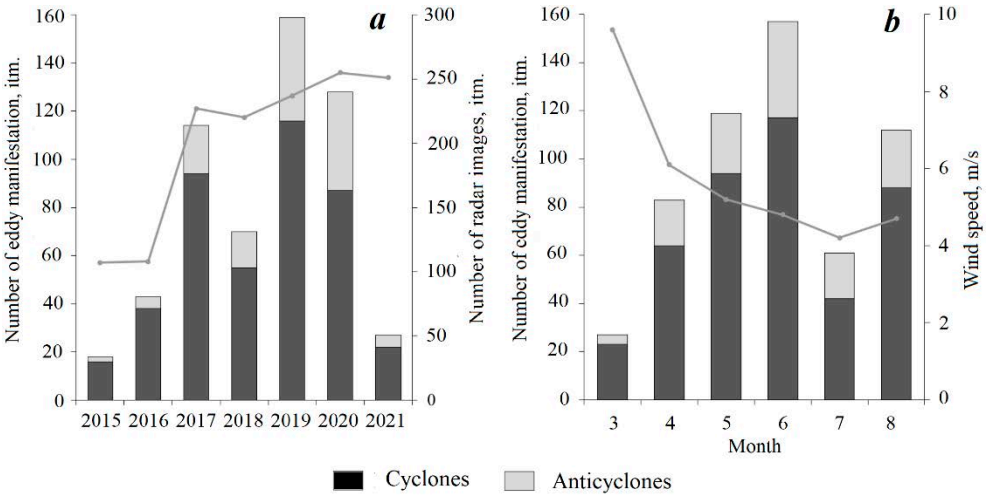

Fig. 6. Distribution of the number of registered manifestations of submesoscale eddies (bars) and the number of radar images (gray line) by year (*a*); intra-annual variability of the number of eddies (bars) and the average monthly speed of the surface wind (gray line) (*b*)

In August, the number of eddies increased again and they were observed more frequently over the shelf. Note that the minimum number of eddies in March can be explained by sufficiently high wind speeds (Fig. 6, *b*), which can lead to their masking on SAR images [37]. In other months, the average wind speed decreases to 5–6 m/s and does not prevent the manifestation of eddy structures on the SAR images, although another minimum in the number of submesoscale eddies is noted in July.

The obtained significant archive of one-time manifestations of submesoscale and mesoscale eddy structures allowed us to consider them together. A preliminary analysis of the coincident data showed that groups of small cyclonic eddies were often observed at the periphery of mesoscale anticyclones. The causes of eddy formation are quite diverse and typical for eddies of different scales [11, 26]. As noted in [26], small-scale eddy structures can be caused by local wind effects, shear instability of currents and frontal dynamics, plume propagation processes, and topographic effects when flowing around shoreline and bottom irregularities. The clustering of submesoscale eddies may indicate the transformation or even destruction of larger eddies. The role of tidal dynamics in this process is a poorly understood phenomenon.

Multiscale eddies and tidal dynamics. The cumulative analysis of satellite imagery showed that intense flow friction at the outer boundary of large eddies repeatedly formed a large number of submesoscale eddies. A total of 76 mesoscale eddies were identified based on the multi-year estimates obtained, with small eddies recorded at the outer boundary of these eddies. It is worth noting that in most cases such a situation occurred during the period of spring-like intensification of the tidal currents. The results of such analyses taking into account the tidal dynamics are presented in the table.

The table shows that the largest number of small eddies near mesoscale structures was observed in Avacha Gulf and the smallest – in the water area near the southeastern tip of Kamchatka. Up to 60 % of the small eddies are generated at the periphery of mesoscale structures during the spring tide. Typically, up to 10 small eddies per day were recorded at the periphery of mesoscale structures at maximum tidal current velocities.

Considering the fisheries interest in the Avacha Gulf area, we have considered here the case of synchronous registration of eddies of different scales, dated 26 June 2018. First, we note that during the period of March–August 2015–2021, 62 mesoscale anticyclones with diameters between 60 and 156 km crossed the Avacha Gulf (see Fig. 2, *b*). Most eddy structures are generated near Cape Shipunsky, move chaotically over the eastern part of the Avacha Gulf, and then dissipate south of 52° N with an average life of ~50 days. These eddies are often 'delayed' in the gulf, apparently falling into the area of weak velocities of the East Kamchatka Current. The eddies are clearly visible in the field of geostrophic velocities calculated from altimetric data (Fig. 7, *a*). Note also that the presence

Occurrence of small eddies in the areas adjacent to the Kamchatka Peninsula and the Kuril Islands from March to August 2015–2021

Area	Total number of SME	Including	
		at the ME periphery	of them during the spring tide
KG	189	80	40
AG	131	117	77
SEK	102	73	31
NK	137	94	65

Note: The occurrence was assessed if there were two or more eddies. SME – submesoscale eddies; ME – mesoscale eddies; KG – Kronotsky Gulf; AG – Avacha Gulf; SEK – south-eastern Kamchatka; NK – the northern Kuril Islands (see Fig. 1)

of the mesoscale eddy in Fig. 7, *a* is not confirmed by the CMEMS GLORYS12v1 reanalysis data. On the same day, 26.06.2018, radar data on the pe-riphery of the mesoscale eddy, mainly in its northwestern part, revealed several submesoscale eddies with an average diameter of 1.5 km, indicated by the points in Fig. 7, *a*. As can be seen from Fig. 7, *b*, the observations fall within the period two days before the maximum spring tide.

To illustrate the role of tidal dynamics, we consider the variability of the total current vorticity in the tidal cycle. The eddy field corresponding to the geostrophic currents in the mesoscale eddy of Fig. 7, *a*, is shown in Fig. 7, *c*. Having chosen the closest moments of maximum tidal currents, we add them to the currents in the mesoscale eddy (assuming they are background) and then recalculate the eddy fields for these two moments. The difference between the two new vorticity fields is shown in Fig. 7, *d*, where it can be seen that the changes in total vorticity associated with the tidal influence are of the same order as its background values. It is clear that in the northwestern and northeastern parts of the mesoscale eddy there is a small-scale spatial inhomogeneity of the flow field when the tide is taken into account, which can be a source of submesoscale eddy generation. This is a manifestation of the known cascade process of vorticity transfer along the scale

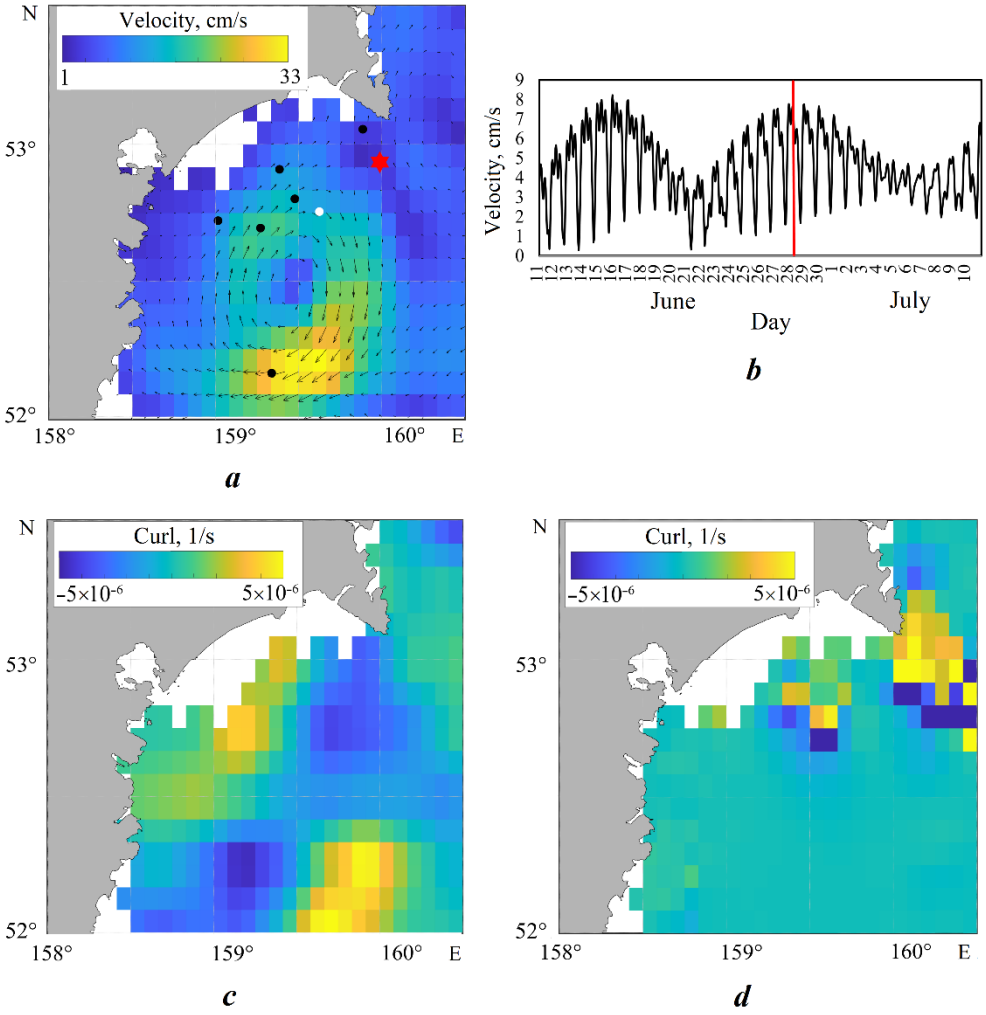

Fig. 7. Geostrophic circulation on 26.06.2018 with the position of the centers submesoscale eddy manifestations from Sentinel-1 SAR data (the red star is the point of tidal current calculation; the black and white points indicate cyclonic and anticyclonic submesoscale eddy structures, respectively) (*a*); the magnitude of tidal currents for 11.06–10.07.2018 (the red line indicates the time when small eddies were recorded on the SAR image) (*b*); the relative curl of the geostrophic circulation (*c*); the difference of the fields of total curl at high tide (04:00) and low tide (16:00) in the Avacha Gulf on 26.06.2018 (*d*). The geostrophic currents were interpolated onto the TPXO9 tidal model grid

spectrum from large to small scales [38]. The above considerations do not take into account the nonlinear interaction between the mesoscale eddy and the tide, baroclinic effects or other mechanisms of eddy formation are not considered. Nevertheless, the analysis presented together with the results of the table gives reason to consider the tidal factor in the occurrence of groups of small eddies as quite plausible, especially since almost all of these eddies are observed far from the coast at sufficiently large depths to exclude the influence of topographic effects. During the neap phase of the tidal oscillations, the currents are at least twice as weak here, and the tidal influence is reduced accordingly.

According to the OST data, the temperature of the core of the anticyclone during this period is 7.8 °C, while at the outer boundary the surface temperature reaches almost 9 °C. Thus, most of the small eddies are registered in the area of the high-gradient thermal zone. It is believed that submesoscale eddies contribute to more intensive vertical mixing and advection, which in turn may influence the surface distribution of chlorophyll a concentration in this part of the Avacha Gulf, which is favourable for biota development. Such a feature can be observed even in the spring period, similar to the one shown in Fig. 4. To conclude the analysis of the special case of 26.06.2018, we note another circumstance. The magnitude of tidal currents in the Avacha Gulf varies within a wide range. South of Cape Shipunsky they are comparable to the background currents and even exceed them. However, on dates close to the example under discussion, small eddies were not registered here due to the lack of radar coverage of this part of the Avacha Gulf.

Conclusion

This paper presents an analysis of heterogeneous satellite observations over the Pacific Ocean water area adjacent to the Kamchatka Peninsula and the Northern Kuril Islands. The comprehensive review of satellite data for a long period (seven years) in the region represents a novel contribution to the existing literature. The analysis demonstrated that eddy dynamics at different scales are subject to interannual and intra-annual variability in the frequency and locations of occurrence of eddy formations, as well as, to a lesser extent, in their size and type of rotation. The peculiarities of variability of mesoscale eddies are related to the behaviour of the East Kamchatka Current, which is largely determined by the atmospheric processes on the interannual and synoptic scales. As evidenced by satellite observations and literature sources, the variability in the characteristics of water masses and the dynamics of their boundaries observed in Avacha and Kronotsky Gulfs, as well as on the shelf of southeast Kamchatka, affects the life cycles of a variety of hydrobionts, including the early stages of pollock development.

The general trends in the interannual variability of submesoscale and mesoscale eddies are revealed. The intra-annual variability of the characteristics of multiscale eddies is demonstrated to depend on the peculiarities of seasonal fluctuations of the East Kamchatka Current and the wind regime.

The interconnection of eddies of varying scales provides an illustrative example of a theoretically described direct cascade of energy transfer in the ocean. The findings of our study indicate that the tidal factor can be a primary contributor to the formation of groups of smaller eddies at the periphery of larger mesoscale eddies, despite the absence of significant topographic effects. This phenomenon can be attributed to unsteady current velocity shifts that occur as a result of tidal currents. It can be hypothesised that such a process may result in the destruction of the mesoscale eddy, as well as influencing the vertical and horizontal distribution of pollock eggs and larvae. The specific example of the Avacha Gulf demonstrates the formation of small eddies in the area of mass spawning and larval development. The data on ocean surface temperature and chlorophyll concentration in the same area indicate that small eddies can exert a significant influence on the development of the prey base, which is of particular importance during the early stages of fish development. It would be highly beneficial to conduct *in situ* observations in order to describe these processes in greater detail.

It is noteworthy that the results of the global, widely used CMEMS ocean reanalysis GLORYS12v1 do not reflect the observed pattern of mesoscale eddies in the Avacha Gulf, which is indicative of multi-scale eddy dynamics in the region. This confirms the need to develop and improve high-resolution models for this region, which motivates further research.

REFERENCES

1. Buslov, A.V. and Tepnin, O.B., 2007. Characteristics of Walleye Pollock Spawn near the Northern Kurile Islands and the Southeast Extremety of Kamchatka. *The Researches of the Aquatic Biological Resources of Kamchatka and the North-West Part of the Pacific Ocean*, (9), pp. 235–245 (in Russian).
2. Buslov, A.V. and Tepnin, O.B., 2002. Conditions of spawning and embryogenesis of pollock Theragra chalcogramma (Gadidae) in deep-water canyons of the Pacific coast of Kamchatka. *Voprosy Ihtiologii*, 42(5), pp. 617–625 (in Russian).
3. Buslov, A.V., Tepnin, O.B. and Dubinina, A.Yu., 2004. Some Features of Spawn Ecology and Embriogenesis of the East Kamchatka Walleye Pollock. *Izvestiya TINRO*, 138, pp. 282–298 (in Russian).
4. Sergeeva, N.P., 2019. Spawning Intensity Walleye Pollock in Kronotsky Gulf (Eastern Kamchatka). In: A. M. Tokranov, ed., 2019. *Conservation of Biodiversity of Kamchatka and Coastal Waters : Materials of the XX International Scientific Conference, Dedicated to the 150th Anniversary of Academic V. L. Komarov's Birthday*. Petropavlovsk-Kamchatsky : Kamchatpress, 300 p. (in Russian).
5. Varkentin, A.I. and Saushkina, D.Y., 2022. Some Issues of Walleye Pollock Reproduction in the Pacific Waters Adjacent to the Kamchatka Peninsula and the Northern Kuril Islands in 2013–2022. *Trudy VNIRO*, 189, pp. 105–119. EDN HQAYWV. https://doi.org/10.36038/2307-3497-2022-189-105-119 (in Russian).
6. Shuntov, V.P., Volkov, A.F., Temnykh, O.S. and Dulepova, E.P., 1993. [*Walleye Pollock in Ecosystems of Far East Seas*]. Vladivostok: Izd-vo TINRO, 426 p. (in Russian).
7. Brodeur, R.D. and Matthew, T.W., 1996. A review of the Distribution, Ecology and Population Dynamics of age-0 Walleye Pollock in the Gulf of Alaska. *Fisheries Oceanography*, 5(S1), pp. 148–166. https://doi.org/10.1111/j.1365-2419.1996.tb00089.x
8. Terziev, F.S., ed., 1999. [*Hydrometeorology and Hydrochemistry of Seas. Vol. 10. The Bering Sea. Iss. 1. Hydrometeorological Conditions*]. Saint Petersburg: Gidrometeoizdat, 301 p. (in Russian).

9. Rogachev, K.A. and Shlyk, N.V., 2019. Characteristics of the Kamchatka Current Eddies. *Russian Meteorology and Hydrology*, 44(6), pp. 416–423. https://doi.org/10.3103/S1068373919060062

10. Tepnin, O.B., 2022. Variability of Hydrological Conditions at Spawning Sites of East Kamchatka Walleye Pollock (*Gadus chalcogrammus*) in 2012–2022. *The Researches of the Aquatic Biological Resources of Kamchatka and the North-West Part of the Pacific Ocean*, 66, pp. 79–93. https://doi.org/10.15853/2072-8212.2022.66.79-93 (in Russian).

11. Prants, S.V., 2021. Trench Eddies in the Northwest Pacific: An Overview. *Izvestiya, Atmospheric and Oceanic Physics*, 57(4), pp. 341–353. https://doi.org/10.1134/S0001433821040216

12. Vakulskaya, N.M., Dubina, V.A. and Plotnikov, V.V., 2019. Eddy Structure of the East Kamchatka Current According to Satellite Observations. In: POI FEB RAS, 2019. *Physics of Geospheres: The Collection of Scientific Articles on Selected Materials XI All-Russian Symposium "Physics of Geospheres"*. Vladivostok: V.I. Il'ichev Pacific Oceanological Institute. Iss. 1, 130 p. (in Russian).

13. Prants, S.V., Budynsky, M.V., Lobanov, V.B., Sergeev, A.F. and Uleysky, M.Yu., 2020. Observation and Lagrangian Analysis of Quasi-Stationary Kamchatka Trench Eddies. *Journal of Geophysical Research: Oceans*, 125(6), e2020JC016187. https://doi.org/10.1029/2020JC016187

14. Bondur, V., Zamshin, V., Chvertkova, O., Matrosova, E. and Khodaeva, V., 2021. Detection and Analysis of the Causes of Intensive Harmful Algal Bloom in Kamchatka Based on Satellite Data. *Journal of Marine Science and Engineering*, 9(10), 1092. https://doi.org/10.3390/jmse9101092

15. Alexanin, A., Kachur, V., Khramtsova, A. and Orlova, T., 2023. Methodology and Results of Satellite Monitoring of Karenia Microalgae Blooms, That Caused the Ecological Disaster off Kamchatka Peninsula. *Remote Sensing*, 15(5), 1197. https://doi.org/10.3390/rs15051197

16. Konik, A.A., Tepnin, O.B., Zimin, A.V., Varkentin, A.I., Atadzhanova, O.A., Sofina, E.V., Romanenkov, D.A., Svergun, E.I., Saushkina, D.Ya. and Rodikova, A.E., 2024. The Influence of Abiotic Factors on Alaska Pollock Distribution at the Early Stages of the Life Cycle in the Pacific Ocean Adjacent to the Kamchatka Peninsula. In: MSU, 2024. *Conference Proceedings of the XII International conference "Marine Research and Education" MARESEDU-2023. Moscow, 23–27 October 2023.* Tver: PoliPRESS. Vol. II(IV), pp. 308–318 (in Russian).

17. Kruglova, K.A., Zimin, A.V. and Atadzhanova, O.A., 2022. Comparative Analysis of the Characteristics of Surface Manifestations of Submesoscale Eddies in the Kuril-Kamchatka Region in the Summer 2020 and 2021. In: B. V. Chubarenko, ed., 2022. *Proceedings of the All-Russian Conference with International Participation "XXIX Coastal Conference: Field-Based and Theoretical Research in Shore Use Practice"*. Kaliningrad: Izdatelstvo IKBFU, pp. 460–463 (in Russian).

18. Zimin, A.V., Atadzhanova, O.A., Konik, A.A. and Kruglova, K.A., 2023. Small Eddy Structures of the Bering Sea and the Shelf of the Kuril-Kamchatka Region Based on Satellite Radar Data in the Warm Period 2020–2021. *Sovremennye Problemy Distantsionnogo Zondirovaniya Zemli iz Kosmosa*, 20(4), pp. 239–249 (in Russian).

19. Kurkin, A., Kurkina, O., Rybin, A. and Talipova, T., 2020. Comparative Analysis of the First Baroclinic Rossby Radius in the Baltic, Black, Okhotsk, and Mediterranean Seas. *Russian Journal of Earth Sciences*, 20(4), ES4008. https://doi.org/10.2205/2020ES000737

20. Thomas, L.N., Tandon, A. and Mahadevan, A., 2008. Submesoscale Processes and Dynamics. In: M. W. Hecht and H. Hasumi, eds., 2008. *Ocean Modeling in an Eddying Regime*. Washington : AGU, pp. 17–38. https://doi.org/10.1029/177GM04

21. Zimin, A.V., 2018. *Sub-Tidal Processes and Phenomena in the White Sea*. Moscow: GEOS, 220 p. (in Russian).

22. Payandeh, A.R., Washburn, L., Emery, B. and Ohlmann, J.C., 2023. The Occurrence, Variability, and Potential Drivers of Submesoscale Eddies in the Southern California Bight Based on a Decade of High-Frequency Radar Observations. *Journal of Geophysical Research: Oceans*, 128(10), e2023JC019914. https://doi.org/10.1029/2023JC019914

23. Nakamura, T., Matthews, J.P., Awaji, T. and Mitsudera, H., 2012. Submesoscale Eddies near the Kuril Straits: Asymmetric Generation of Clockwise and Counterclockwise Eddies by Barotropic Tidal Flow. *Journal of Geophysical Research: Oceans*, 117(C12), C12014. https://doi.org/10.1029/2011jc007754

24. Atadzhanova, O.A. and Zimin, A.V., 2019. Analysis of the Characteristics of the Submesoscale Eddy Manifestations in the Barents, the Kara and the White Seas Using Satellite Data. *Fundamental and Applied Hydrophysics*, 12(3), pp. 36–45. https://doi.org/10.7868/S2073667319030055

25. Goyens, C., Jamet, C. and Schroeder, T., 2013. Evaluation of Four Atmospheric Correction Algorithms for MODIS-Aqua Images over Contrasted Coastal Waters. *Remote Sensing of Environment*, 131, pp. 63–75. https://doi.org/10.1016/j.rse.2012.12.006

26. Karimova, S.S., 2012. Seasonal and Interannual Variability of Submesoscale Eddy Activity in the Baltic, Black and Caspian Seas. *Sovremennye Problemy Distantsionnogo Zondirovaniya Zemli iz Kosmosa*, 9(4), pp. 173–185 (in Russian).

27. Bashmachnikov, I.L., Kozlov, I.E., Petrenko, L.A., Glok, N.I. and Wekerle, C., 2020. Eddies in the North Greenland Sea and Fram Strait from Satellite Altimetry, SAR and High-Resolution Model Data. *Journal of Geophysical Research: Oceans*, 125(7), e2019JC015832. https://doi.org/10.1029/2019JC015832

28. Belonenko, T.V. and Sholeninova, P.V., 2016. On Identification of Mesoscale Eddies from Satellite Altimetry Based on the Area in the NW Pacific. *Sovremennye Problemy Distantsionnogo Zondirovaniya Zemli iz Kosmosa*, 13(5), pp. 79–90 (in Russian).

29. Egbert, G.D. and Erofeeva, S.Y., 2002. Efficient Inverse Modeling of Barotropic Ocean Tides. *Journal of Atmospheric and Oceanic Technology*, 19(2), pp. 183–204. https://doi.org/10.1175/1520-0426(2002)019<0183:EIMOBO>2.0.CO;2

30. Zhabin, I.A., Dmitrieva, E.V. and Taranova, S.N., 2021. Mesoscale Eddies in the Bering Sea from Satellite Altimetry Data. *Izvestiya, Atmospheric and Oceanic Physics*, 57(12), pp. 1627–1642. https://doi.org/10.1134/S0001433821120240

31. Zhabin, I.A., 2006. Evolution of the East Kamchatka Current Eddy as Detected by Satellite Observation. *Issledovanie Zemli iz Kosmosa*, (1), pp. 53–58 (in Russian).

32. Shlyk, N.V. and Rogachev, K.A., 2016. Rapid Freshening of the Kamchatka Current. *Vestnik of Far Eastern Branch of Russian Academy of Sciences*, (5), pp. 113–119 (in Russian).

33. Khen, G.V. and Zaochny, N.A., 2009. Variability of the Kamchatka Current Transport and Water Properties in the Kamchatka Strait. *Izvestija TINRO*, 158, pp. 247–260 (in Russian).

34. Bulatov, N.V. and Samko, E.V., 2002. [Main Features of the Frontal Zones Structure of the North-West Pacific Ocean]. *Izvestija TINRO*, 130-1, pp. 12–23 (in Russian).

35. Kubryakov, A.A., Belonenko, T.V. and Stanichny, S.V., 2016. Impact of Mesoscale Eddies on Sea Surface Temperature in the North Pacific Ocean. *Sovremennye Problemy Distantsionnogo Zondirovaniya Zemli iz Kosmosa*, 13(2), pp. 34–43 (in Russian).

36. Fedorov, K.N., 1986. *The Physical Nature and Structure of Oceanic Fronts*. New York: Springer-Verlag, 333 p.

37. Lavrova, O.Yu., Kostianoy, A.G., Lebedev, S.A., Mityagina, V.I., Ginzburg, A.I. and Sheremet, N.A., 2011. *Complex Satellite Monitoring of the Russian Seas*. Moscow: IKI RAS, 470 p. (in Russian).

38. Monin, A.S., Kamenkovich, V.M. and Kort, V.G., 1977. *Variability of the Ocean*. London: John Wiley & Sons Ltd., 241 p.

Submitted 13.05.2024; accepted after review 7.06.2024;
revised 17.06.2024; published 25.09.2024

About the authors:

Aleksey V. Zimin, Head of Laboratory, Shirshov Institute of Oceanology of Russian Academy of Sciences (30 1st Line of Vasilevsky Island, Saint Petersburg, 119053, Russian Federation), Dr.Sci. (Geogr.), **ResearcherID: C-5885-2014, Scopus Author ID: 55032301400**, *zimin2@mail.ru*

Dmitry A. Romanenkov, Leading Research Associate, Shirshov Institute of Oceanology of Russian Academy of Sciences (30 1st Line of Vasilevsky Island, Saint Petersburg, 119053, Russian Federation), Ph.D. (Geogr.), **ResearcherID: U-8280-2017, Scopus Author ID: 6506855768**, *dmromanenkov@yandex.ru*

Aleksandr A. Konik, Research Associate, Shirshov Institute of Oceanology of Russian Academy of Sciences (30 1st Line of Vasilevsky Island, Saint Petersburg, 119053, Russian Federation), Ph.D. (Geogr.), **ResearcherID: AAB-7195-2020, ORCID ID: 0000-0002-2089-158X, Scopus Author ID: 57203864647**, *konikrshu@gmail.com*

Oksana A. Atadzhanova, Senior Research Associate, Shirshov Institute of Oceanology of Russian Academy of Sciences (30 1st Line of Vasilevsky Island, Saint Petersburg, 119053, Russian Federation), Research Associate, Marine Hydrophysical Institute of Russian Academy of Sciences (2 Kapitanskaya St., Sevastopol, 299011, Russian Federation), Ph.D. (Geogr.), **ResearcherID: R-7835-2018, Scopus Author ID: 57188718743**, *oksanam07@list.ru*

Egor I. Svergun, Research Associate, Shirshov Institute of Oceanology of Russian Academy of Sciences (30 1st Line of Vasilevsky Island, Saint Petersburg, 119053, Russian Federation), Ph.D. (Geogr.), **ResearcherID: AAC-7289-2020, ORCID ID: 0000-0002-9228-5765, Scopus Author ID: 57195066881**, *egor-svergun@yandex.ru*

Aleksandr I. Varkentin, Leading Research Associate, Shirshov Institute of Oceanology of Russian Academy of Sciences (30 1st Line of Vasilevsky Island, Saint Petersburg, 119053, Russian Federation), Deputy Head of Kamchatka branch of Federal State Budget Scientific Institution "Russian Federal Research Institute of Fisheries and oceanography" ("KamchatNIRO") (18 Naberezhnaya St., Petropavlovsk-Kamchatskiy, 683000, Russian Federation), Ph.D. (Biol.), *a.varkentin@kamniro.vniro.ru*

Oleg B. Tepnin, Senior Research Associate, Shirshov Institute of Oceanology of Russian Academy of Sciences (30 1st Line of Vasilevsky Island, Saint Petersburg, 119053, Russian Federation), Head of Oceanography Sector of Kamchatka branch of Federal State Budget Scientific Institution "Russian Federal Research Institute of Fisheries and Oceanography" ("KamchatNIRO") (18 Naberezhnaya St., Petropavlovsk-Kamchatskiy, 683000, Russian Federation), **ORCID ID: 0000-0001-9596-4336, ResearcherID: KIL-1378-2024**, *tenpin@yandex.ru*

Contribution of the authors:

Aleksey V. Zimin – article concept, complex analysis and interpretation of the results, final version of the manuscript

Dmitry A. Romanenkov – analysis and interpretation of the data on section *Multiscale eddies*, significant alterations while revising the article text

Aleksandr A. Konik – analysis and interpretation of the data on sections *Mesoscale eddies* and *Multiscale eddies and tidal dynamics*, work on the article draft

Oksana A. Atadzhanova – analysis and interpretation of the data on section *Submesoscale eddies*, writing the article draft

Egor I. Svergun – work on the data of section *Multiscale eddies and tidal dynamics*, work on the article draft

Aleksandr I. Varkentin – complex interpretation of the results, work on the article draft

Oleg B. Tepnin – complex data analysis, work on the article draft

All the authors have read and approved the final manuscript.

Original article

Estimation of Carbon Dioxide Fluxes through the Surface of the Black Sea from Numerical Simulation Results

V. L. Dorofeev, L. I. Sukhikh *

Marine Hydrophysical Institute of RAS, Sevastopol, Russia
* *e-mail: l.sukhikh@gmail.com*

Abstract
Based on numerical simulation, the paper studies the spatiotemporal distribution of CO_2 fluxes through the free surface of the Black Sea. The basic equation for solving this problem is the three-dimensional evolutionary transport–diffusion equation for the concentration of dissolved inorganic carbon. The simulation uses hydrodynamic fields resulting from a previous physical reanalysis as input parameters. A model of the lower level of the Black-Sea ecosystem food chain is used to describe the influence of biological factors on the dissolved carbon dioxide distribution. The concentration and equilibrium partial pressure of dissolved carbon dioxide in the surface layer of the Black Sea were calculated from the numerical simulation results. It is shown that the time dependence of these quantities is highly seasonal. The seawater temperature significantly affects the solubility of carbon dioxide and therefore its fluxes. The equilibrium partial pressure of carbon dioxide averaged over the area of the Black Sea is minimal in January–February and maximal in June–July. Accordingly, in the warm season, the flux of carbon dioxide is directed mainly from the sea to the atmosphere; in the cold season, the sea mainly absorbs carbon dioxide. Biological factors also influence the CO_2 content in the sea. Thus, at the beginning of the year, a high concentration of phytoplankton is observed almost throughout the entire Black Sea water area, which is why the absorption of carbon dioxide predominates during photosynthesis. In summer, the release of carbon dioxide predominates due to plankton respiration and oxidation of organic matter. The simulation results are in fairly good agreement with *in situ* measurements of the partial pressure of dissolved carbon dioxide obtained during scientific cruises.

Keywords: carbonate system, carbon dioxide, partial pressure of carbon dioxide, Black Sea, marine ecosystem, numerical simulation

Acknowledgments: The work was carried out under topic of state assignment of FSBSI FRC MHI FNNN-2023-0001. The authors thank the staff of the Biogeochemistry Department of the FSBSI FRC MHI for providing the results of field data processing.

For citation: Dorofeev, V.L. and Sukhikh, L.I., 2024. Estimation of Carbon Dioxide Fluxes through the Surface of the Black Sea from the Numerical Simulation Results. *Ecological Safety of Coastal and Shelf Zones of Sea*, (3), pp. 36–48.

Оценка потоков углекислого газа через поверхность Черного моря по результатам численного моделирования

В. Л. Дорофеев, Л. И. Сухих *

Морской гидрофизический институт РАН, Севастополь, Россия
** e-mail: l.sukhikh@gmail.com*

Аннотация
На основе численного моделирования изучается пространственно-временное распределение потоков CO_2 через свободную поверхность Черного моря. Основным уравнением для решения этой задачи является трехмерное эволюционное уравнение переноса – диффузии для концентрации растворенного неорганического углерода. При моделировании в качестве входных параметров используются гидродинамические поля, являющиеся результатом проведенного ранее физического реанализа. Для описания влияния биологических факторов на распределение растворенного углекислого газа используется модель нижнего уровня пищевой цепи экосистемы Черного моря. По результатам численного моделирования были рассчитаны концентрация и равновесное парциальное давление растворенного углекислого газа в поверхностном слое Черного моря. Показано, что зависимость от времени этих величин носит выраженный сезонный характер. На растворимость углекислого газа и, следовательно, на его потоки существенно влияет температура морской воды. Осредненное по площади Черного моря равновесное парциальное давление углекислого газа минимально в январе – феврале и максимально в июне – июле. Соответственно в теплый сезон поток углекислого газа направлен преимущественно из моря в атмосферу, в холодный сезон море в основном поглощает углекислый газ. На содержание CO_2 в море влияют также биологические факторы. Так, в начале года почти по всей акватории Черного моря наблюдается высокая концентрация фитопланктона, из-за чего преобладает поглощение углекислого газа в процессе фотосинтеза. Летом преобладает выделение углекислого газа вследствие дыхания планктона и окисления органического вещества. Результаты моделирования достаточно хорошо согласуются с натурными измерениями равновесного парциального давления растворенного углекислого газа, полученными в ходе научных рейсов.

Ключевые слова: карбонатная система, углекислый газ, парциальное давление углекислого газа, Черное море, морская экосистема, численное моделирование

Благодарности: работа выполнена в рамках государственного задания ФГБУН ФИЦ МГИ по теме FNNN-2023-0001. Авторы благодарят сотрудников отдела биогеохимии моря ФГБУН ФИЦ МГИ за предоставленные результаты обработки натурных данных.

Для цитирования: *Дорофеев В. Л., Сухих Л. И.* Оценка потоков углекислого газа через поверхность Черного моря по результатам численного моделирования // Экологическая безопасность прибрежной и шельфовой зон моря. 2024. № 3. С. 36–48. EDN WRBJXJ.

Introduction

A large number of papers (e. g. [1–7]) have been devoted to the study of the Black Sea carbonate system and, in particular, the flux of carbon dioxide through the surface. These studies are mainly based on measurement data. The disadvantage of these data is that they are limited in space and time. To obtain spatial distributions and temporal evolution of carbonate system components, it is necessary to use numerical three-dimensional models of the marine environment. Recently, numerical simulation of marine ecosystems has become widespread, including the Black Sea ecosystem simulation [8–11]. As an example of a model for the entire world ocean, the PISCES model can be mentioned [12]. Numerical ecosystem models describe the evolution of biological and hydrochemical fields as well as the carbonate system elements. They advantage the possibility of obtaining a sequence of the marine environment parameters on a regular grid. Of course, simulation results cannot replace *in situ* measurements, but they can extrapolate their results over time and over wider spatial areas. This paper presents preliminary results of estimation of carbon dioxide fluxes between the Black Sea and the atmosphere based on numerical simulation.

Method of study

Quantitative estimation of carbon dioxide fluxes through the sea–atmosphere interface is one of the main tasks in the study of the carbon cycle. This paper solves this problem by numerical simulation. The basic equation is three-dimensional evolutionary transport–diffusion equation for the dissolved inorganic carbon concentration

$$\frac{\partial C}{\partial t}+\frac{\partial (uC)}{\partial x}+\frac{\partial (vC)}{\partial y}+\frac{\partial (wC)}{\partial z}=K_h\nabla^2 C+\frac{\partial}{\partial z}\left(K_v\frac{\partial C}{\partial z}\right)+R\,, \qquad (1)$$

Where u, v, w are current velocity components; K_h, K_v are coefficients of horizontal and vertical turbulent diffusion, respectively. Representing the coefficients of equation (1), these fields, are provided by the Black Sea circulation model. Summand R in the right-hand side of equation (1) has the form $R = Res - upt + Ox$, where *Res* describes the input of carbon dioxide due to the respiration of all plankton species; $-$ *upt* describes reduction of dissolved inorganic carbon from photosynthesis during primary production and *Ox* – its input due to oxidation of suspended organic matter [13].

An existing three-dimensional model of the lower level of the Black Sea ecosystem food chain is used to calculate these values [14, 15]. From the mathematical point of view, the biogeochemical part of the model represents a system of fifteen (according to the number of state variables) transport-diffusion equations similar to equation (1). The summands in the right-hand sides of this system describe biogeochemical interactions among the state variables of the ecosystem model. A view of

these sources for the ecosystem model is presented in [15]. Variable units are converted from nitrogen to carbon using the C:N ratios for the Black Sea taken from [16].

The connection of the circulation model with the biogeochemical part is one-way in this work. That is, current velocity fields, temperature, salinity and turbulent diffusion coefficients obtained from the hydrodynamic model in advance are then used to calculate the biogeochemical model parameters and in equation (1). The calculation domain for equation (1) and the biogeochemical part of the model coincides horizontally with the corresponding domain for the circulation model (grid steps equal to 4.8 km coincide, accordingly) and occupies vertically the upper 200 m layer of the Black Sea. At the same time, the computational horizons correspond to the circulation models. The results of a 28-year physical reanalysis of the Black Sea fields (1993–2020) were used as hydrodynamic fields in this work [17].

To obtain the initial fields, the calculation for 2017 was carried out in a cycle in which the input parameters of the ecosystem model (current velocity, temperature and salinity fields for 2017) were taken from the reanalysis. Once the biogeochemical fields reached the stationary regime, the calculation was terminated and the obtained fields were used as initial fields for the main calculation.

Dissolved CO_2 concentration was calculated from the obtained dissolved inorganic carbon fields using formula

$$[DIC] = [\mathrm{CO_2}] \times \left\{ 1 + \frac{K_1}{[\mathrm{H^+}]} + \frac{K_1 K_2}{[\mathrm{H^+}][\mathrm{H^+}]} \right\},$$

where effective dissociation constants of carbonic acid K_1, K_2 depend on seawater temperature and salinity. Then its equilibrium partial pressure is determined from the concentration of dissolved carbon dioxide using Henry coefficient K_0 by formula $[CO_2] = K_0\, pCO_2$ [18]. The Henry coefficient is not a constant as it depends on seawater temperature and salinity.

To calculate the concentration of dissolved carbon dioxide from the total inorganic carbon concentration in water, it is necessary to know the concentration of hydrogen ions in addition to coefficients K_1, K_2. To estimate the fluxes of carbon dioxide through the sea surface, only surface values of carbon dioxide concentration are necessary. In this work, the pH parameter was not calculated by the model, but approximated in time and space according to the data from atlas [1)] containing maps of pH distribution on the Black Sea surface for four seasons.

The partial pressure of carbon dioxide in the atmosphere surface layer was assumed to be constant and equal to 410 μatm. The carbon dioxide flux between the sea and the atmosphere was calculated by formula $F = Tr\,(pCO_{2w} - pCO_{2a})$, where Tr is carbon dioxide transport coefficient between the sea and the atmosphere; pCO_{2w} and pCO_{2a} are partial pressure values in water and in the atmosphere. The value

[1)] Mitin, L.I.. ed., 2006. *Atlas of the Black Sea and Sea of Asov Nature Protection*. Saint Petersburg: GUN i O, 436 p. (in Russian).

of coefficient *Tr* was chosen to be 0.5 $gC \cdot m^{-2} \cdot \mu atm^{-1} \cdot month^{-1}$ (the World Ocean average according to [19]).

Results

The main calculation covered four years from 2017 to 2020. Fig. 1 shows the evolution of basin area averaged concentration of carbon dioxide at the sea surface and its partial pressure obtained from simulation results. Temporal dependence is highly seasonal. Dissolved carbon dioxide pressure values are minimal around January–February and maximal around June–July. When the partial pressure of carbon dioxide dissolved in seawater exceeds the pressure in the atmosphere, the flux is directed from the sea to the atmosphere through the free surface, and vice versa. Thus, it follows from the graph of pCO_2 change that invasion is observed on average in the Black Sea water area during cold times (approximately from October to April) because the partial pressure of CO_2 dissolved in the sea is lower than the partial pressure in the atmosphere. On the contrary, evasion is observed on average during the warm period (approximately from April to October).

The maxima and minima on the graph of temporal variability of carbon dioxide concentration in the Black Sea surface layer do not coincide with the corresponding extremes on the graph of pressure. They are shifted by about three months. This is stipulated by the fact that the Henry constant, which relates the values of CO_2 concentration in the sea and its equilibrium partial pressure, depends, among other things, on the sea water temperature, which varies considerably during the year.

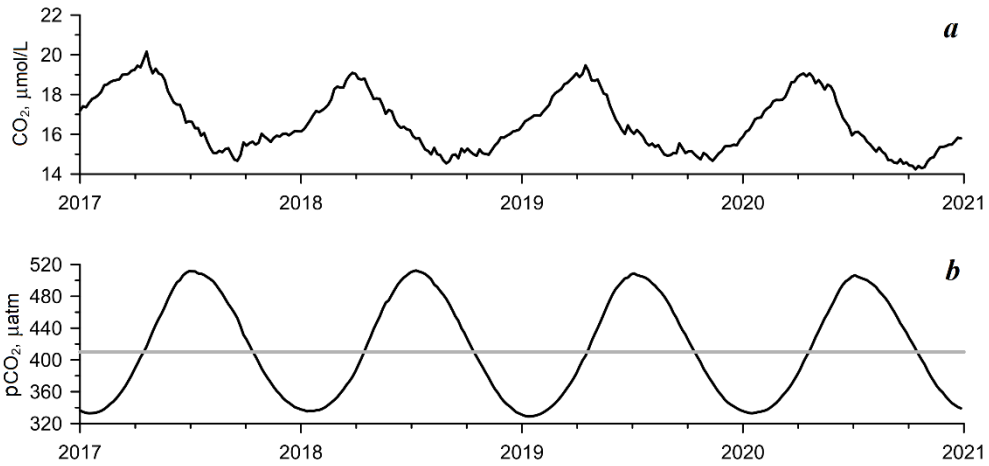

Fig. 1. Evolution of the average over the basin area concentration of carbon dioxide at the sea surface (*a*) and its partial pressure (*b*) obtained from simulation results. The straight line shows the CO_2 partial pressure in the atmospheric surface layer

At the same time, the range of fluctuations of the basin area averaged concentration of carbon dioxide (approximately 25 % of the maximum value) is significantly smaller than the range of pressure fluctuations. The graphs (Fig. 1) also show the inverse dependence of dissolved carbon dioxide concentration on partial pressure clearly: the CO_2 concentration increases in those periods of time when the CO_2 flux is directed from the atmosphere to the sea, and vice versa, the concentration decreases when the flux is directed to the atmosphere.

Figure 2, *a* shows the graph of the time dependence of the sea area averaged value of the Henry coefficient. The temperature and salinity fields obtained from the reanalysis of the Black Sea hydrodynamic fields were used to calculate the value of the coefficient at each grid point. The variability of the Henry coefficient is also highly seasonal and is almost antiphased to the change in the carbon dioxide partial pressure (see Fig. 1, *b*). Over the course of a year, the area average of the Henry coefficient changes by almost a factor of two. Figure 2, *b* shows the graph of sea surface temperature evolution. These two graphs change in antiphase and it can be concluded that the variation of the sea area averaged value of the Henry coefficient is determined mainly by the sea water temperature. That is, the main contribution to the intra-annual variability of the CO_2 partial pressure in the sea surface layer is made by hydrological factors (mainly water temperature). The partial pressure decreases as the water temperature decreases and increases as the temperature increases. Accordingly, as long as the dissolved CO_2 pressure is greater than the atmospheric one, the flux through the sea surface is directed towards the atmosphere which is accompanied by a decrease in the dissolved CO_2 concentration. Then, when the dissolved gas pressure becomes less than the atmospheric one, the flux through the surface changes direction with an increase in the dissolved carbon dioxide concentration.

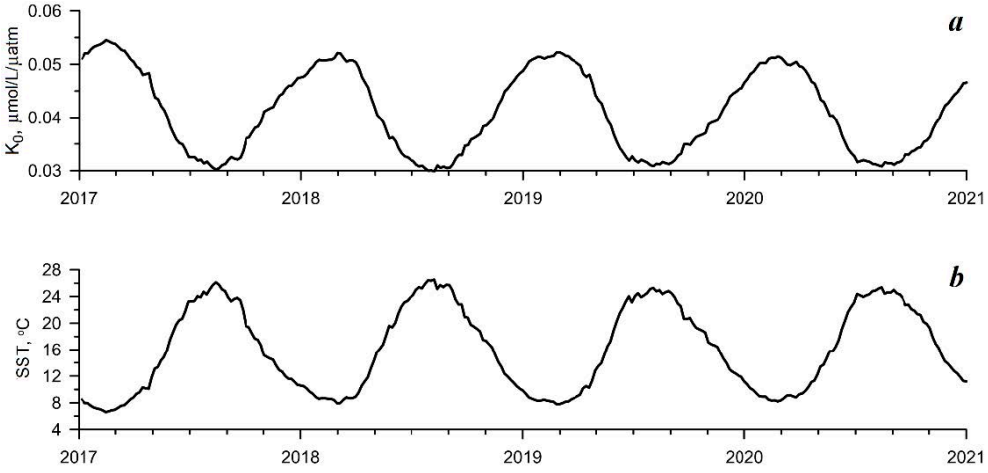

F i g . 2 . Evolution of sea area averaged values of the Henry coefficient (*a*) and sea surface temperature (*b*)

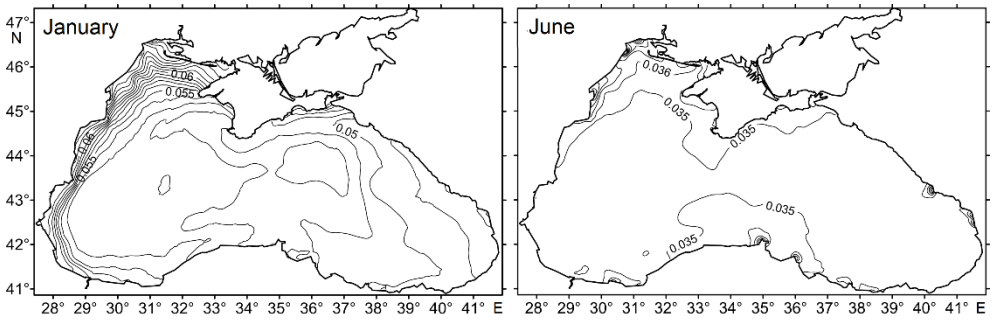

Fig. 3. Spatial distributions of the Henry coefficient (μmol/L/μatm) for January and June 2017

Figure 3 shows the spatial distribution of the Henry coefficient. In summer, the distribution of the Henry coefficient is almost uniform over the entire water area except for the river confluences where the water is much freshened. In winter, the coefficient value is higher than in summer. In addition, an increase in the coefficient values is clearly visible in the north-western shelf (NWS) and along the western coast of the Black Sea. This is due to the fact that the NWS water is the coldest and most freshened in winter. The Black Sea Rim Current, intense in winter, carries this water along the western coast.

Figure 4, *a*, *b* provides an insight into the spatial distribution of the carbon dioxide partial pressure in the Black Sea surface layer. It shows the monthly average maps for two months, January and June 2017 (which corresponds to the minimum and maximum in Fig. 1, *b*). Spatial distributions of pCO_2 are similar for both months: the maxima are observed in the centre of the basin and in the NWS (only in its northern part in January). However, the average level varies significantly. Thus, the surface partial pressure of dissolved carbon dioxide is lower than the atmospheric pressure (410 μatm) in the entire water area in January and it is higher practically in the entire water area in June.

Biological processes also affect the dissolved carbon dioxide pressure distribution. Figure 4, *c*, *d* shows average monthly maps of the surface distribution of value $R = Res - upt + Ox$ describing the input of dissolved carbon dioxide from the plankton respiration and organic oxidation and its loss during photosynthesis for the same months.

In January, this value is negative almost over the entire water area (except for a small area in Karkinitski and Tendrovski Bays). A local maximum is identified at this location on the pCO_2 distribution map (Fig. 4, *a*). That is, the absorption of carbon dioxide prevails over its production due to biological processes in January. In June, most of the area has positive values, except for the central part of the sea, where it is close to zero.

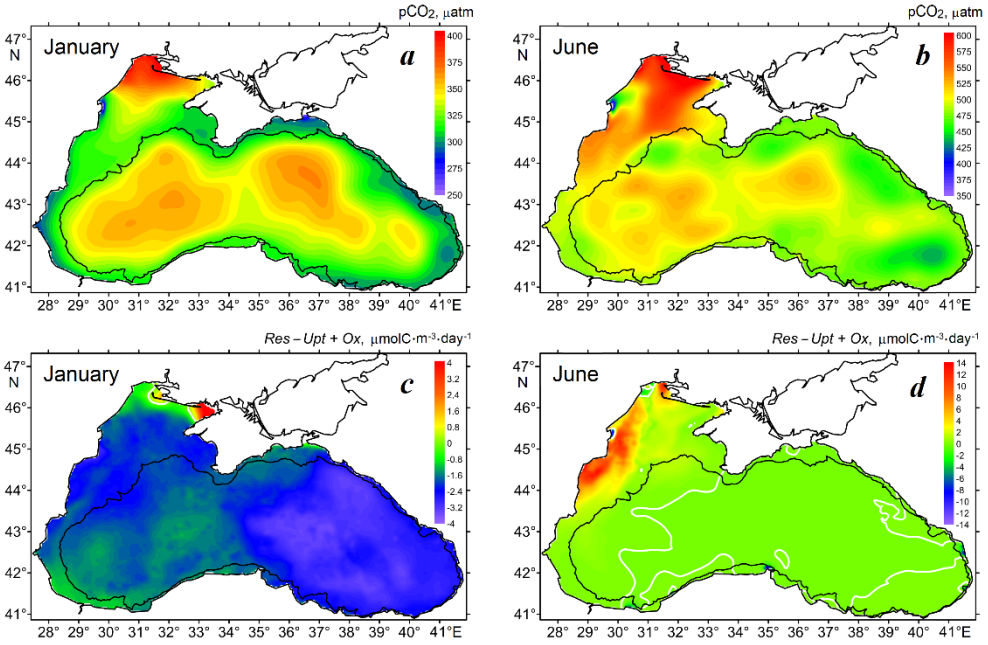

Fig. 4. Spatial distribution of partial pressure of carbon dioxide in the surface layer of the Black Sea (*a*, *b*) and monthly average maps of the surface distribution of the $R = Res - upt + Ox$ value (*c*, *d*) for January and June 2017 (the white line in Fig. 4, *d* indicates the zero isoline)

The predominance of carbon dioxide absorption over its production as a consequence of biological processes or vice versa is directly related to plankton concentrations in the sea upper layer. Figure 5 shows surface phytoplankton concentrations (*a*, *b*) and total plankton concentrations (*c*, *d*) for the same two months.

In January, the surface phytoplankton concentration is relatively high throughout the Black Sea area (Fig. 5, *a*), including its deep water. Total plankton concentration also shows high values (Fig. 5, *c*), but mainly due to phytoplankton. Accordingly, the absorption of carbon dioxide in the process of photosynthesis predominates in Fig. 5, *c*.

In June, concentrations of both phytoplankton and total plankton are low in the deep sea and high in the NWS (Fig. 5, *b*, *d*). Moreover, the total plankton biomass is significantly greater than the phytoplankton biomass in the NWS. Accordingly, Fig. 4, *d* shows that the CO_2 production caused by the plankton respiration dominates in the western Black Sea, especially in the NWS.

The obtained numerical simulation results were compared with observational data, unfortunately, few and local. Fig. 6 shows the pCO_2 distribution maps based

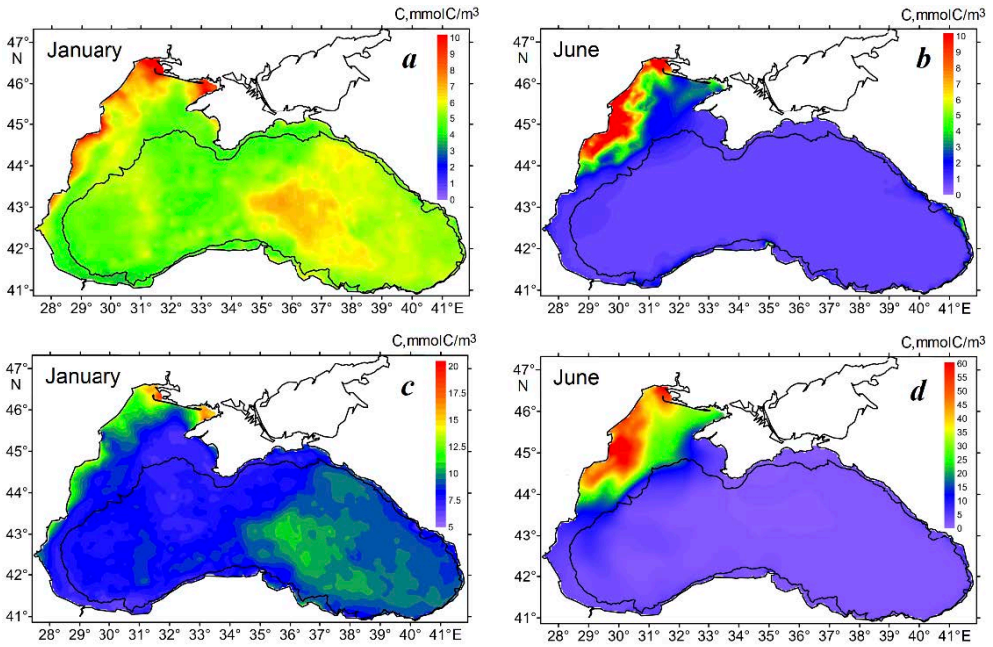

Fig. 5. Spatial distribution of surface phytoplankton concentrations (*a*, *b*) and total plankton concentration (*c*, *d*) for January and June 2017

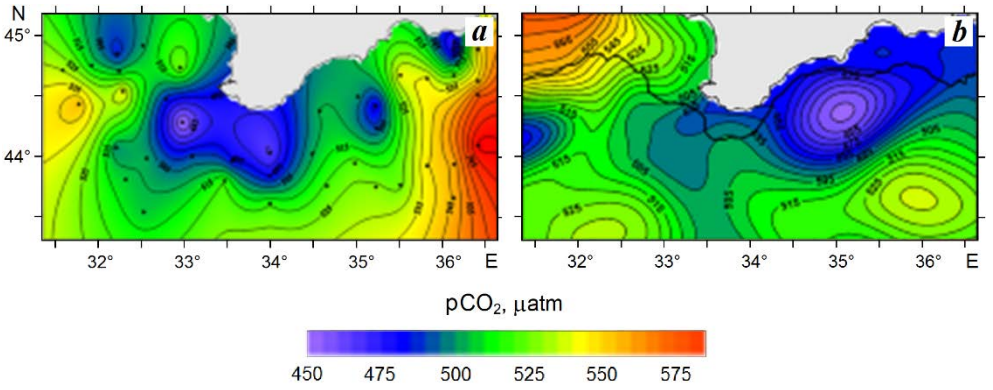

Fig. 6. pCO_2 distribution maps based on observational data (*a*) and numerical simulation results (*b*)

on observational data (Fig. 6, *a*) [20] and numerical simulation results (Fig. 6, *b*). The left map (Fig. 6, *a*) represents the result of processing samples taken at 132 stations during the 95th cruise of R/V *Professor Vodyanitsky* from 14 June to 4 July 2017.

In general, the values of the CO_2 equilibrium partial pressure near the sea surface obtained from the simulation results are quite close to the measurement data. The spatial distribution of pressure on two maps does not coincide, however, a characteristic decrease of pressure values near the Southern Coast of Crimea and Sevastopol is observed on both maps. It should also be noted that the map obtained from the model refers to a specific date (26 June), while the survey, on the results of which the left map is based (Fig. 6, *a*), lasted more than two weeks.

Figure 7 shows graphs of intra-annual variability of the Black Sea water area average values of equilibrium partial pressure of carbon dioxide pCO_2 obtained from measurements and simulation results averaged over four years. The left graph (Fig. 7, *a*) was kindly provided by the Marine Biogeochemistry Department of Marine Hydrophysical Institute. It is based on the processing of data obtained in 2015–2021 during the R/V *Professor Vodyanitsky* expedition studies of Marine Hydrophysical Institute. The location of stations is given in [7, p. 871].

Both graphs are relatively similar. Thus, the intra-annual variability of the Black Sea average equilibrium partial pressure of dissolved carbon dioxide in the sea surface layer is reproduced well by the model.

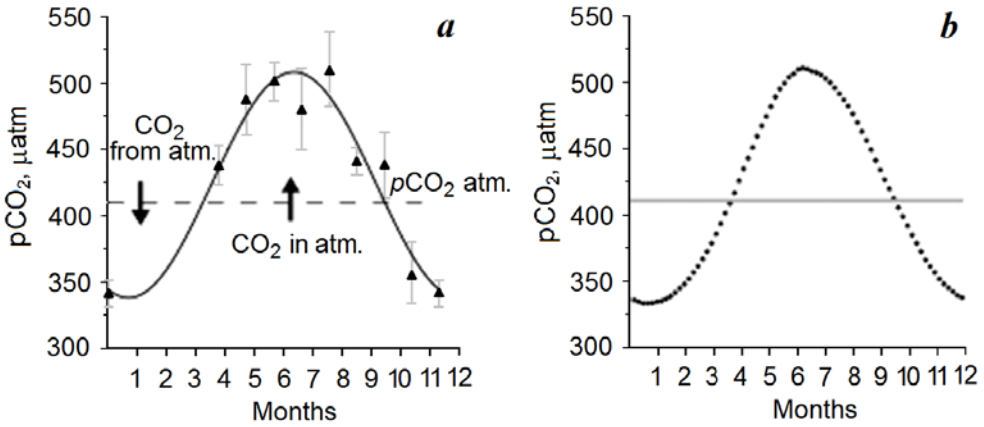

Fig. 7. Intra-annual variability of pCO_2 from observational data (*a*) and numerical simulation results (*b*)

Conclusions

Based on the results of numerical simulation, the time course and spatial distribution of such elements of the carbonate system as the concentration of dissolved carbon dioxide in the surface layer of the sea and its equilibrium partial pressure were obtained. The time course of these parameters is highly seasonal.

It has been shown that during the time period approximately from October to April, i. e. during the cold season, invasion is observed on average in the Black Sea water area because the equilibrium partial pressure of CO_2 dissolved in the sea is lower than the partial pressure in the atmosphere. Evasion occurs during the warm season, approximately from April to October, when pCO_2 in water is on average higher than in the atmosphere.

At constant partial pressure of CO_2 in the atmosphere (it changed during the year by 5 % according to the measurement data in 2017, according to atlas [1)]), the direction of carbon dioxide flux through the Black Sea surface is mainly influenced by seawater temperature. The equilibrium partial pressure of the dissolved gas decreases when the temperature decreases and increases with its increase. As long as the CO_2 pressure in the water is greater than the atmospheric one, the flux through the sea surface is directed towards the atmosphere, which is accompanied by a decrease in dissolved CO_2 concentration. When the dissolved gas pressure becomes lower than the atmospheric one, the flux through the surface reverses its direction, which is accompanied by an increase in dissolved carbon dioxide concentration.

The flux of carbon dioxide through the sea free surface is also influenced by biological processes. In winter, almost the entire Black Sea area is dominated by carbon dioxide absorption over carbon dioxide production due to high phytoplankton concentration near the Black Sea surface. In summer, however, carbon dioxide release predominates over most of the water area due to the plankton respiration.

The equilibrium partial pressure of dissolved carbon dioxide obtained as a result of simulation was compared with the data of hydrochemical surveys. The comparison showed a fairly good agreement between the results of numerical simulation and measurements.

References

1. Zhorov, V.A., Abakumova, T.N., Sovga, E.E. and Lyashenko, S.V., 1981. On CO_2 Exchange between the Sea and the Atmosphere in Some Regions of the Black Sea. *Okeanologiya*, 21(1), pp. 55–62 (in Russian).
2. Khoruzhiy, D.S. and Konovalov, S.K., 2014. Diurnal Variation and Inter-Diurnal Changes of Carbonic Acid and Dissolved Inorganic Carbon Content in the Black Sea Coastal Waters. *Morskoy Gidrofizicheskiy Zhurnal*, (1), pp. 28–43 (in Russian).
3. Konovalov, S.K., Kondratev, S.I., Khoruzhiy, D.S., Medvedev, E.V. and Moiseenko O.G., 2014. [Total Inorganic Carbon, Carbonate System and Carbon Dioxide Fluxes in the Coastal Zone of the Southern Coast of Crimea: Monitoring, Characteristics, Dynamics]. In: V. A. Ivanov and V. A. Dulov, eds., 2014. *Monitoring of the Coastal Zone in the Black Sea Experimental Sub-Satellite Testing Area*. Sevastopol: ECOSI-Gidrofizika, pp. 250–271 (in Russian).

4. Khoruzhii, D.S., 2016. Variability of Equilibrium Partial Pressure of Carbon Dioxide (pCO2) and Concentration of Dissolved Inorganic Carbon (TCO2) in the Black Sea Coastal Waters in 2010–2014. *Physical Oceanography*, (4), pp. 34–46. https://doi.org/10.22449/1573-160X-2016-4-34-46
5. Orekhova, N.A., Konovalov, S.K. and Medvedev, E.V., 2019. Features of Inorganic Carbon Regional Balance in Marine Ecosystems under Anthropogenic Pressure. *Physical Oceanography*, 26(3), pp. 225–235. https://doi.org/10.22449/1573-160X-2019-3-225-235
6. Silkin, V.A., Podymov, O.I. and Lifanchuk, A.V., 2022. Biological Carbon Pump in the Black Sea. *Hydrosphere Ecology*, (2), pp. 69–92. https://doi.org/10.33624/2587-9367-2022-2(8)-69-92 (in Russian).
7. Varenik, A.V., Kondratyev, S.I., Medvedev, E.V., Khoruzhiy, D.S. and Orekhova, N.A., 2023. Characteristics of State and Evolution of the Black Sea Hydrochemical Structure. *Physical Oceanography*, 30(6), pp. 826–850.
8. Grégoire, M., Soetaert, K., Nezlin, N. and Kostianoy, A., 2004. Modeling the Nitrogen Cycling and Plankton Productivity in an Enclosed Environment (The Black Sea) Using a Three-Dimensional Coupled Hydrodynamical-Ecosystem Model. *Journal of Geophysical Research: Oceans*, 109(C5), C05007. https://doi.org/10.1029/2001JC001014
9. Tsiaras, K.P., Kourafalou, V.H., Davidov, A. and Staneva, J., 2008. A Three-Dimensional Coupled Model of the Western Black Sea Plankton Dynamics: Seasonal Variability and Comparison to SeaWiFS Data. *Journal of Geophysical Research: Oceans*, 113(C7), C07007. https://doi.org/10.1029/2006JC003959
10. Dorofeev, V.L., 2009. Modeling of Decadal Variations in the Black-Sea Ecosystem. *Physical Oceanography*, 19(6), pp. 400–409. https://doi.org/10.1007/s11110-010-9062-6
11. Capet, A., Meysman, F.J.R., Akoumianaki, I., Soetaert, K. and Grégoire, M., 2016. Integrating Sediment Biogeochemistry into 3D Oceanic Models: A Study of Benthic-Pelagic Coupling in the Black Sea. *Ocean Modelling*, 101, pp. 83–100. https://doi.org/10.1016/j.ocemod.2016.03.006
12. Aumont, O., Ethé, C., Tagliabue, A., Bopp, L. and Gehlen, M., 2015. PISCES-v2: An Ocean Biogeochemical Model for Carbon and Ecosystem Studies. *Geoscientific Model Development*, 8(8), pp. 2465–2513. https://doi.org/10.5194/gmd-8-2465-2015
13. Van den Meersche, K., Middelburg, J.J., Soetaert, K., Van Rijswijk, P., Boschker, H.T.S. and Heip, C.H.R., 2004. Carbon Nitrogen Coupling and Algal-Bacterial Interactions during an Experimental Bloom: Modeling a ^{13}C Tracer Experiment. *Limnology and Oceanography*, 49(3), pp. 862–878. https://doi.org/10.4319/lo.2004.49.3.0862
14. Dorofeyev, V. and Sukhikh, L., 2018. A Model for Monitoring the Evolution of the Black Sea Ecosystem on the Basis of Remote Sensing Data Assimilation. *International Journal of Remote Sensing*, 39(24), pp. 9339–9355. https://doi.org/10.1080/01431161.2018.1523589
15. Dorofeev, V.L. and Sukhikh, L.I., 2019. Studying Long-Term Variations in Black-Sea Ecosystem Based on the Assimilation of Remote Sensing Data in a Numerical Model. *Water Resources*, 46(1), pp. 65–75. https://doi.org/10.1134/S0097807819010032
16. Grégoire, M., Raick, C. and Soetaert, K., 2008. Numerical Modeling of the Central Black Sea Ecosystem Functioning During the Eutrophication Phase. *Progress in Oceanography*, 76(3), pp. 286–333. https://doi.org/10.1016/j.pocean.2008.01.002
17. Dorofeev, V.L. and Sukhikh, L.I., 2023. Analysis of Long-Term Variability of Hydrodynamic Fields in the Upper 200-Meter Layer of the Black Sea Based on the Reanalysis Results. *Physical Oceanography*, 30(5), pp. 581–593.
18. Millero, F.J., 2007. The Marine Inorganic Carbon Cycle. *Chemical Reviews*, 107(2), pp. 308–341. https://doi.org/10.1021/cr0503557

19. Takahashi, T., Sutherland, S.C., Wanninkhof, R., Sweeney, C., Feely, R.A., Chipman, D.W., Hales, B., Friederich, G., Chavez, F. [et al.], 2009. Climatological Mean and Decadal Changes in Surface Ocean pCO_2, and Net Sea-Air CO_2 Flux over the Global Oceans. *Deep-Sea Research II: Topical Studies in Oceanography*, 56(8–10), pp. 554–577. https://doi.org/10.1016/j.dsr2.2008.12.009

20. Zabegaev, I.A. and Medvedev, E.V., 2019. [Equilibrium Partial Pressure of Carbon Dioxide in the Surface Water Layer of the Northern Black Sea Based on Direct Observations in 2017]. In: MHI, 2019. [*Seas of Russia: Fundamental and Applied Studies. Proceedings of the All-Russian Scientific Conference. Sevastopol, September 23–28, 2019*]. Sevastopol: FGBUN FITS MGI, pp. 76–78 (in Russian).

Submitted 25.01.2024; accepted after review 25.03.2024;
revised 17.06.2024; published 25.09.2024

About the authors:

Viktor L. Dorofeev, Leading Research Associate, Marine Hydrophysical Institute of RAS (2 Kapitanskaya St., Sevastopol, 299011, Russian Federation), PhD (Phys.-Math.), **ResearcherID: G-1050-2014**, *viktor.dorofeev@mhi-ras.ru*

Larisa I. Sukhikh, Research Associate, Marine Hydrophysical Institute of RAS (2 Kapitanskaya St., Sevastopol, 299011, Russian Federation), **ResearcherID: M-4381-2018**, *l.sukhikh@gmail.com*

Contribution of the authors:

Viktor L. Dorofeev – general scientific supervision of the study, formulation of the goals and objectives of the study, carrying out numerical simulations, analysis of the obtained results and their interpretation

Larisa I. Sukhikh – literature review, numerical simulations, analysis of the results

All the authors have read and approved the final manuscript.

Original article

Statistical Distributions of Crests and Trough of Sea Surface Waves

A. S. Zapevalov

Marine Hydrophysical Institute of RAS, Sevastopol, Russia

e-mail: sevzepter@mail.ru

Abstract

In many practical applications, a statistical description of waves is needed to calculate and predict their impact on ships, coastal structures and beaches. This paper investigates the statistics of the trough *Th* and the crest *Cr* of sea surface waves in the coastal zone of the Black Sea. The analysis uses data from direct wave measurements obtained on a stationary oceanographic platform of the Marine Hydrophysical Institute of the Russian Academy of Sciences. In all situations, the mode of the *Th* and *Cr* distributions is shifted to the region of higher values relative to the Rayleigh distribution mode. As a rule, the analysis of the distributions of trough and crest is carried out within a second-order nonlinear model based on the Stokes wave. It is shown that within the framework of this model it is possible to describe only the average distribution over an ensemble of situations, while for practical tasks it is necessary to know the deviations from these values. The type of *Th* and *Cr* distributions significantly depends on the skewness of the distribution of sea surface elevations A_η. With $A_\eta < 0$, the probability density function *Th* and *Cr* are almost identical. The second-order nonlinear model, in which the condition $A_\eta > 0$ is always fulfilled, does not describe this situation. The probability density functions *Th* and *Cr* obtained with $A_\eta > 0$ correspond qualitatively to this model. Changes in the excess kurtosis of the distribution of sea surface elevations have a lesser effect on the probability density functions *Th* and *Cr*.

Keywords*:* sea surface, waves, trough, crest, statistical distributions, Black Sea

Acknowledgements: the work was completed under state assignment on topic FNNN-2021-0004 “Fundamental studies of the processes that determine fluxes of matter and energy in the marine environment and at its boundaries, the state and evolution of the physical and biogeochemical structure of marine systems in modern conditions” (“Oceanological processes” code). The author thanks A.V. Garmashov, who provided wave measurement data on a stationary oceanographic platform.

For citation: Zapevalov, A.S., 2024. Statistical Distributions of Crests and Trough of Sea Surface Waves. *Ecological Safety of Coastal and Shelf Zones of Sea*, (3), pp. 49–58.

Статистические распределения высоты гребней и глубины впадин морских поверхностных волн

А. С. Запевалов

Морской гидрофизический институт РАН, Севастополь, Россия
e-mail: sevzepter@mail.ru

Аннотация
В настоящей работе исследуются статистические распределения глубины впадин *Th* и высоты гребней *Cr* морских поверхностных волн в прибрежной зоне Черного моря. Для анализа используются данные прямых волновых измерений, полученные на стационарной океанографической платформе Морского гидрофизического института РАН. Во всех ситуациях мода распределений *Th* и *Cr* смещена в область более высоких значений относительно моды распределения Рэлея. Как правило, анализ распределений глубин впадин и высот гребней проводится в рамках нелинейной модели второго порядка, построенной на основе волны Стокса. Показано, что в рамках указанной модели можно описать только средние по ансамблю ситуаций распределения, в то время как для практических задач необходимо знать отклонения от этих значений. Вид распределений *Th* и *Cr* существенно зависит от асимметрии распределения возвышений морской поверхности A_η. При $A_\eta < 0$ функции плотности вероятностей *Th* и *Cr* почти совпадают. Нелинейная модель второго порядка, в рамках которой всегда выполняется условие $A_\eta > 0$, не описывает эту ситуацию. Полученные при $A_\eta > 0$ функции плотности вероятностей *Th* и *Cr* качественно соответствуют данной модели. Изменения эксцесса распределения возвышений морской поверхности в меньшей мере влияют на функции плотности вероятностей *Th* и *Cr*.

Ключевые слова: морская поверхность, волны, впадина, гребень, статистические распределения, Черное море

Благодарности: работа выполнена в рамках государственного задания по теме FNNN-2024-0001 «Фундаментальные исследования процессов, определяющих потоки вещества и энергии в морской среде и на ее границах, состояние и эволюцию физической и биогеохимической структуры морских систем в современных условиях» (шифр «Океанологические процессы»). Автор благодарит А. В. Гармашова, предоставившего данные волновых измерений на стационарной океанографической платформе.

Для цитирования: *Запевалов А. С.* Статистические распределения высоты гребней и глубины впадин морских поверхностных волн // Экологическая безопасность прибрежной и шельфовой зон моря. 2024. № 3. С. 49–58. EDN CYOWEE.

Introduction

The study of sea wave statistical distributions and the identification of rogue waves are among the urgent tasks of modern oceanology [1]. In a linear wave field, which represents a superposition of sinusoidal waves with random phase, provided that the wave spectrum is sufficiently narrow, the distribution of wave heights is described by the Rayleigh distribution [2]. It also describes the distributions of crest heights and trough depths [3]. The Rayleigh distribution is generally regarded as the lower limit giving the lowest probabilities for rogue waves [4]. The linear model also underestimates strongly the probability of high crests [5].

Crest *Cr* refers to the maximum value of wave record $\eta(t)$ between the time it crosses the zero level from bottom to top and the time it crosses that level from top to bottom [6]. Similarly, trough *Th* is minimum value $\eta(t)$ between two consecutive crossings of the zero level from top to bottom and from bottom to top. Wave height is defined as the sum of consecutive maximum and minimum values between two points where the wave record crosses $\eta(t)$ the zero level upwards or downwards, i. e., $H = Cr + Th$ [7].

Deviations of sea wave statistical distributions from the linear model are usually described within a second-order nonlinear model which is based on the decomposition of the wave profile into small parameter powers (steepness) [8]. In the above model, the skewness of the sea surface elevation distribution is always higher than zero [9], the crests are higher and the troughs are shallower than predicted by linear theory [10]. Both of these conditions are not always fulfilled in marine environments. Measurements made in different areas of the world ocean have shown that the lower limit of the range where the skewness varies lies in the region of negative values [11, 12]. The second-order nonlinear model describes only average trends of skewness and excess kurtosis changes not allowing to describe the whole variety of situations occurring in the sea [13].

The ratios of crest and trough vary widely. Some situations are observed when the maximum trough is greater than the maximum crest during a measurement session [14, 15]. According to measurements in the Black Sea, the probability of an event in which the trough of the highest wave in the measurement session is greater than its crest reaches 10% [16].

Less attention has been paid to the analysis of the distribution of sea wave troughs than to the statistical description of their crests, although the distribution of troughs is of great importance for a number of engineering applications [9]. The purpose of this paper is to analyse jointly the distributions of crests and troughs of surface waves.

Measurement equipment and conditions

Wave measurement data obtained on the stationary oceanographic platform of Marine Hydrophysical Institute of the Russian Academy of Sciences were used to study the statistical characteristics of surface waves. The stationary oceanographic platform is located in the coastal part of the Black Sea off the Southern Coast of Crimea at a depth of about 30 metres. Two types of wave recorders were used to measure surface waves. The wave recorders of the first type contain a vertically stretched nichrome string as a sensor [17] and the nichrome string is coiled with a constant pitch on a vertically oriented supporting cable-tether in wave recorders of the second type [18].

This paper analyses the measurement data obtained in the summer and autumn of 2006 as well as in the winter of 2018. In 2006, measurements were taken in sessions lasting several hours; in 2018, wave measurements were taken continuously for a month. Continuous recordings of sea surface elevations were divided into 20 min fragments. A total of 2380 twenty-minute fragments were used for the analysis.

For each fragment, crest *Cr* and trough *Th* of separate waves were determined and significant wave height H_S, skewness *A* and excess kurtosis *E* of surface elevation were calculated. Only waves satisfying the conditions of *Cr* > 5 cm and *Th* > 5 cm were considered in the analysis. Hereinafter, parameter *Th* is equal to the trough modulus.

Wave measurements carried out in different seasons made it possible to cover a wide range of meteorological parameters. The average wind speed during the measurement session varied from conditional zero (the threshold of propeller starting) to 26 m/s. The wind speed reached 35 m/s in gusts. The wave periods calculated from the maximum of the wave spectrum were in the range from 1.1 s to 9 s. Significant wave height varied from 0.1 m to 2.3 m. The values of wave steepness (nonlinearity parameter) ranged mainly from 0.009 to 0.09.

Distributions of troughs and crests

For statistical moments $\eta(t)$, we introduce the following notation

$$\mu_n = \langle \eta^n(t) \rangle ,$$

where $\langle \ldots \rangle$ is averaging. Let us assume that the average value of a random variable is $\mu_1 = 0$, then the skewness and excess kurtosis of the surface elevation distribution are equal to $A_\eta = \mu_3/\mu_2^{3/2}$ and $E_\eta = \mu_4/\mu_2^2 - 3$, respectively.

To compare the statistical distributions of troughs and crests determined in different situations, we will use normalised wave records

$$\tilde{\eta}(t) = \eta(t)/H_S , \qquad (1)$$

where H_S is significant wave height connected to the second statistical moment of sea surface elevations by relation $H_S = 4\sqrt{\mu_2}$.

The probability density function of the Rayleigh distribution describing distributions of *Cr* and *Th* under the linear model is as follows

$$F_R(x) = \frac{x}{a^2} \exp\left(-\frac{x^2}{2a^2} \right), \quad x \geq 0 , \qquad (2)$$

where $a = H_S / 4$. Considering (1), we obtain that in our case mode of distribution (2) is defined as $Mo_R = 0.25$.

Empirical probability density functions of *Cr* and *Th* were calculated based on histograms constructed with equal intervals of 0.05. Fig. 1 shows the empirical probability density functions of crests $F_{Cr}(x)$ and troughs $F_{Th}(x)$ calculated over the entire measurement data set. It can be seen that modes of empirical distributions Mo_{Cr} and Mo_{Th} are shifted relative to the Rayleigh distribution mode towards higher values *x*, i. e., the following conditions are fulfilled

$$Mo_{Cr} > Mo_R , \quad Mo_{Th} > Mo_R .$$

The modes of the *Cr* and *Th* distributions are located in neighbouring intervals, with their centers $Mo_{Cr} = 0.375$ and $Mo_{Th} = 0.325$.

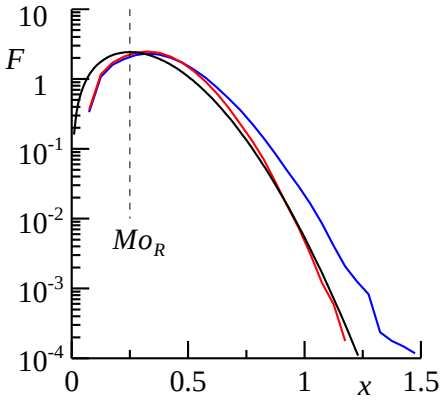

Fig. 1. Probability density functions F (average over an ensemble of situations). The blue curve is $F_{Cr}(x)$, the red curve is $F_{Th}(x)$, the black curve is $F_R(x)$

The consideration of nonlinearity leads to the fact that the probability of high crests becomes greater than in the linear model, in which this probability is described by the Rayleigh distribution, and the probability of deep troughs is smaller [9]. It follows from Fig. 1 that inequality $F_{Cr}(x) > F_R(x)$ is true in region $x > Mo_{Cr}$. The ratio between $F_{Th}(x)$ and $F_R(x)$ changes at $x_0 \approx 0.8$, inequality $F_{Th}(x) > F_R(x)$ takes place in region $x_0 > x > Mo_{Cr}$, reciprocal ratio $F_{Th}(x) < F_R(x)$ takes place at $x > x_0$. Thus, in the area of high crests and deep troughs, deviations $F_{Cr}(x)$ and $F_{Th}(x)$ from $F_R(x)$ occur in the direction predicted by the second-order nonlinear model [19], i. e., the average distribution of crests and troughs over an ensemble of situations corresponds to this model qualitatively.

Earlier studies of senior statistical moments of sea surface elevations have shown that the second-order nonlinear model makes it possible to describe only average trends of skewness and excess kurtosis, but does not allow describing the whole variety of situations occurring under sea conditions [13]. The skewness and excess kurtosis values vary over a much wider range than the model suggests. In particular, the model estimates of surface elevation distribution skewness A_η and excess kurtosis E_η are always positive [20], while situations in which $A_\eta < 0$ and/or $E_\eta < 0$ are often observed under sea conditions [12]. Fig. 2 shows at what values of A_η and E_η the wave records analysed in this paper were obtained.

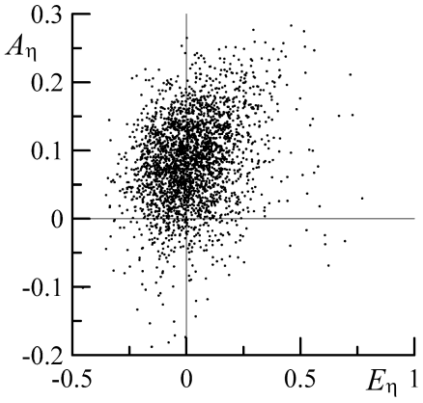

Fig. 2. Changes in the skewness A_η and excess kurtosis E_η of sea surface elevations

Effect of skewness A_η and excess kurtosis E_η

Usually, the distributions of crests and troughs are analysed within a second-order nonlinear model based on the decomposition of the wave profile into a series of small parameter powers [19–22]. In [8], a simplified second-order nonlinear model, which is the sum of linear $\eta_L(x, t)$ and nonlinear $\eta_N(x, t)$ components, is proposed to describe the sea surface statistical characteristics. The model is constructed for waves propagating in deep water in the narrowband spectrum approximation. It is described by the amplitude-modulated Stokes wave equation with average frequency ω and random phase ε

$$\eta(x,t) = \eta_L(x,t) + \eta_N(x,t) = a_r(x,t)\cos\theta + \frac{1}{2}k_p a_r^2(x,t)\cos(2\theta), \qquad (3)$$

where $a_r(x, t)$ is envelope; $\theta = k_p x - \omega t + \varepsilon$; k_p is wave number corresponding to the wave spectrum peak. The local maxima of nonlinear term $\eta_N(x, t)$ coincide with the crest and trough of the linear wave $\eta_L(x, t)$, hence, the ridge and trough within model (3) are equal [9]

$$Cr_N = a_r + \frac{1}{2}k_p a_r^2, \quad Th_N = a_r - \frac{1}{2}k_p a_r^2.$$

In order to assess how applicable this model is to the description of statistical distributions of crests and troughs, it is necessary to analyse how functions $F_{Cr}(x)$ and $F_{Th}(x)$ change in different situations, in particular, when the skewness or excess kurtosis is negative. Fig. 3 shows the results of this analysis.

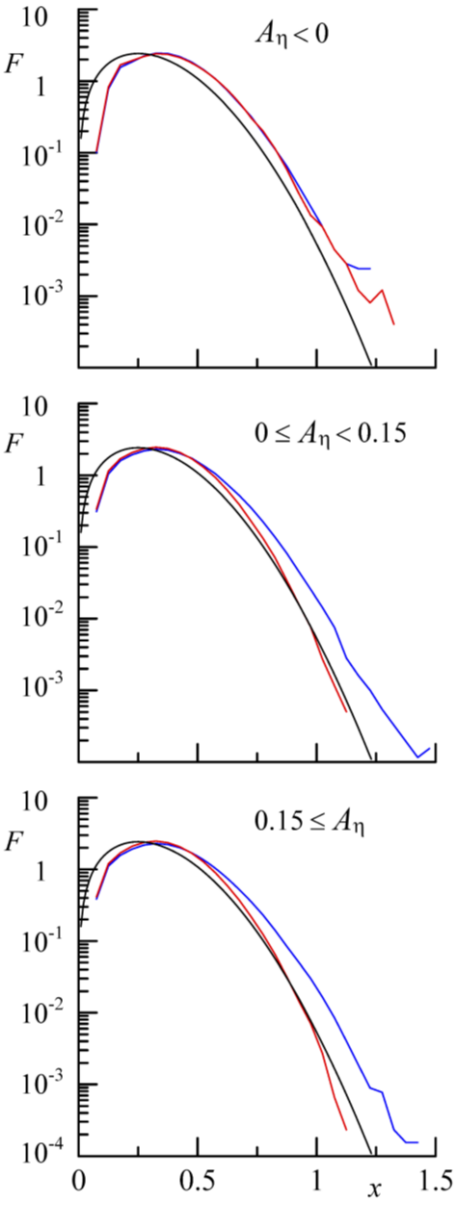

Fig. 3. Probability density functions F calculated for three ranges of skewness A_η. The blue curve is $F_{Cr}(x)$, the red curve is $F_{Th}(x)$, the black curve is $F_R(x)$

It follows from Fig. 3 that when changing the sign of skewness A_η, the type of function $F_{Th}(x)$ changes significantly. If condition $A_\eta < 0$ takes place, equality $F_{Th}(x) \approx F_{Cr}(x)$ is observed. Note that equality $F_{Th}(x) = F_{Cr}(x)$ takes place within the linear model when the *Cr* and *Th* distributions are described by the Rayleigh distribution. In this case, the difference from the linear model at $A_\eta < 0$ is that inequalities $F_{Cr}(x) > F_R(x)$ and $F_{Th}(x) > F_R(x)$ are fulfilled in region $x > 0.45$.

As follows from Fig. 4, changes in the excess kurtosis have a lesser effect on the type of functions $F_{Cr}(x)$ and $F_{Th}(x)$.

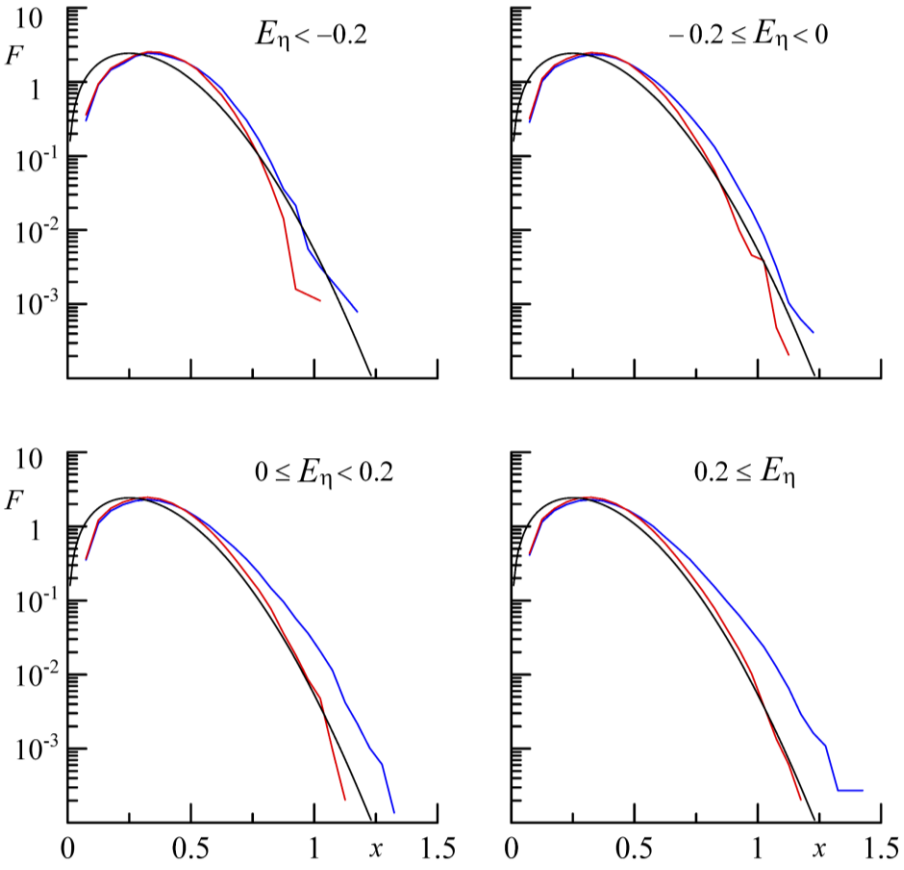

Fig. 4. Probability density functions F calculated for four ranges of excess kurtosis E_η. The blue curve is $F_{Cr}(x)$, the red curve is $F_{Th}(x)$, the black curve is $F_R(x)$

Conclusion

Based on direct wave measurements carried out under sea conditions, the distributions of troughs *Th* and crests *Cr* of sea surface waves were analysed. On average over an ensemble of situations, the greater values of crests calculated from the measurement data have higher probability than the Rayleigh distribution suggests, and the probability of deep troughs is smaller. Such distributions of crests and troughs correspond to a second-order nonlinear model qualitatively.

At the same time, the second-order nonlinear model fails to describe $F_{Th}(x)$ and $F_{Cr}(x)$ when sea surface elevation distribution skewness A_η is negative. It is shown that functions $F_{Th}(x)$ and $F_{Cr}(x)$ are approximately equal at $A_\eta < 0$.

Changes in the excess kurtosis of the distribution of sea surface elevations have a lesser effect on the probability density functions of *Th* and *Cr* than changes in the skewness of the distribution.

References

1. Slunyaev, A.V., Kokorina, A.V., Zaytsev, A.I., Didenkulova, E.G., Moskvitin, A.A., Didenkulov, O.I. and Pelinovsky, E.N., 2023. The Dependence of Wave Height Probability Distributions on Physical Parameters from Measurements near Sakhalin Island. *Fundamental and Applied Hydrophysics*, 16(3), pp. 18–29. https://doi.org/10.59887/2073-6673.2023.16(3)-2 (in Russian).
2. Longuet-Higgins, M.S., 1952. On the Statistical Distribution of the Heights of Sea Waves. *Journal of Marine Research*, 11(3). Available at: https://elischolar.library.yale.edu/journal_of_marine_research/774 [Accessed: 25 July 2024].
3. Naess, A., 1985. On the Distribution of Crest to Trough Wave Heights. *Ocean Engineering*, 12(3), pp. 221–234. https://doi.org/10.1016/0029-8018(85)90014-9
4. Gemmrich, J. and Thomson, J., 2017. Observations of the Shape and Group Dynamics of Rogue Waves. *Geophysical Research Letters*, 44(4), pp. 1823–1830. https://doi.org/10.1002/2016GL072398
5. Dysthe, K., Krogstad, H.E. and Muller, P., 2008. Oceanic Rogue Waves. *Annual Review of Fluid Mechanics*, 40, pp. 287–310. https://doi.org/10.1146/annurev.fluid.40.111406.102203
6. Forristall, G.Z., 2000. Wave Crest Distributions: Observations and Second-Order Theory. *Journal of Physical Oceanography*, 30(8), pp. 1931–1943. https://doi.org/10.1175/1520-0485(2000)030<1931:WCDOAS>2.0.CO;2
7. Nieto-Reyes, A., 2022. On the Non-Gaussianity of Sea Surface Elevations. *Journal of Marine Science and Engineering*, 10(9), 1303. https://doi.org/10.3390/jmse10091303
8. Tayfun, M.A., 1980. Narrow-Band Nonlinear Sea Waves. *Journal of Geophysical Research*, 85(C3), pp. 1548–1552. https://doi.org/10.1029/JC085iC03p01548
9. Toffoli, A., Bitner-Gregersen, E., Onorato, M. and Babanin, A.V., 2008. Wave Crest and Trough Distributions in a Broad-Banded Directional Wave Field. *Ocean Engineering*, 35(17), pp. 1784–1792. https://doi.org/10.1016/j.oceaneng.2008.08.010
10. Longuet-Higgins, M.S, 1963. The Effect of Nonlinearities on Statistical Distributions in the Theory of Sea Waves. *Journal of Fluid Mechanics*, 17(4), pp. 459–480. https://doi.org/10.1017/S0022112063001452
11. Guedes Soares, C., Cherneva, Z. and Antão, E.M., 2004. Steepness and Asymmetry of the Largest Waves in Storm Sea States. *Ocean Engineering*, 31(8–9), pp. 1147–1167. https://doi.org/10.1016/j.oceaneng.2003.10.014

12. Zapevalov, A.S. and Garmashov, A.V., 2022. The Appearance of Negative Values of the Skewness of Sea-Surface Waves. *Izvestiya, Atmospheric and Oceanic Physics*, 58(3), pp. 263–269. https://doi.org/10.1134/S0001433822030136
13. Zapevalov, A.S. and Garmashov, A.V., 2021. Skewness and Kurtosis of the Surface Wave in the Coastal Zone of the Black Sea. *Physical Oceanography*, 28(4), pp. 414–425. doi:10.22449/1573-160X-2021-4-414-425
14. Glejin, J., Sanil Kumar, V., Nair, T.B., Singh, J. and Nherakkol, A., 2014. Freak Waves off Ratnagiri, West Coast of India. *Indian Journal of Geo-Marine Sciences*, 43(7), pp. 1339–1342.
15. Didenkulova, I. and Anderson, C., 2010. Freak Waves of Different Types in the Coastal Zone of the Baltic Sea. *Natural Hazards and Earth System Sciences*, 10(9), pp. 2021–2029. https://doi.org/10.5194/nhess-10-2021-2010
16. Zapevalov, A.S. and Garmashov, A.V., 2024. Ratio between Trough and Crest of Surface Waves in the Coastal Zone of the Black Sea. *Physical Oceanography*, 31(1), pp. 71–78.
17. Zapevalov, A.S., Bol'shakov, A.N. and Smolov, V.E., 2009. Studying the Sea Surface Slopes Using an Array of Wave Gauge Sensors. *Oceanology*, 49(1), pp. 31–38. https://doi.org/10.1134/S0001437009010044
18. Toloknov, Yu.N. and Korovushkin, A.I., 2010. Hydrometeorological Information Collection System. *Monitoring Systems of Environment*, 13, pp. 50–53 (in Russian).
19. Toffoli, A., Onorato, M., Babanin, A.V., Bitner-Gregersen, E., Osborne, A.R. and Monbaliu, J., 2007. Second-Order Theory and Setup in Surface Gravity Waves: A Comparison with Experimental Data. *Journal of Physical Oceanography*, 37(11), pp. 2726–2739. https://doi.org/10.1175/2007JPO3634.1
20. Tayfun, M.A. and Alkhalidi, M.A., 2016. Distribution of Surface Elevations in Nonlinear Seas. In: OTC, 2016. *Proceedings of Offshore Technology Conference. Kuala Lumpur, Malaysia, 22–25 March 2016*. pp. 1274–1287. https://doi.org/10.4043/26436-MS
21. Forristall, G.Z., 2000. Wave Crest Distributions: Observations and Second-Order Theory. *Journal of Physical Oceanography*, 30(8), pp. 1931–1943. https://doi.org/10.1175/1520-0485(2000)030<1931:WCDOAS>2.0.CO;2
22. Prevosto, M. and Forristall, G.Z., 2004. Statistics of Wave Crests from Models vs. Measurements. *Journal of Offshore Mechanics and Arctic Engineering*, 126(1), pp. 43–50. https://doi.org/10.1115/1.1641795

Submitted 15.02.2024; accepted after review 26.03.2024;
revised 17.06.2024; published 25.09.2024

About the author:

Aleksandr S. Zapevalov, Chief Research Associate, Marine Hydrophysical Institute of RAS (2 Kapitanskaya St., Sevastopol, 299011, Russian Federation), Dr.Sci. (Phys.-Math.), **Scopus Author ID: 7004433476, ResearcherID: V-7880-2017, ORCID ID: 0000-0001-9942-2796**, *sevzepter@mail.ru*

The author has read and approved the final manuscript.

Original article

Transformation of the Lake Bogaily Barrier Beach (Western Crimea) under the Influence of Extreme Storms

V. V. Krylenko [1] *, Yu. N. Goryachkin [2], M. V. Krylenko [1], B. V. Divinsky [1]

[1] *Shirshov Institute of Oceanology of RAS, Moscow, Russia*

[2] *Marine Hydrophysical Institute of RAS, Sevastopol, Russia*

* *e-mail: krylenko.slava@gmail.com*

Abstract

Accumulative marine coastal forms of the Azov-Black Sea basin are a key element of coastal abrasion-accumulative geosystems and a valuable commercial resource. Monitoring of the accumulative forms dynamics in the region is a necessary component for successful management of the coastal zone and timely adoption of measures for coastal protection. The purpose of the work is to determine the qualitative and quantitative characteristics of the transformation of the Lake Bogaily Barrier Beach influenced by storms, in particular the extreme storm of November 26–27, 2023. The work uses materials from long-term monitoring observations, satellite images, simulation results of hydrological and lithodynamic processes, literary and archival sources. It was established that in the last 60 years the configuration and topography of the studied accumulative form have changed significantly. Periods were noted when the morphological and dynamic features of the accumulative form did not undergo fundamental changes as well as periods of their significant transformation. In particular, during the storm on November 26–27, 2023, the configuration and topography of the Lake Bogaily Barrier Beach was completely redesigned. The paper reveals characteristic features of the accumulative form dynamics during the storm. The accumulative body was displaced into the water area of the lake. The magnitude of this displacement significantly exceeded that of the retreat of the adjacent bedrock shores. The longitudinal and transverse structure within the barrier beach that existed for several decades has been completely transformed. It is concluded that any extreme storms play a decisive role in the variability of coastal accumulative forms in the region.

Keywords: Black Sea, Crimean Peninsula, coastal geosystem, barrier beach, accumulative form, extreme storm, coastal relief, coastline

Acknowledgments: The work was carried out under state assignments no. FMWE-2024-0027 and FNNN-2024-0016.

For citation: Krylenko, V.V., Goryachkin, Yu.N., Krylenko, M.V. and Divinsky, B.V., 2024. Transformation of Lake Bogaily Barrier Beach (Western Crimea) under the Influence of Extreme Storms. *Ecological Safety of Coastal and Shelf Zones of Sea*, (3), pp. 59–78.

Трансформация пересыпи озера Богайлы (Западный Крым) под воздействием экстремального шторма

В. В. Крыленко [1] *, Ю. Н. Горячкин [2], М. В. Крыленко [1], Б. В. Дивинский [1]

[1] *Институт океанологии им. П.П. Ширшова РАН, Москва, Россия*

[2] *Морской гидрофизический институт РАН, Севастополь, Россия*

* *e-mail: krylenko.slava@gmail.com*

Аннотация

Аккумулятивные морские береговые формы Азово-Черноморского бассейна являются ключевым элементом береговых абразионно-аккумулятивных геосистем и ценным хозяйственным ресурсом. Мониторинг динамики аккумулятивных форм региона является необходимой составляющей успешного управления береговой зоной и своевременного принятия мер по защите берегов. Цель работы – определение качественных и количественных характеристик трансформации пересыпи оз. Богайлы под действием штормов, в частности экстремального шторма 26–27 ноября 2023 г. Использованы материалы многолетних мониторинговых наблюдений, спутниковые снимки, результаты математического моделирования гидрологических процессов, литературные и архивные источники. Установлено, что в последние 60 лет наблюдались значительные изменения конфигурации и рельефа изучаемой аккумулятивной формы. Отмечены периоды, когда морфологические и динамические особенности аккумулятивной формы не претерпевали принципиальных изменений, и периоды ее значительной трансформации. В частности, во время шторма 26–27 ноября 2023 г. конфигурация и рельеф пересыпи оз. Богайлы были значительно изменены. Выявлены характерные черты динамики аккумулятивной формы в ходе шторма. Произошло смещение аккумулятивного тела в акваторию озера, величина этого смещения существенно превысила величину отступания прилегающих коренных берегов. Преобразована существовавшая несколько десятилетий продольная и поперечная структура в пределах пересыпи. Сделан вывод, что экстремальные по тем или иным характеристикам штормы играют определяющую роль в изменчивости береговых аккумулятивных форм региона.

Ключевые слова: Черное море, полуостров Крым, береговая геосистема, пересыпь, аккумулятивные формы, экстремальный шторм, береговой рельеф, береговая линия

Благодарности: работа выполнена в рамках государственных заданий FMWE-2024-0027 и FNNN-2024-0016.

Для цитирования: Трансформация пересыпи озера Богайлы (Западный Крым) под воздействием экстремальных штормов / В. В. Крыленко [и др.] // Экологическая безопасность прибрежной и шельфовой зон моря. 2024. № 3. С. 59–78. EDN HQBWYY.

Introduction

Shirshov Institute of Oceanology of RAS and Marine Hydrophysical Institute of RAS have been engaged in research into the dynamics of the Azov–Black Sea coasts for several decades. Particular attention is paid to the investigation of the formation and transformation of coastal accumulative forms, encompassing spits and barrier beaches [1–3].

The combination of anthropogenic and natural factors, particularly storm impacts, has resulted in the transformation of coastal accumulative forms, in some instances leading to their degradation [1]. It is indicated in [4] that transformations of sandy beaches, defined as seasonal, can occur as a result of a single storm event. An improved version of the CROSS P storm deformation model was proposed in [5], incorporating the impact of overflow over the foredune during storm surges. The modelling results demonstrated that during periods of overflow across the foredune, a portion of the transported sediment was transferred to the rear slope. This resulted in a gradual inland migration of the dune belt, accompanied by a decrease in height. The potential for material transport to the rear of the barrier beach and the possibility of its displacement towards the lagoon as a result of an extreme storm are also discussed in [6]. In [7], it was demonstrated that the XBeach model is capable of accurately simulating morphological changes, including those induced by storm activity, such as erosion of dunes and beaches. In [8], the XBeach mathematical model was employed to examine the effects of storm waves on the Lake Bogaily area. The findings revealed that these waves induce significant beach erosion and active reformation of the upper part of the underwater coastal slope. The objective of this study was to obtain quantitative estimates of the water edge retreat rate and bottom topography deformation values for different wave exposure times.

Extreme storm surge tends to have the strongest effect on the redistribution of material in the coastal zone. There are known cases [9] when the volumes of flows transverse to the shoreline reached 200 m^3/m, leading to significant changes in the relief of the accumulative form. However, recent studies [10, 11] have shown that extreme storms can redistribute sediment and, in some cases, stabilise shorelines. The results presented in these studies demonstrate the complex and not always predictable nature of storm effects on accumulative forms.

It is uncommon for extreme storms to occur, and the scientific observations of the transformation of marine coastal accumulative forms in the Azov–Black Sea region as a result of such events are limited in number and nature. No such purposeful observations have been conducted along the coastline of the Crimean Peninsula. Furthermore, there has been an observed increase in the frequency and intensity of storm waves in the Azov–Black Sea basin [12, 13].

In November 2023, the Black Sea was under the influence of a series of deep Mediterranean cyclones. Winds of up to 40 m/s were observed over most of the water area. A storm wave was formed on 26–27 November 2023, exhibiting numerous parameters that surpassed those observed in the region earlier that same year. This allows us to categorise the event as an extreme natural phenomenon [14].

It is relevant to consider the impact of an extreme storm on the Bogaily Lake Barrier Beach in the context of the development of this accumulative form over the past 60 years. The objective of this study is to determine the qualitative and quantitative characteristics of the transformation of the Lake Bogaily Barrier Beach in response to the impact of an extreme storm on 26–27 November 2023.

Materials and methods of research

For the study region (Fig. 1), the first available remote sensing materials are space images from the 1960s–1980s [1)]. Satellite images of different years from open sources (Google Earth, Yandex, Bing, etc.) were used to analyse the coastal dynamics. For operational assessment of changes caused by the storm on 26–27 November 2023, data from the Sentinel-2 spacecraft of the European Space Agency were used [2), 3)]. To achieve accurate spatial referencing, geometric correction of satellite data was performed. The 9+ GCP (Ground Control Points) polynomial method was used for geometric correction of the images. To improve accuracy, the number of points was significantly increased (more than 20 GCPs were used most often), and they were distributed evenly over the area of the corrected image [15]. Subsequently, for each image, the accuracy of the acquired vector data was evaluated using reference linear objects (street networks and airfield runways) situated in proximity to the coastal area under study. The line of the sea edge and, if possible, the lagoon and cliff edge were digitised based on the multi-temporal images presented in these resources. Taking into account the steep sea slope of the beach, the maximum possible sea level rise at the storm peak of about 0.4 m, as well as the low intensity of surge events, the change in the planned position of the shoreline as a result of sea level fluctuations is significantly lower than the accuracy of measurements. As a result of this work, information on the dynamics of the shoreline and other morphological elements of the studied natural objects in different periods was obtained.

In order to undertake an in-depth examination of the relief and associated dynamics, the generation of digital elevation models was essential. In fulfilling this task, materials from aerial surveys carried out using unmanned aerial vehicles (UAVs) were used. A combination of planned and panoramic surveys was conducted in areas with cliffs [16–18]. High-accuracy digital relief models (DRMs) and orthophotomaps were constructed utilising photogrammetric image processing technology. The Agisoft Metashape software was employed to generate high-quality 3D models of objects and orthophoto maps based on digital photographs.

[1)] U.S. Department of the Interior U.S. Geological Survey (USGS). Available at: http://earthexplorer.usgs.gov [Accessed: 30 August 2024]

[2)] MultiSpectral Instrument (MSI). Available at: https://sentinel.esa.int/web/sentinel/missions/sentinel-2/instrument-payload [Accessed: 30 August 2024]

[3)] The operational Copernicus optical high resolution land mission. Available at: http://esamultimedia.esa.int/ docs/S2-Data_Sheet.pdf [Accessed: 30 August 2024]

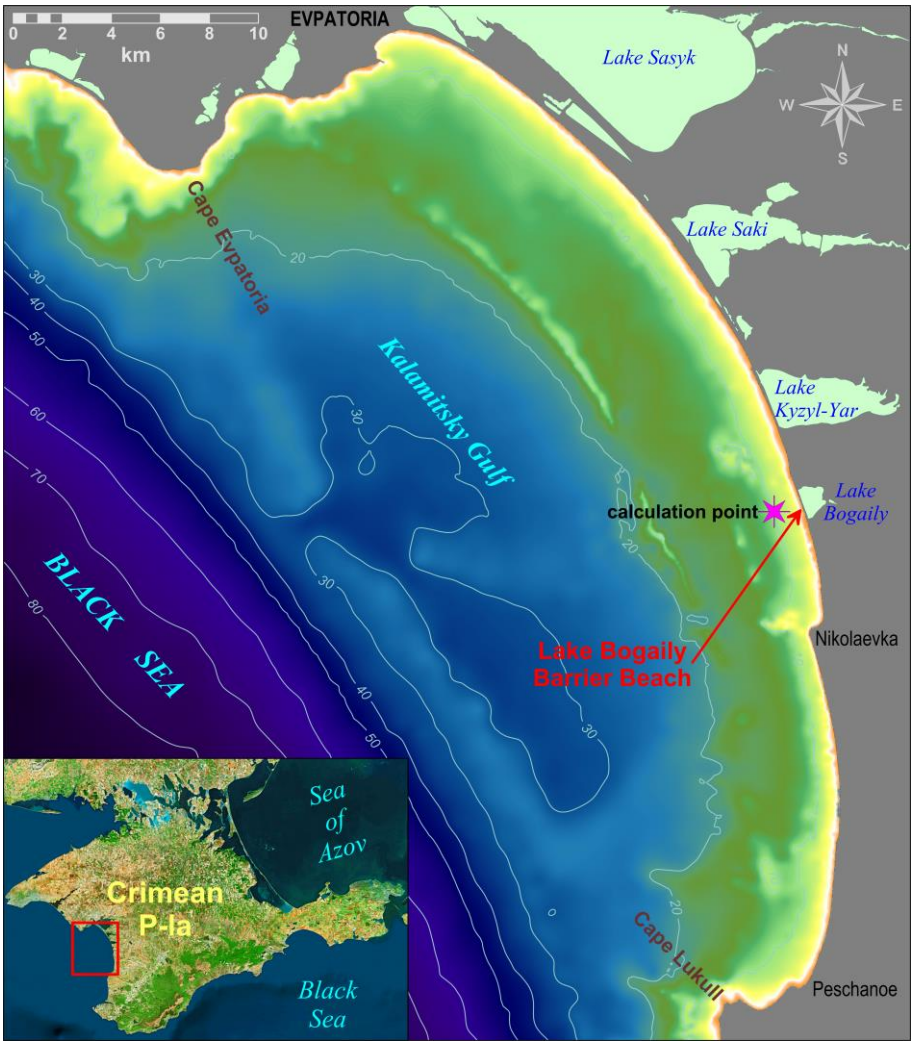

Fig. 1. Map-chart of the Kalamitsky Gulf in the Black Sea (data on underwater topography are given using SonarChart™ materials (https://webapp.navionics.com)). The calculation point is the point for which the main wave parameters were calculated

TerraScan Bentley MicroStation module was used to classify photogrammetric point clouds [4]. The digital images obtained from UAVs were processed to create orthophotos with a resolution of 0.05 m and digital relief models (DRMs) with a grid step of 0.15 × 0.15 m. These materials were employed in the analysis of the topography of the barrier beach.

In addition to remote sensing materials, data of granulometric analysis of beach and bottom sediment samples, morphometric characteristics, geobotanical descriptions obtained during expedition works, as well as archival cartographic materials were used.

The climatic characteristics of wind waves in the Black Sea were calculated using the modern spectral wave model MIKE 21 SW [19] [5]. A full description of the model, as well as the issues of model verification and tuning are described in [19]. Based on the results of calculations, an array of spatial fields of surface wave parameters was formed with a discreteness of 1 h covering the entire sea area for the period from January 1979 to December 2023.

General characterisation of the Lake Bogaily Barrier Beach

Lake Bogaily is situated in the central region of the Kalamitsky Gulf (Fig. 1), representing an estuary formed at the convergence of the Sukhaya and Bogaily gullies. The lake has a surface area of approximately 0.95 km², with a maximum depth of 20–40 cm near the barrier beach for the majority of the year. The lake barrier beach is 1.4 km in length and 40–70 m in width. The accumulation formation is sustained by sedimentary material derived from the abrasion of the adjacent bank structures on either side. The area is characterised by cliffs reaching heights of up to 8–10 m, comprising clay deposits interlayered with sandstones, gravelites and conglomerates of ancient alluvial origin. The structure of cliffs is described in great detail in [2]. It can be observed that the migration of material typically occurs within a narrow nearshore zone. However, the formation of submarine shafts was not noted. A mixture of fine and medium sand with fine gravel is the predominant composition on the marine underwater slope of the barrier beach, at a depth of 1–1.5 m. Deeper than 2.5 m, siltstones become the predominant composition. In the depth range of 2 to 4 m, no particles larger than 0.25 mm were observed in the samples. It can be concluded that the zone of migration of beach-forming sediment in the area of the Lake Bogaily Barrier Beach is limited to isobaths of 2–2.5 m. Furthermore, it has been observed that fine-grained silty fractions accumulate at greater depths [20].

The barrier beach constitutes part of the Kalamite lithodynamic system of order I [21], which extends between Cape Lukull and Cape Yevpatoria (Fig. 1). The resulting longshore sediment flow is directed northwards as far as Yevpatoria Bay [22]. However, in some areas the direction and intensity of longshore sediment flow is characterised by considerable seasonal and interannual variability [23].

---

[4] Sentinel Online technical website. Available at: https://sentinel.esa.int/web/sentinel/technical-guides/sentinel-2-msi/level-1c/product-formatting [Accessed: 30 August 2024].

[5] DHI Water&Environment. MIKE21/3 Coupled Model FM, 2007. 190 p.

The cliff, and with it the shoreline at Lake Bogaily, is actively retreating. Satellite data show that between 1984 and 2016, the cliff retreated an average of 42 m along the abrasion section north of the barrier beach, and the barrier beach retreated 30–35 m inland. Thus, the rate of retreat of the seashore of the barrier beach is close to the rate of retreat of the adjacent cliffs. The rate of the process in the multiannual regime varies significantly depending on the frequency and strength of storms.

The multiannual regime is dominated by the west-southwest swell [24]. An analysis of the distribution of heights and periods of significant waves over 30 years [25] has shown that the highest wave heights in the adjacent Black Sea area can reach 5.5–6 m with a period of 6.5–7 s during the autumn-winter period. Between April and September, the average monthly height of significant waves does not exceed 4 m and corresponds to the minimum of wind activity. In the area of the Barrier Beach of Lake Bogaly, there are two dominant directions of approach of significant waves (from the northeast and southwest), which determine the reversible nature of the sediment movement along the shore. Mathematical modelling [24] suggests the existence of two sediment flows towards each other with the formation of a convergence zone at the barrier beach in summer [24]. It is likely that the two-way movement of sediment predetermines high shoreline variability in some areas, but increases the stability of the accumulation body as a whole due to the input of sediment from adjacent abrasion areas under all wave conditions.

Prior to the storm of 26–27 November 2023, the cross-sectional profile of the Bogaily Lake Barrier Beach was based on a full profile sand and gravel beach [2]. There were three longitudinal zones within the barrier beach: the beach zone, the ridge zone (dune and vegetation zone) and the estuary zone. The width and other morphometric parameters of these zones changed from time to time, but the general structure of the relief was preserved for decades. Thus, the width of the beach (up to the vegetation strip and the dunes) was 30–40 m. The beach near the shoreline is composed predominantly of gravel, while up the slope it is composed of medium-grained sand. Changes in the topography within the beach during the normal regime were characterised by alternating areas of surface rise and fall or widening and narrowing of the beach due to shoreline migration. Even small storms caused a change in the cross-sectional profile of the beach, most commonly in the nearshore zone. Formation and subsequent destruction of storm rolls and terraces was most commonly observed. In some parts of the barrier beach, formation of washout scarps up to 1 m high was recorded during strong storms accompanied by an increase in longshore currents.

The uplifted part of the barrier beach was originally the crest of a full profile beach (1.8–1.9 m above sea level). As vegetation developed along it, accumulative aeolian forms were formed. In recent decades, until the storm of 26–27 November 2023, a dune ridge up to 0.5 m high (2–2.5 m above sea level), covered with herbaceous vegetation characteristic of coastal aeolian forms, existed along the crest of the barrier beach. Some parts of the dune ridge were separated by depressions – scour holes – where waves overtopped during strong storms. During these periods

there was an increase in the width and depth of the scour hole, partial destruction of the aeolian moulds along its sides, and removal of material to the lagoonal shore of the barrier beach and into the lake. In addition to storm damage, the top of the barrier beach has been subject to anthropogenic impacts from vehicle traffic, with significant damage to the relief of the aeolian forms and vegetation.

During the most severe storms, the transfer of gravel and sand material from the seashore to the lakeshore by wave splash has been recorded within the scour holes. This process can be considered as an element of the sediment budget for the shore adjacent to the Lake Bogaily Barrier Beach. In the vicinity of the scour holes on the lake shore of the barrier beach, export cones were formed which determined a peculiar configuration of the lake shore in the form of festoons. No active redistribution of the incoming material along the lake shore was observed, which can be explained by insufficient wave intensity. The near shore depression, except for the cones, was covered with halophytic herbaceous vegetation, which in dry years forms the part of the dried lake bed adjacent to the barrier beach. A berm of vegetation and debris was observed along the lake shore. Until the 1970s, Lake Bogaily was salty and periodically dried up. Subsequently, the discharge water from the poultry farm commenced flowing into the lake, resulting in the lake becoming full year-round. In the southern part, there was a pipeline for the discharge of freshwater and the conveyance of wastewater, which has since been destroyed. Following a reduction in discharge during dry years, the lake dries up completely again in summer.

Dynamics of the shoreline and relief of the Lake Bogaily Barrier Beach

The available archival cartographic materials and satellite images allow us to distinguish several characteristic periods in the development of the accumulative body of the Lake Bogaily Barrier Beach.

In some maps of the nineteenth century, the lake is depicted as a sea bay, with Kichik-Bel Island situated along the line of the modern barrier beach. During this period, it would appear that there was no continuous barrier beach in existence; the lake was connected to the sea by a strait (or straits) of variable width.

The space images of 19 July 1963 and 19 September 1968 reveal the presence of a scour between the lake and the sea in the southern part of the barrier beach, although its precise location varies. It is likely that the cause of this phenomenon is anthropogenic.

The analysis of space images allows us to state with a high degree of confidence that the structure of the over-water body of the barrier beach was completely different to what it became later, at least between the years 1963 and 1968. The images of 19 July 1963 and 19 September 1968 (Fig. 2) demonstrate that the shorelines on the sea and lake sides are straight and almost parallel, and that the barrier beach, with an average width of 80 m, exhibits minimal transverse hydrogenic forms, with the exception of a large scour in the southern part. The longitudinal zones are evident in the structure of the coastal embankments and vegetation along the barrier beach.

An alternative perspective is offered by the image of 21 June 1975. The width of the barrier beach ranges from 60 m in the north to 40 m in the south, which is associated with the elevated water level in the lake. The seaward shoreline remained straight, but the lake shoreline became curved, especially in the southern part.

The longitudinal structure shows a curved shoreline berm crest with no evidence of vegetation, indicating that storm surge has impacted the entire surface of the barrier beach. The most probable cause of these changes is the extreme storms recorded during 1969 [26–28].

The image dated 31 July 1984 (Fig. 3) illustrates the restoration of the barrier beach structure in the form of a beach strip, a dune ridge with developed lagoonal slope vegetation, and a drying strip with emergent vegetation along the lakeshore. The width of the barrier beach varies from 40 m in the southern part to 60 m in the northern part. The seaward edge line is almost straight, with a few gentle bends in the southern part of the lake edge line. Trails traversing the dune and vegetative bands are discernible, yet there is no indication of substantial transverse scouring or evidence of drift cone formation along the lakeshore.

Unfortunately, detailed images of the period 1984–2005 could not be located. As a result, it is challenging to determine the extent to which the extreme storm of 15 November 1992 impacted the Barrier Beach of Lake Bogaily.

The configuration of the barrier beach (Fig. 3) in the 2005 image is very similar to that observed in 1975, showing a levelled sea-front line and a curved lake-front line. The width of the barrier beach at two-thirds of the northern extent is approximately 50 m, subsequently increasing to 60 m. Thereafter, at approximately 100 m from the southern boundary, there is a notable narrowing to 30 m. In the longitudinal structure, the strip of beach, dunes and adjacent vegetation is clearly discernible. The width of these zones along the barrier beach varies in a gradual manner without exhibiting abrupt changes. The 08 May 2005 image also displays transverse scour holes that separate the vegetation strip. The largest of these holes on the lagoonal shore correspond to export cones. The general configuration of the sea and estuarine banks in the image dated 31 October 2009 (Fig. 3) has remained largely unchanged in comparison with the image dated 08 May 2005. However, the export cones are now much more visible and are present at the majority of scour holes. It can thus be concluded that the extreme storm of November 2007 did not have a significant impact on the morphological structure of the Lake Bogaily Barrier Beach. Rather, its impact was limited to the expansion of scour holes and export cones. As illustrated in Fig. 4, the aforementioned structure was largely preserved until the November 2023 storm.

One should note significant variations in the mean annual rate of sea level retreat. Fig. 5 shows that in 1963–1984 the shore retreated insignificantly – from 5 m in the central part of the barrier beach to 15 m in the areas adjacent to the bedrock shore. The rate of shore retreat was considerably more pronounced between 1984 and 2005 (Fig. 5). The retreat is 25–30 m along the barrier beach and to the north of it, and 20 m along the cliff to the south of the barrier beach. It is important to note the impact of the cross structure (reinforced concrete boathouse) at the junction of the northern part of the barrier beach with the cliff. The filling of the inlet corner to the north and the downward scour to the south of the structure are clearly visible. The impact of this structure can be observed in subsequent periods, even in instances where it has undergone partial destruction. It is noteworthy that there were instances when the position of the inlet corner and the downstream scour zone were reversed.

In view of the distribution and composition of sediment on the submarine slope along the Lake Bogaily Barrier Beach and adjacent abrasion-prone bedrock

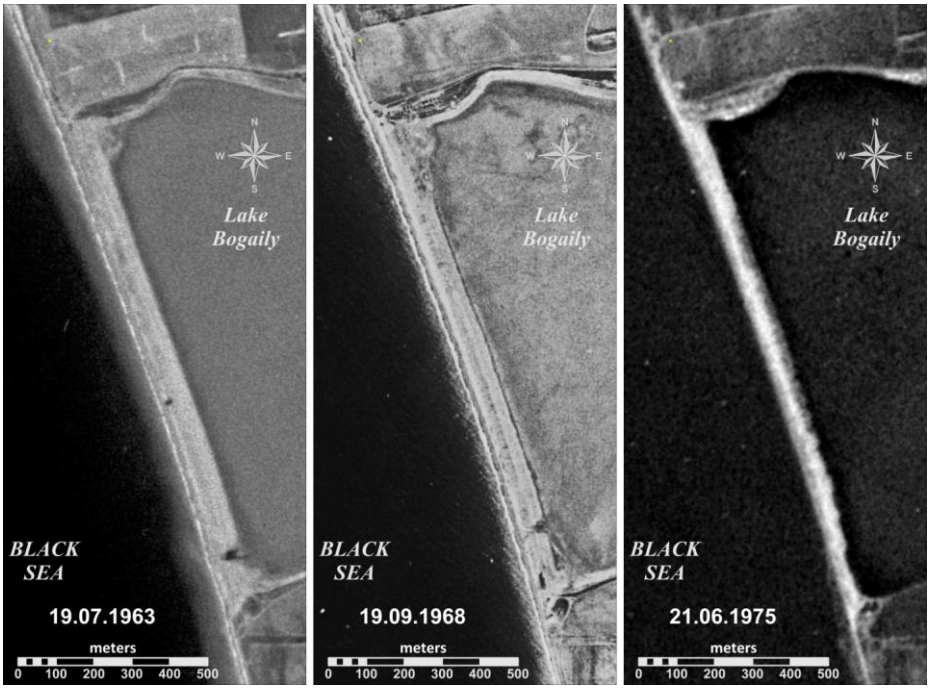

Fig. 2. Development of the Lake Bogaily Barrier Beach in 1963–1975

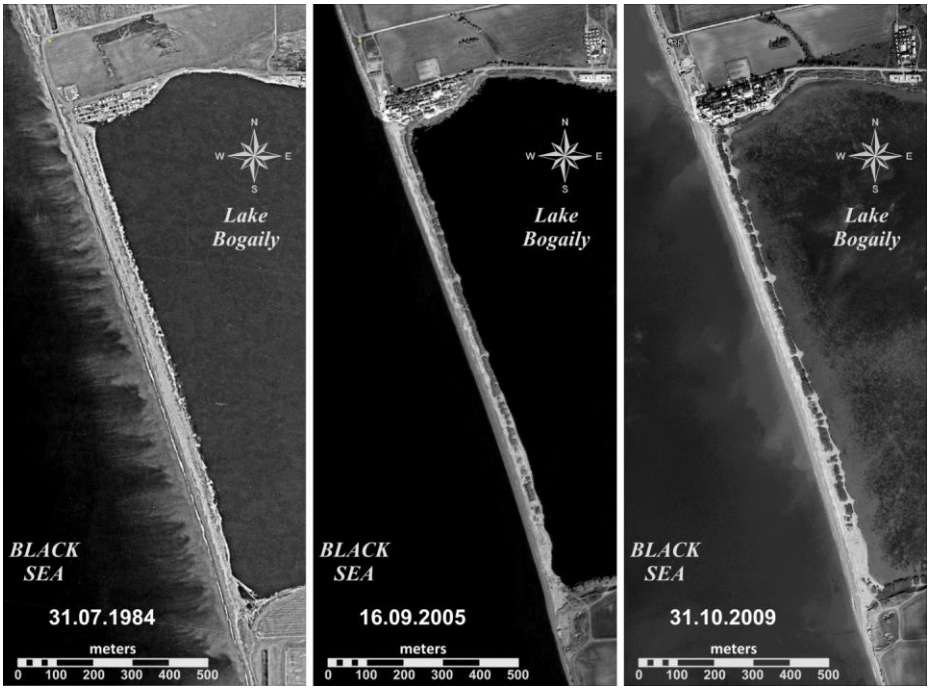

Fig. 3. Development of the Lake Bogaily Barrier Beach in 1984–2009

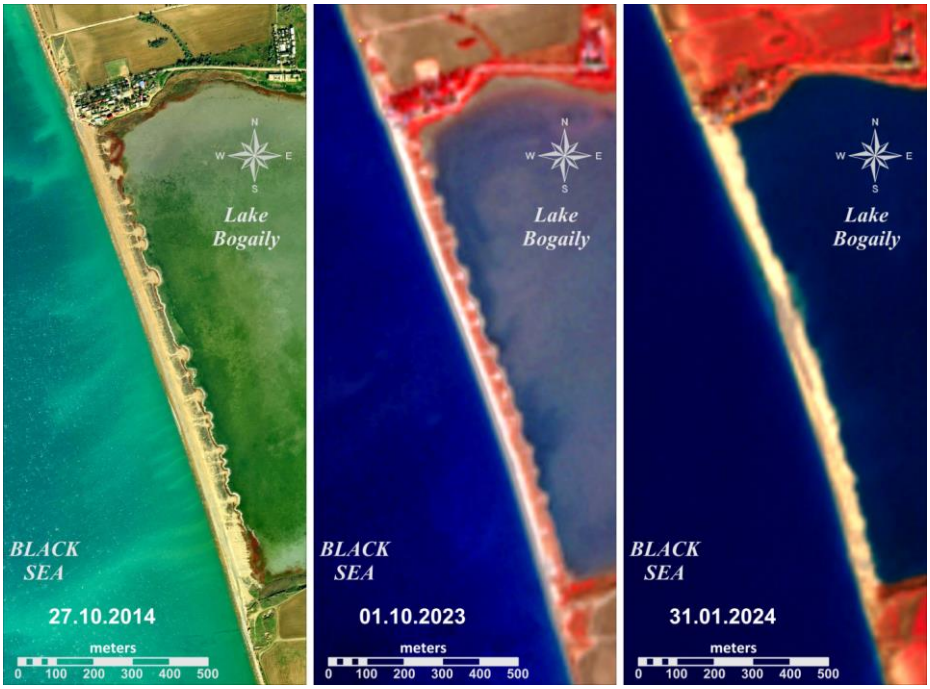

Fig. 4. Development of the Lake Bogaily Barrier Beach in 2014–2024

shores [20], as well as analyses of remote sensing data, it can be concluded that the actual capacity of the longshore sediment flux is relatively small. It is worth noting here that from the 1960s onwards the sediment flow in the system has been decreasing, due to river regulation, the blocking of cliffs by bank protection structures, the construction of transverse structures and other factors. The southern boundary of the lithodynamic system, which encompasses the overflow of Lake Bogaily, can currently be identified as an unnamed cape situated in the southern region of the Nikolaevka settlement. This is characterised by a system of two groins. In contrast, the northern boundary is represented by the transverse structure of the water intake at Lake Kyzyl-Yar. The absence of substantial sedimentary deposits within the lithodynamic system, mobilised by storms of varying directions and with a notable longshore component, contributes to the absence of significant fluctuations in the volume of material arriving at the barrier beach. This determines the relative flatness of the seaward edge of the barrier beach and uniformity of the transverse profile along its entire length. The absence of bends in the shoreline and underwater slope favours uniform distribution of wave energy and increases the overall stability of the overwater part of the accumulative form. This is probably the reason why the position and configuration of scour holes and associated drift cones on the lagoonal shore have been stable for several decades. In recent decades, significant wave damage to vegetation along the sea slope of the dunes and on the sides of stationary scour holes has rarely been observed.

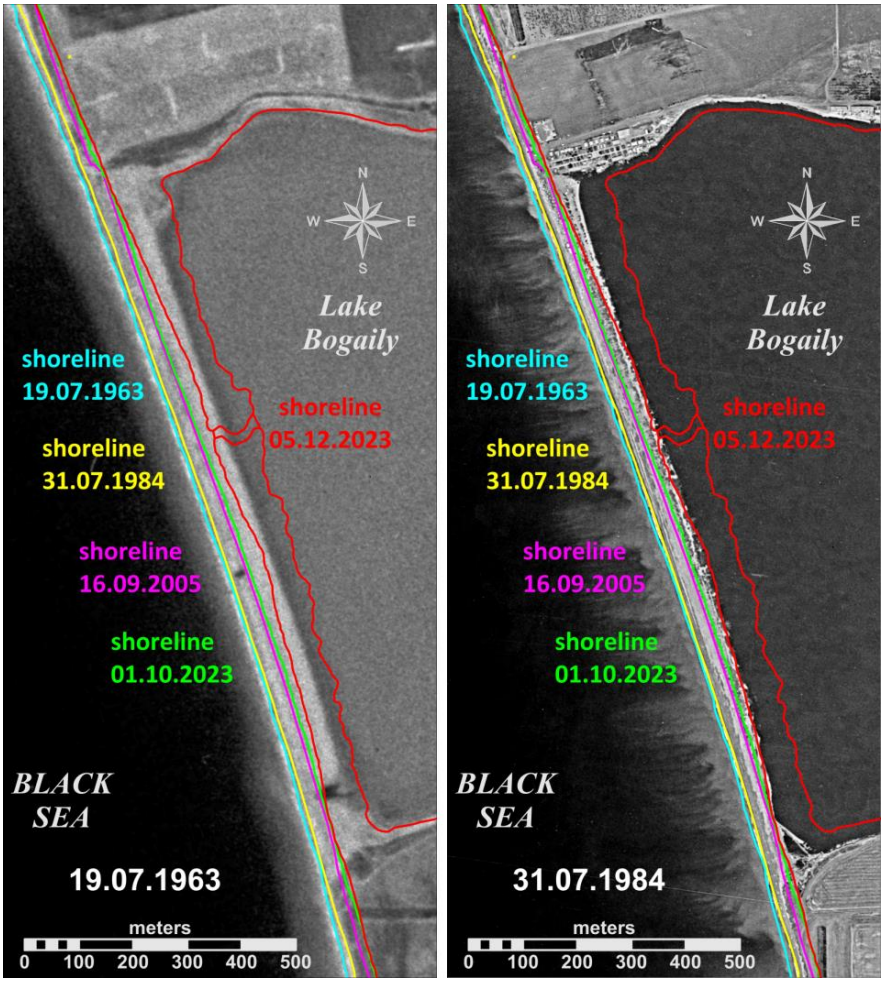

Fig. 5. Development of the Lake Bogaily Barrier Beach in 1963–2023

Characteristics of the 26–27 November 2023 storm

To analyse the nature of storm impact on the shore, the main wave parameters (significant wave heights, spectrum peak periods, average propagation directions) were calculated. The calculation point was located 4500 m from the shore at an isobath of 10 m (see Fig. 1). In addition, wave power was calculated, which is a representative characteristic because it depends on two integral wave parameters, namely wave height and wave energy period. In essence, the power period is the period of a monochromatic wave with a power equivalent to the power of a given irregular swell. The power of a wave is expressed in kilowatts per metre of wave front.

Fig. 6 shows the maximum wave heights and power in individual storms over the past 45 years in the area of the Lake Bogaily Barrier Beach. The selection was limited to storms with significant wave heights exceeding 2.5 m. It is acknowledged that the selection of an appropriate threshold level is always a matter for debate. In this instance, the objective is to identify the most intense storms that occurred in a specific year from a multitude of storms. As can be seen from Fig. 6, the 2023 storm is the most powerful in terms of energy over the past 45 years, with wave heights slightly inferior to those recorded, for example, in 1981, 1988, 1999 and 2003.

Fig. 7 shows a series of significant wave heights, periods, strengths and directions at the Lake Bogaily Barrier Beach for November 2023. It shows that the Lake Bogaily Barrier Beach was under the influence of developed wave action for almost the entire month. Three storms with power greater than 30 kW/m were observed, including an extreme storm on 26–27 November. As shown in Fig. 6, *b*, this storm is the strongest in terms of power (109 kW/m) for the Lake Bogaily Barrier Beach in the last 45 years. Previously, the strongest storm was the storm of 2000 (82 kW/m). At the time of the largest storm development on 26 November 2023 at the isobath of 10 m near the Barrier Beach of Lake Bogaily, the wave parameters were as follows: significant wave height – 3.4 m, period – 12.8 s, length – 160 m. The surge height during the storm was 0.21–0.54 m.

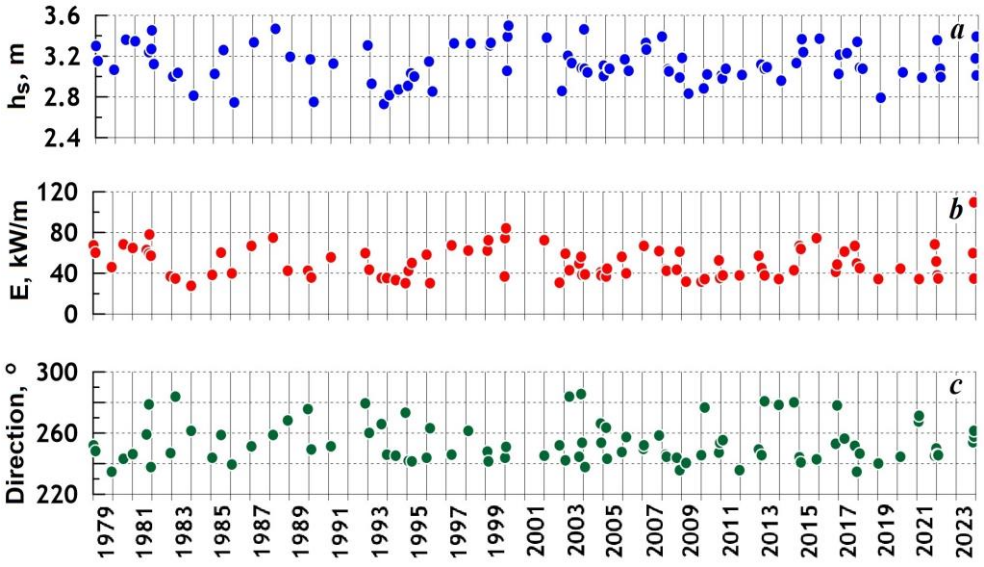

Fig. 6. Parameters of the largest storms near the Lake Bogaily Barrier Beach: *a* – maximum significant wave heights; *b* – maximum wave power; *c* – general directions of storms

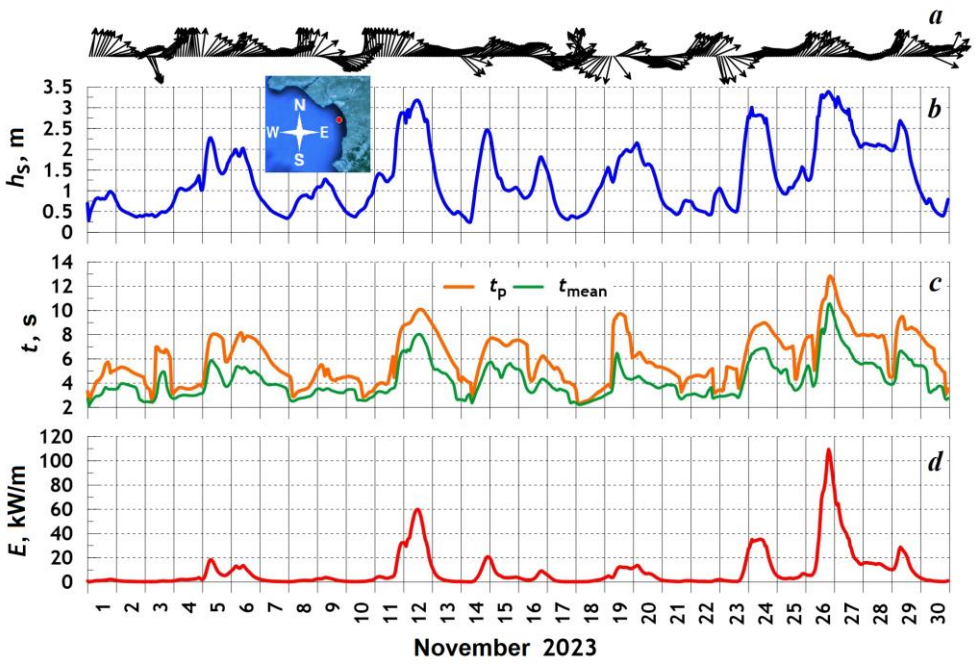

Fig. 7. The main parameters of wind waves near the Lake Bogaily Barrier Beach: *a* – propagation directions; *b* – significant wave heights; *c* – peak and mean wave periods; *d* – wave power

Realignment of the barrier beach topography during the storm of 26–27 November 2023

It is clear that the storm of 26–27 November 2023 is an extreme storm in terms of the scale and nature of the changes to the configuration and relief of the Lake Bogaily Barrier Beach on a scale of several decades. Direct wave action with overtopping of the beach crest was observed along the entire length of the barrier beach. The transfer of material from the seaward to the lagoon side of the barrier beach shifted the seaward edge line to the east (Fig. 8). The seaward retreat of the seaward side of the barrier beach near the abutment to the cliffs of the rocky shore was 5–10 m, which is close to the amount of storm induced cliff retreat. In the central part of the barrier beach, the retreat increases to 20 m, and in the area of the formed rill and slightly to the north, the retreat exceeds 30 m, even with subsequent coastal levelling. The magnitude of the retreat can be estimated by comparing it with a 60-year (1963–2023) retreat of 40–45 m (Figs. 5, 8).

It should be noted that there is no evidence of longshore sediment movement during the storm, with all changes being caused by cross-shore water movement. This is probably a consequence of the long length of the waves approaching

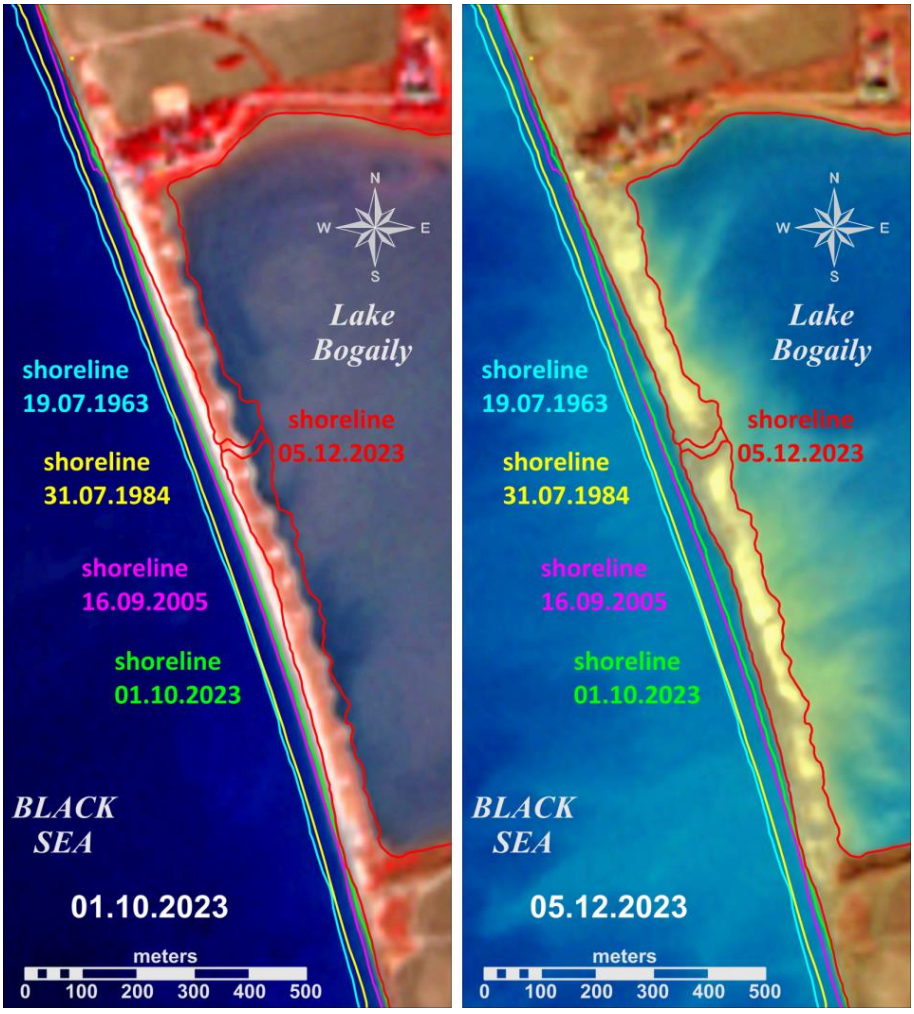

Fig. 8. Development of the Lake Bogaily Barrier Beach since 1963 and during the storm in November 2023. *Left* – the barrier beach before the storm, *right* – that after the storm

from the open sea, the front of which turned parallel to the coastline on contact with the seabed at a considerable distance from the shore. It is possible that the same circumstance caused a significant rise in sea level during the storm.

The storm surge covered even the highest parts of the barrier beach and destroyed pre-existing landforms. The storm surge completely destroyed the characteristic longitudinal structure that had existed for several decades, including bands of dunes and vegetation (Fig. 9). In essence, the former orderly longitudinal and transversal structure that had been formed and maintained over decades was transformed into a full profile beach with steep marine and gentle lagoonal slopes.

Fig. 9. View of the Lake Bogaily Barrier Beach from the south side (2021)

A similar process was observed both before and during the storm of 26–27 November 2023 on a number of accumulation forms in the Black Sea, in particular on the Solyonoye Lake Barrier Beach and in the southern part of the Anapa Barrier Beach. As noted above, a similar large-scale transformation of the relief of the Lake Bogaily Barrier Beach may have occurred in the late 1960s and early 1970s.

As a result of the extreme storm, the system of transverse scour holes with export cones in the inner (lake) part of the barrier beach has completely disappeared. During normal heavy storms, these scour holes acted as a safety valve, allowing some of the wave surge to pass into the lake and helping to attenuate the wave energy. It is likely that the presence of such stationary scour holes on the sandy barrier beach is a sign of its maturity and the prolonged absence of extreme storm events.

The formation of a lake outflow channel occurred in the central part of the barrier beach where the lake outflow was concentrated in one of the pre-existing stationary scour holes. In the southern part of the barrier beach, where the cross-sectional height and width were minimal prior to the storm and where rills had been observed in the past, water flow was impeded by concrete structures. In the central part of the barrier beach, several depressions formed after the storm on what had previously been an almost straight line at the seaward edge. By the end of January 2024, the depression formed during the storm was completely washed out, but the depression in the body of the barrier beach remained. At the same time, there was a tendency for the seaward line to flatten out. Given the continued high water level in the lake and the complete destruction of the vegetation

along the lagoon shore of the barrier beach, partial levelling of the lake shore line by wave action is expected, although the general configuration is likely to be maintained. As can be seen from the dynamics of the barrier beach after the storm, self-recovery processes are evident.

Conclusion

The analysis of the long-term dynamics of the Lake Bogaily Barrier Beach confirms the assumption of the leading role of strong storms in the development of marine coastal accumulation forms. In particular, during and as a result of the extreme storm of 26–27 November 2023, the following was observed:

1. The configuration and relief of the Barrier Beach at Lake Bogaily was completely changed, the accumulation was displaced into the lake water area, and the magnitude of this displacement significantly exceeded the retreat of the adjacent bedrock shores.

2. The seaward edge line, which had previously been almost straight, formed several concavities in the central part of the barrier beach after the storm.

3. The retreat of the barrier beach near the abutment to the cliffs of the bedrock shore was 5–10 m, in the central part of the barrier – up to 20 m, in the area of the formed rill and slightly to the north – more than 30 m, even taking into account the subsequent levelling of the shore.

4. The previously existing system of transverse scour holes with export cones in the inner (lake) part of the barrier beach completely disappeared.

5. The impact of the storm surge completely destroyed the characteristic longitudinal structure that had existed for several decades, including strips of dunes and vegetation.

6. By the end of January 2024, the rill formed during the storm was completely washed out and a levelling of the seaward edge line was observed.

As a result, the storm has completely altered the decades-old relief and vegetation structure within the barrier beach. The Bogaily Lake Barrier Beach has undergone much greater change than in the previous 40-year period. It is clear that extreme storms play a critical role in the development of both the Bogaily Lake Barrier Beach and similar coastal accumulation forms in the region.

REFERENCES

1. Kosyan, R.D., Krylenko, V.V. and Krylenko, M.V., 2021. *Geosystem of the Anapa Bay-Bar*. Moscow: Nauchny Mir, 262 p. (in Russian).
2. Krylenko, V.V., Goryachkin, Yu.N., Kosyan, R.D., Krylenko, M.V. and Kharitonova, L.V., 2021. Similarities and Differences of Small Bay-Bars of the North-Eastern Part of the Black Sea. *Ecological Safety of Coastal and Shelf Zones of Sea*, (1), pp. 63–83. https://doi.org/10.22449/2413-5577-2021-1-63-83 (in Russian).
3. Goryachkin, Yu.N., Kosyan, R.D. and Krylenko, V.V., 2018. A Comprehensive Assessment of the Crimea West Coast. *Ecological Safety of Coastal and Shelf Zones of Sea*, (3), pp. 41–55. https://doi.org/10.22449/2413-5577-2018-3-41-55 (in Russian).

4. Korzinin, D.V., 2021. Special Aspects of Deformation of Coastal Profile During a Full Storm Cycle. *Journal of Oceanological Research*, 49(2), pp. 45–56. https://doi.org/10.29006/1564-2291.JOR-2021.49(2).3 (in Russian).
5. Leont'yev, I.O., Ryabchuk, D.V. and Sergeev, A.Y., 2015. Modeling of Storm-Induced Deformations of a Sandy Coast (Based on the Example of the Eastern Gulf of Finland). *Oceanology*, 55(1), pp. 131–141. https://doi.org/10.1134/S000143701406006X
6. Leont'yev, I.O. and Akivis, T.M., 2020. Modeling of Coastal Dynamics of the Anapa Bay-Bar. *Oceanology*, 60(2), pp. 279–285. https://doi.org/10.1134/S000143702002006X
7. Bugajny, N., Furmańczyk, K., Dudzińska-Nowak, J. and Paplińska-Swerpel, B., 2013. Modelling Morphological Changes of Beach and Dune Induced by Storm on the Southern Baltic Coast Using XBeach (Case Study: Dziwnow Spit). *Journal of Coastal Research*, 65(sp1), pp. 672–677. https://doi.org/10.2112/SI65-114.1
8. Gurov, K.I., Udovik, V.F. and Fomin, V.V., 2019. Modeling of the Coastal Zone Relief and Granulometric Composition Changes of Sediments in the Region of the Bogaily Lake Bay-Bar (the Western Crimea) during Storm. *Physical Oceanography*, 26(2), pp. 170–180. https://doi.org/10.22449/1573-160X-2019-2-170-180
9. Scott, T., Masselink, G., O'Hare, T., Saulter, A., Poate, T., Russell, P., Davidson, M. and Conley, D., 2016. The Extreme 2013/2014 Winter Storms: Beach Recovery Along the Southwest Coast of England. *Marine Geology*, 382, pp. 224–241. http://dx.doi.org/10.1016/j.margeo.2016.10.011
10. Harley, M.D., Masselink, G., Ruiz de Alegría-Arzaburu, A., Valiente, N.G. and Scott, T., 2022. Single Extreme Storm Sequence Can Offset Decades of Shoreline Retreat Projected to Result from Sea-Level Rise. *Communications Earth and Environment*, 3, 112. https://doi.org/10.1038/s43247-022-00437-2
11. Kim, T.-K., Lim, C., Lee, J.-L., 2021. Vulnerability Analysis of Episodic Beach Erosion by Applying Storm Wave Scenarios to a Shoreline Response Model. *Frontiers in Marine Science*, 8, 759067. https://doi.org/10.3389/fmars.2021.759067
12. Belokopytov, V.N., Fomin, V.V. and Ingerov, A.V., 2017. On Multidisciplinary Investigations of Dangerous Natural Phenomena in the Azov-Black Sea Basin. *Physical Oceanography*, (3), pp. 28–44. https://doi.org/10.22449/1573-160X-2017-3-28-44
13. Divinsky, B.V., Kubryakov, A.A. and Kosyan, R.D., 2020. Interannual Variability of the Wind-Wave Regime Parameters in the Black Sea. *Physical Oceanography*, 27(4), pp. 337–351. https://doi.org/10.22449/1573-160X-2020-4-337-351
14. Bogdanovich, A.Yu., Lipka, O.N., Krylenko, M.V., Andreeva, A.P. and Dobrolyubova, K.O., 2021. Climate Threats in the North-West Caucasus Black Sea Coast: Modern Trends. *Fundamental and Applied Climatology*, 7(4), pp. 44–70, https://doi.org/10.21513/2410-8758-2021-4-44-70 (in Russian).
15. Krylenko, M., Krylenko, V. and Kosyan, R., 2015. Accumulative Coast Dynamics Estimation by Satellite Camera Records. In: D. G. Hadjimitsis, K. Themistocleous, S. Michaelides, G. Papadavid, eds., 2015. *Proceedings of SPIE, Third International Conference on Remote Sensing and Geoinformation of the Environment*. Paphos, Cyprus. Vol. 9535, 95351K. https://doi.org/10.1117/12.2192495
16. Boyko, E., Krylenko, V. and Krylenko, M., 2015. LIDAR and Airphoto Technology in the Study of the Black Sea Accumulative Coasts. In: D. G. Hadjimitsis, K. Themistocleous, S. Michaelides, G. Papadavid, eds., 2015. *Proceedings of SPIE, Third International Conference on Remote Sensing and Geoinformation of the Environment*. Paphos, Cyprus. Vol. 9535, 95351Q. https://doi.org/10.1117/12.2192577

17. Krylenko, V.V. and Rudnev, V.I., 2018. Technique of Photographic Aerial Survey of the Bakalskaya Spit. *Ecological Safety of Coastal and Shelf Zones of Sea*, (4), pp. 59–64. https://doi.org/10.22449/2413-5577-2018-4-59-64 (in Russian).

18. Krylenko, M. and Krylenko, V., 2020. Features of Performing High-Precision Survey of the Abrasion Coast Relief by UAV. *Bulletin of Science and Practice*, 6(2), 10–19. https://doi.org/10.33619/2414-2948/51/01 (in Russian).

19. Divinsky, B. and Kosyan, R., 2017. Spatiotemporal Variability of the Black Sea Wave Climate in the Last 37 Years. *Continental Shelf Research*, 136, pp. 1–19. https://dx.doi.org/10.1016/j.csr.2017.01.008

20. Gurov, K.I., 2018. Results of Sediment Granulometric Composition Monitoring in Coastal Zone of the Kalamitsky Bay. *Ecological Safety of Coastal and Shelf Zones of Sea*, (3), pp. 56–63. https://doi.org/10.22449/2413-5577-2018-3-56-63 (in Russian).

21. Shuisky, Yu.D., 2005. Basical Peculiarities of Morphology and Dynamic of the Western Crimea Peninsula Coast. In: MHI, 2005. *Ekologicheskaya Bezopasnost' Pribrezhnykh i Shel'fovykh Zon i Kompleksnoe Ispol'zovanie Resursov Shel'fa* [Ecological Safety of Coastal and Shelf Zones and Comprehensive Use of Shelf Resources]. Sevastopol: ECOSI-Gidrofizika. Iss. 13, pp. 62–72 (in Russian).

22. Goryachkin, Yu.N. and Dolotov, V.V., 2019. *Sea Coasts of Crimea*. Sevastopol: Colorit, 256 p. (in Russian).

23. Udovik, V.F. and Goryachkin, Yu.N., 2013. [Interannual Variability of the Alongshore Sediment Flow in the Coastal Zone of the Western Crimea]. In: MHI, 2013. *Ecological Safety of Coastal and Shelf Zones and Comprehensive Use of Shelf Resources*. Sevastopol: ECOSI-Gidrofizika. Iss. 27, pp. 363–368 (in Russian).

24. Kharitonova, L.V. and Fomin, V.V., 2017. Spatial Structure of Sediment Flow in the Coastal Zone of the Western Crimea on according Numerical Simulation. *Ecological Safety of Coastal and Shelf Zones of Sea*, 1, pp. 48–58 (in Russian).

25. Kharitonova, L.V. and Fomin, V.V., 2012. Statistical Characteristics of Wind Waves in the Coastal Zone of the Western Crimea according to Retrospective Calculations for 1979–2010. In: MHI, 2012. *Ekologicheskaya Bezopasnost' Pribrezhnykh i Shel'fovykh Zon i Kompleksnoe Ispol'zovanie Resursov Shel'fa* [Ecological Safety of Coastal and Shelf Zones and Comprehensive Use of Shelf Resources]. Sevastopol: ECOSI-Gidrofizika. Iss. 26, pp. 24–33 (in Russian).

26. Gippius, F.N. and Arkhipkin, V.S., 2017. Interannual Variability of Storm Waves in the Black Sea According to Numerical Modeling Results. *Vestnik Moskovskogo Universiteta. Seria 5, Geografia*, (1), pp. 38–47 (in Russian).

27. Zhuk, V.O. and Yergina, E.I., 2018. Space-Time Variability of Climate of Winter Seasons in Crimea. *Scientific Notes of V.I. Vernadsky Crimean Federal University. Geography. Geology*, 4(1), pp. 104–121 (in Russian).

28. Krinko, E.F. and Semenov, V.S., 2021. The Consequences of the 1969 Pitsunda Storm and Measures to Overcome Them. *Science in the South of Russia*, 17(2), pp. 90–97. https://doi.org/10.7868/S25000640210210 (in Russian).

Submitted 6.03.2024; accepted after review 3.05.2024;
revised 17.06.2024; published 25.09.2024

About the authors:

Viacheslav V. Krylenko, Senior Research Associate, Shirshov Institute of Oceanology of RAS (36 Nakhimov Avenue, Moscow, 117997, Russian Federation), Ph.D. (Geogr.), **ORCID ID: 0000-0001-8898-8479, ResearcherID: N-1754-2017**, *krylenko.slava@gmail.com*

Yuri N. Goryachkin, Chief Research Associate, Marine Hydrophysical Institute of RAS (2 Kapitanskaya St., Sevastopol, 299011, Russian Federation), Dr.Sci. (Geogr.), **ORCID ID: 0000-0002-2807-201X, ResearcherID: I-3062-2015,** *yngor@mhi-ras.ru*

Marina V. Krylenko, Leading Research Associate, Shirshov Institute of Oceanology of RAS (36 Nakhimov Avenue, Moscow, 117997, Russian Federation), Ph.D. (Geogr.), **ORCID ID: 0000-0003-4407-0548, ResearcherID: R-2210-2016**, *krylenko@mail.ru*

Boris V. Divinsky, Senior Research Associate, Shirshov Institute of Oceanology of RAS (36 Nakhimov Avenue, Moscow, 117997, Russian Federation), Ph.D. (Geogr.), **ORCID ID: 0000-0002-2452-1922, ResearcherID: C-7262-2014**, *divin@ocean.ru*

Contribution of the authors:

Viacheslav V. Krylenko – task setting, processing, analysis and description of research results, preparation of the text and graphic materials

Yuri N. Goryachkin – task setting, processing and analysis of literary sources, field studies, preparation of the article text

Marina V. Krylenko – processing and analysis of the results of field research, preparation of the text of the article and the list of references

Boris V. Divinsky – mathematical modeling of hydrodynamic processes

All the authors have read and approved the final manuscript.

Original article

Testing of a Piled (Permeable) Breakwater Made of Composite Material for Coastal Protection. Part 1: Installation Conditions and Stability Assessment

D. I. Dikii [1]*, V. I. Efremov [2], B. V. Chubarenko [1], D. A. Domnin [1], R. B. Zakirov [1], E. M. Burnashov [3], K. V. Karmanov [4], O. V. Bass [5]

[1] *Shirshov Institute of Oceanology, Russian Academy of Sciences, Moscow, Russia*

[2] *LLC Trading House Basalt Pipes, Moscow, Russia*

[3] *GBU KO Baltberegozashhita, Svetlogorsk, Kaliningrad Oblast, Russia*

[4] *Kaliningrad State Technical University, Kaliningrad, Russia*

[5] *Immanuel Kant Baltic Federal University, Kaliningrad, Russia*

* *e-mail: dimandikiy@mail.ru*

Abstract

The article discusses the results of an experiment (03 October 2021–30 April 2023) to test a "Grebenka" breakwater (breakwater of a through structure, or wave-breaking piled wall) made of composite material. The purpose of the study is to prove or disprove the hypothesis that the structures under study are sufficiently resistant to natural effects of the marine environment and can be considered as an alternative to existing coastal protection methods and means. The test breakwater in the form of five 12-meter modules, four of which were arranged in a line, was installed on the northern shore of the Sambia Peninsula (Baltic Sea, Kaliningrad Oblast'). The state of the breakwater was registered by various methods, including underwater and aerial photography. The results of the study showed that the installation of modules on the unprepared bottom caused their shear and tilt as a result of wave action. In order to improve the resistance of the "Grebenka" breakwater to such impact, it is necessary to prepare the bottom by flushing out the sand cover up to the consolidated layer level. Despite the fact that one of the breakwater modules split into two parts following the longitudinal fracture of its base (due to a violation of installation technology), all vertical pipe-piles forming the wave-dampening pile rows with cantilevered sealing at the base and free upper ends did not break off or corrode. This indicates that the composite material is strong enough for use in marine conditions with wave and ice loads. Algae biofouling has demonstrated the friendliness of the composite material to the biota.

Keywords: breakwater, coastal protection, composite material, Baltic Sea, natural experiment

Acknowledgments: Production and installation of the construction were funded by LLC Trading House Basalt Pipes (Moscow). The publication was prepared under topic no. FMWE-2024-0025 of the state assignment of Shirshov Institute of Oceanology, Russian Academy of Sciences.

For citation: Dikii, D.I., Efremov, V.I., Chubarenko, B.V., Domnin, D.A., Zakirov, R.B., Burnashov, E.M., Karmanov, K.V. and Bass, O.V., 2024. Testing of a Piled (Permeable) Breakwater Made of Composite Material for Coastal Protection. Part 1: Installation Conditions and Stability Assessment. *Ecological Safety of Coastal and Shelf Zones of Sea*, (3), pp. 79–92.

Испытание свайного (проницаемого) волнолома из композитного материала для берегоукрепления. Часть 1. Условия установки и оценка устойчивости

Д. И. Дикий [1] *, В. И. Ефремов [2], Б. В. Чубаренко [1], Д. А. Домнин [1], Р. Б. Закиров [1], Е. М. Бурнашов [3], К. В. Карманов [4], О. В. Басс [5]

[1] *Институт океанологии им. П. П. Ширшова РАН, Москва, Россия*

[2] *ООО «Торговый дом «Базальтовые трубы», Москва, Россия*

[3] *ГБУ КО «Балтберегозащита», Светлогорск, Россия*

[4] *Калининградский государственный технический университет, Калининград, Россия*

[5] *Балтийский федеральный университет имени Иммануила Канта, Калининград, Россия*

* *e-mail: dimandikiy@mail.ru*

Аннотация

Рассмотрены итоги испытания (03.10.2021–30.04.2023) волнолома «Гребенка» (волнолома сквозной конструкции, или волногасящей проницаемой стенки) из композитного стеклобазальтопластика. Цель исследования – доказать или опровергнуть гипотезу о том, что исследуемые конструкции достаточно устойчивы к естественным воздействиям морской среды и могут быть рассмотрены в качестве альтернативы традиционным берегозащитным средствам. Тестовый волнолом в виде пяти 12-метровых модулей, четыре из которых были расположены в один ряд, установили на северном побережье Самбийского полуострова (Балтийское море, Калининградская область). Состояние волнолома фиксировали разными способами, включая подводную съемку и аэросъемку. Результаты показали, что установка модулей на неподготовленное дно спровоцировала их сдвиг и наклон вследствие волнового воздействия. Для повышения устойчивости волнолома «Гребенка» к таким воздействиям необходимо подготавливать грунт путем размыва песчаного чехла до уровня консолидированного слоя. Несмотря на то, что один из модулей волнолома разделился на две части при продольном разломе его основания (из-за нарушения технологии монтажа), все вертикальные трубы-сваи, образующие волногасящие свайные ряды с консольной заделкой в основании и свободными верхними концами, не обломились и не подверглись коррозии. Это говорит о достаточной прочности композитного материала для использования в морских условиях с волновыми и ледовыми нагрузками. Биообрастание водорослями свидетельствует о дружественности материала к биоте.

Ключевые слова: волнолом, берегоукрепление, композитный материал, Балтийское море, натурный эксперимент

Благодарности: создание и установка конструкции – ООО «Торговый дом «Базальтовые трубы», г. Москва; подготовка публикации – тема № FMWE-2024-0025 государственного задания ИО РАН.

Для цитирования: Испытание свайного (проницаемого) волнолома из композитного материала для берегоукрепления. Часть 1. Условия установки и оценка устойчивости / Д. И. Дикий [и др.] // Экологическая безопасность прибрежной и шельфовой зон моря. 2024. № 3. С. 79–92. EDN GNODYF.

Introduction

The concept of the Kaliningrad Oblast' coastal protection [1] involves the application of several methods of coastline reinforcement, as well as their testing before implementation. Modern materials based on natural or man-made polymers, such as geosynthetics [2, 3], are used in the construction of coastal protection structures to increase the reliability of the soil or construction materials [4]. Such a material is glass-basalt-plastic [5], of which the "Grebenka" breakwater considered in this article is made.

In [6], it was demonstrated that the installation of a 300 m long breakwater at a distance of 250 m from the shore resulted in beach growth and coastline extension of up to 40 m per year.

The practice and rules for the utilisation of breakwaters for the purpose of coastal protection are defined by Regulations 277.1325800.2016 [1)]. In [7], it was demonstrated that the efficiency of permeable structures depended on the ratio of the area of openings to the total area of the structure.

The present study concerns a natural experiment designed to assess the feasibility of utilising the "Grebenka" breakwaters. It is presumed that such breakwaters are capable of dampening waves effectively, resistant to severe storm damage and safe for people and natural environment. Furthermore, it has been demonstrated that the "Grebenka" breakwaters exhibit superior technical performance in comparison to both concrete and wooden breakwaters [8]. The site where the experiment was conducted is located in the South-Eastern Baltic on the northern coast of the Sambia Peninsula (Kaliningrad Oblast', the Russian Federation) west of the city of Zelenogradsk (Fig. 1, *a*).

The objective of this article is to analyse the results of the natural experiment, to evaluate the resistance of the "Grebenka" breakwater to destructive environmental impacts and to propose recommendations for optimising the technology of its installation.

As the first part of the description, this article presents the initial findings of the experiment, with a particular focus on the technical aspects of breakwater installation, its resistance to natural storm loads and other external factors. The results of the data analysis examining the impact of the breakwater on the shoreline, gathered during the experiment, are extensive and will be presented in the second part.

[1)] JSC TsNIITS, 2017. *Book of Rules СП 277.13258000.2016. Coastal protection constructions. Design rules*. Moscow, 91 p. (in Russian).

Materials and methods of study

The five-module "Grebenka" breakwater was installed (Fig. 1, *b*, *c*) opposite the last inter-groin pocket at the eastern end of the site with old, partially collapsed groins (Fig. 1, *c*). Depths at the experimental site ranged from 1.2 m near the shore to more than 2.5 m at the point where the modules were installed. The estimated closure depth for this area varies considerably, with figures ranging from 7.5 m [9] to 8.4 m [10]. As indicated in [11], the wave collapse zone in the vicinity of the breakwater installation commences at a distance of over 200 m from the shore.

In contrast to traditional through pile breakwaters [2)], a special feature of the "Grebenka" breakwater design is the use of pipes (hollow piles) of different diameters. The pipes are made of glass-basalt-plastic – a corrosion-resistant composite

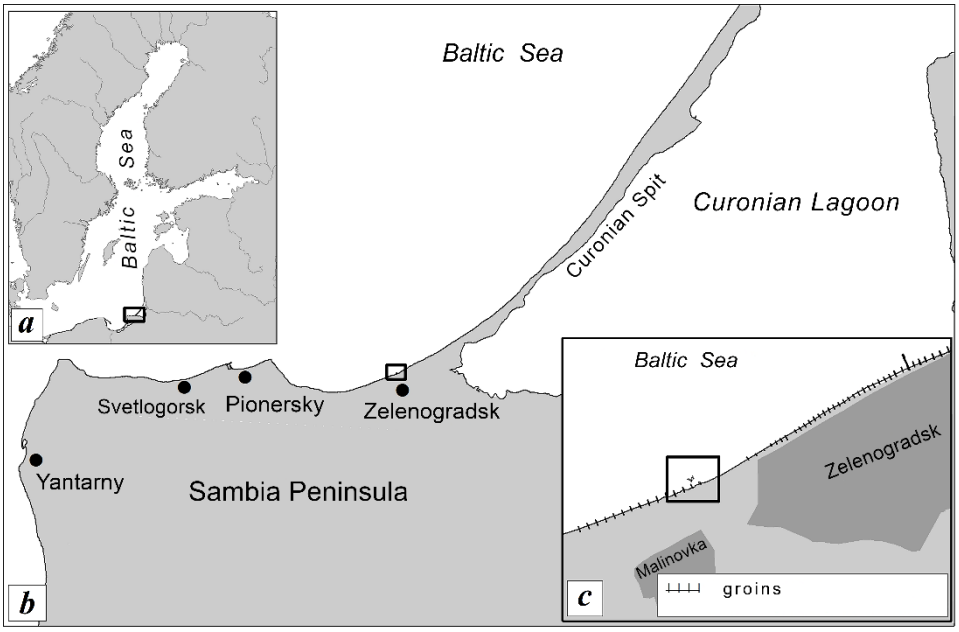

F i g . 1 . Place of the experiment: *a* – the Baltic Sea; *b* – the northern shore of the Sambia Peninsula, Kaliningrad Oblast'; *c* – a section of the shore adjacent from the west to the Zelenogradsk city beach. From left to right: old groins (dashes on the shore line), a breakwater in the sea (the breakwater and four old groins are highlighted by a rectangle), a group of new groins and a pier protruding into the sea

[2)] Sedrisev, D.N. and Rubinskaya, A.V., 2011. [*Fundamentals of Design of Hydraulic Structures, Woodyards and Log Receiving Ports: Training Manual*]. Krasnoyarsk: SibGTU, 119 p. (in Russian).

material that has already been adopted on a wide scale in numerous sectors of the construction industry [5]. The primary benefits of glass-basalt plastic, along with the findings from testing a set of pipes in a wave flume, are presented in comprehensive detail in [8].

A modular breakwater design [3)] was selected with a maximum length per module of 12 m (based on the ability to transport materials to the installation site) and a width of 3 m. The breakwater module (Fig. 2) consisted of a grid base (three horizontal rows of parallel 12 m long, 0.5 m diameter base pipes and an additional pipe at 0.5 m distance, connected by 3 m long, 0.25 m diameter cross pipes) served as a bottom-mounted base. All base pipes were filled with concrete. Vertically installed pipe-piles with diameters of 0.2 and 0.1 m were inserted into the main pipes of the grid base and formed a comb (*grebenka*) of three rows – the analogue of a pile row. The vertical pipes were 3 m high in three modules and 2.5 m high in two modules (*4* and *5*). An additional horizontal pipe (located seaward) at the base was without piles and functioned as a ballast pipe (visible in Fig. 2, *a*) to increase the module resistance to shear and overturning. The weight of the module after filling the horizontal base pipes with concrete was about 28 t. The modules were installed in a line parallel to the shore.

In order to achieve the most effective wave dampening, it is recommended that the relative open area of a row of vertical pipes should be no more than 30–40 %. Furthermore, it is advised that the relative open area should decrease from row to row towards the shore, in accordance with the recommendations set forth by "Central Scientific Research Institute of Construction" JSC.

The most effective scheme, as determined through testing at "Sea Coasts" Research and Development Centre, exhibited a relative open area of 30–20–10 %. To assess the resistance of the vertical rows to storm conditions, the structure was tested with a relative open area of 40–30–20 %. The reflection coefficient, as determined by wave flume tests, was found to be 0.2 [8].

a ***b***

Fig. 2. The module (with pontoons) on the shore (*a*), a line of modules (*1–4*) and a number of installation slips in May 2021 (*b*)

[3)] Efremova, M.V., 2019. Utility Model Patent 187014 U1 Russian Federation. МПК E02B 3/06. [*Breakwater*]: 2018137512. Applied 23.10.2018, published 13.02.2019. 10 p. (in Russian).

From the point of view of functional application, the “Grebenka” wave-dampening piled structure can be considered as a type of through breakwater or wave-dampening permeable wall.

Traditionally, piled breakwaters and other piled barrier structures are constructed on piles that are pounded, hammered, screwed into undrained dense soil, which does not correspond to the “Grebenka” installation technology. On the other hand, Annex A of Regulations 24.13330.2021 mentions a post pile that transmits the load to the foundation only through a heel (in the case of the “Grebenka”, this heel is the grid base of the structure). The investigated structure also contains elements of the piled breakwater mentioned in Regulations 277.1325800.2016 “Marine Coastal Protection Structures. Design Rules.” What is new in the design of the “Grebenka” breakwater compared to traditional through breakwaters is the composite cover, modularity and mobility of assembly and installation.

Regulations 277.1325800.2016 recommend that for sandy beaches, underwater breakwaters should be installed at least 100 m from the shore line. As the tested breakwater is permeable, the designers decided to reduce this distance.

With a total module line length of 60 m and a distance from the shore of 75–80 m, the ratio of the length of the structure to its distance from the shore was between 0.75 and 0.8, which could result in either material accumulation and extension of the shore towards the structure, or even a tombolo.

The modules were assembled from prefabricated sets, then the base was poured with concrete onshore. Vertical pipe-piles were fixed in the base pipes simultaneously with concrete pouring. The assembly of five modules took two days in addition to 3–4 days for the concrete to harden and gain transport strength.

The modules were launched and transported to the sea using inflatable pontoons (Fig. 2, *a*, *b*) with a carrying capacity of 8 t (4 pieces per module). From the sea, the modules with pontoons were towed by the boat through 33 m long prefabricated slips (Fig. 2, *c*).

The modules were placed on the bottom without bedding preparation. Module *5* was placed at a depth of 1.5 m at a distance of 35 m from the shore at the level of the middle of the visible part of the easternmost destroyed old groin. Other four modules (*1–4*) were placed at a depth of 2.5 m at a distance of 75–80 m from the shore (in line with a slight curve, distance between modules 1.5–2 m (Fig. 3)). Module *5* was installed in one day in October 2020 and other four modules were installed in two days in May 2021.

After installation, module *5* (2.5 m high pipe-piles) protruded 1 m above the water and modules *1–3* (3 m high pipe-piles) – 0.5 m above the water. Module *4* (2.5 m high pipe-piles) did not protrude much from the water and the tops of the piles were in the near-surface layer.

The tests of the “Grebenka” breakwater were carried out from 03 October 2021 to 30 April 2023. Expedition surveys were carried out by the manufacturers (LLC Trading House Basalt Pipes), the employees of the Atlantic Branch of Shirshov Institute of Oceanology of RAS, Immanuel Kant Baltic Federal University and GBU KO Baltberegozashhita.

Changes in the location and characteristics of the modules were recorded during visual and tactile inspections and photography, which made it possible to assess the degree of mechanical damage and corrosion, as well as the degree of immersion of the base of the modules in the sand and their position relative to sea level. Photographs from the shore were taken 2–4 times a month throughout the experiment.

Satellite images from the Google and Yandex open sources were used to assess the change in position of the breakwater modules, as in [3]. The coordinates of stationary reference points on the site were used to georeference the satellite images. The accuracy of the module coordinates was improved by GPS georeferencing. The final error was up to 2.7 m.

Aerial visual observations were carried out using an unmanned aerial vehicle (UAV – DJI Mini2) during the 2022 autumn–summer period and during the 2023 winter–spring period. The flight altitude was limited to 120 m taking into account necessary safety measures and the requirements of flight regulations. Similar examples of aerial visual observation are presented for the Black Sea and the Sea of Azov in [12], for the Tsimlyansk Reservoir in [13] and for the rivers of the Yamalo-Nenets Autonomous Okrug in [14].

Underwater photography of the structures using an SJCAM 5000 action camera was conducted on 07 September 2022 and 12 April 2023. Photographs of each module of the structure were taken from a distance of approximately 1 m, with a clockwise traverse of the structure from the west corner off the sea or west side of the module. A bottom-to-surface depth scale was applied to the photographs that showed the bottom.

Results and their discussion

At the time of studying the main morphological parameters during the 2022 summer season, the position of the modules of the "Grebenka" breakwater became relatively stable. The composite material used proved its durability under storm conditions. The "Grebenka" breakwater withstood ice loads successfully during the 2020–2021 winter.

A series of heavy storms during the 2020–2021 winter period disrupted the linear arrangement of modules *1–4* (Fig. 3): three out of five modules were displaced or rotated. From the second year of the experiment, the disturbed linear array of modules acted as a disjointed set of modules and did not provide the expected wave-dampening effect.

Photographs of the underwater section of the breakwater modules and measurements provided an indication of the extent to which the base of the modules was submerged in sand, the tilt of the structures, their integrity and algae fouling.

The most complete survey of the structure was carried out on 07 September 2022 (Figs. 3–5). Module *1* was 1.5 m above the ground, had not been destroyed or overturned and was almost completely covered by water, although it was 0.5 m above the water level when installed; the top 2/3 of the unsanded part of the piles were covered with filamentous algae. Segment *2a* of module *2* was 1 m above the ground,

F i g . 3 . Initial and final location of the “Grebenka” breakwater modules: *a* – initial (red lines) and final (blue lines) location of the modules (Google Maps image, 2021. https://www.google.ru/maps); *b* – location of the “Grebenka” breakwater modules on 12 April 2023

tilted westwards towards the shore and was completely covered by water. The entire visible part of the piles was covered with algae. The depth at the location of module *3* was 1.2 m. It was not destroyed or overturned. Some of the piles were 0.1–0.3 m above the water. The piles were covered with algae along the entire length of the underwater section. Module *4* was up to 0.5 m above the bottom, tilting to the west and completely covered by water. The western part of the module was almost completely hidden by the sand, with only the upper eastern, unsanded part up to 1/3 of its height covered with algae. Fig. 3, *b* shows that the module split into two parts following the longitudinal fracture of its base, as its eastern third is clearly outside the unified line of the first two thirds.

The repeated photography of all modules was carried out from the UAV on 12 April 2023 (Fig. 3, *b*). It uncovered module *2*, which was not visible in the UAV photography dated 07 September 2022 because it was under the sand layer of the underwater berm. The tops of the vertical piles rose 0.4–1.0 m above the bottom and tilted towards the sea. Module *2* appeared to be split into two parts. Probably, the splitting of the module into several parts occurred due to the violation of installation technology of the structure. The reason for this will be definitively determined when the module is dismantled. The most probable explanation is that the connecting cross pipes of the module grid base, which were not cast in concrete, fell onto an uneven part of the bottom under the layer of sand causing the module to break when the sand was eroded.

There was no algae fouling on the piles of module *2* as they were hidden by the sandy underwater berm for most of the time. The fact that it became bare and was observed during the photography on 12 April 2023 is a consequence of the deformation of the berm and the increase in depth at the module site.

In Fig. 3, the dark colour of the piles is associated with algae fouling (except for module *2* (Fig. 3, *b*), which was entirely under sand); part *2a*, separated from module *2*, was not completely covered, so its piles were partially covered with algae.

The upper parts of the piles of all the modules (which were in the water) were covered with algae, indicating a certain friendliness of the glass-basalt-plastic to biota and its ability to form the basis of an underwater reef. If the lower part of the piles was free of vegetation, this meant that it had been covered by sand during the growing season up to the time of the survey. During the resurvey on 12.04.2023, an increase in the lower bare part of all modules was recorded, indicating that sand had been partially washed away from the underwater slope.

The location of the breakwater did not take into account the fact that the breakwater was in the zone of influence of an extensive longshore berm and several types of currents. The migration of the underwater berm ensured that the base of all the modules was covered with sand.

Prior to the installation of the “Grebenka” breakwater modules, necessary engineering survey of the bottom area was not carried out, in particular, the height of the sand layer above the compacted bottom was not established. The modules were not only sanded up, but also subsided by 0.5 m or more (Fig. 5). To avoid such subsidence, it is necessary to place the modules on a hard bottom. This can be achieved, for example, by flushing out the sand at the installation site to the moraine bed, which is much cheaper than preparing a rock bed under stationary stone-concrete breakwaters.

It was assumed that subsidence of the breakwater would increase the shear stability of the modules during storms. In the first year of the experiment, this dynamic was observed, but then the modules tilted during heavier storms.

Since storm wave lengths ranged from 120–140 m, a structure of four modules exposed along a single line provided only the minimum acceptable ratio of wave-dampening structure length to wavelength, i.e. approximately 1:2. Initially, the organisers of the experiment understood that the local impact of the structure could

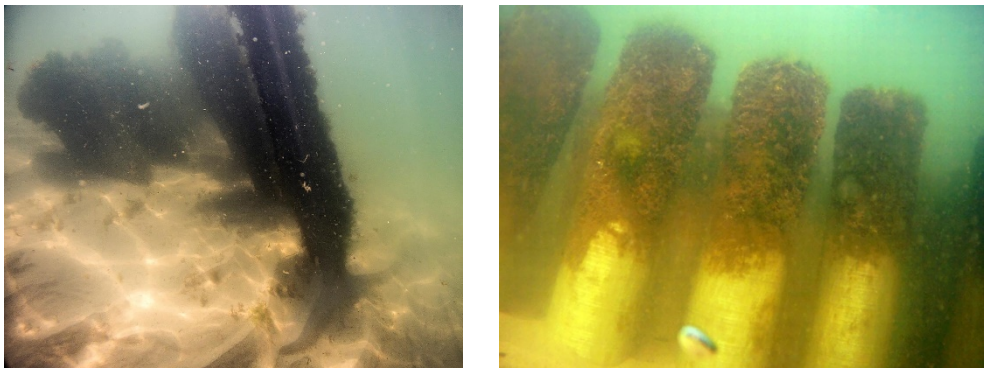

a *b*

F i g . 4 . State of the “Grebenka” breakwater modules: *a* – algae fouling and tilt of the structure (survey on 7 September 2022); *b* – post-storm partial exposure of the wave-damping piles from under sand (survey on April 12, 2023)

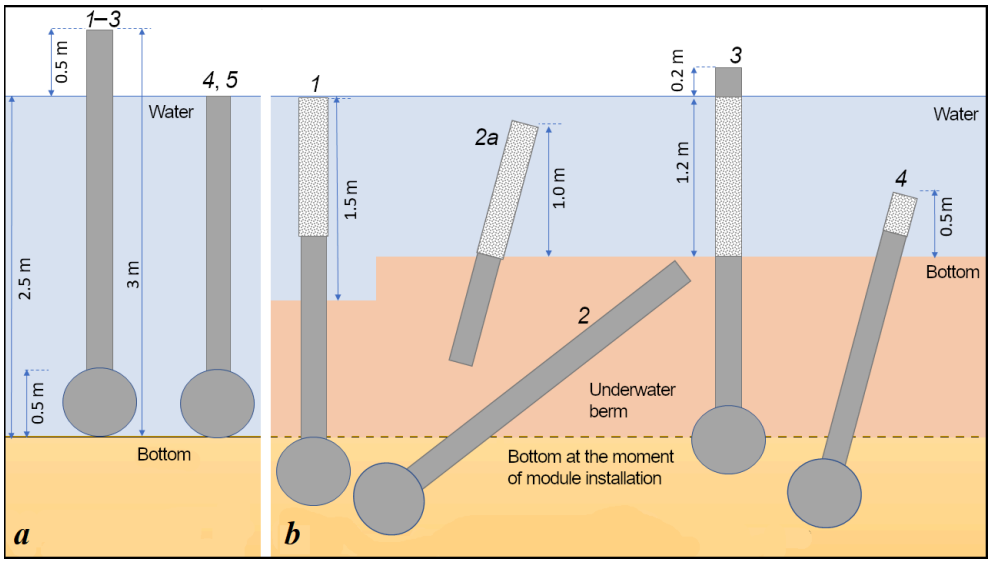

F i g . 5 . Schematic initial position of the modules (*1–5*) during installation in May 2021 (*a*) and their final position during the survey on 07.09.2022 (*b*). The parts fouled with algae are highlighted in light gray. The diagram shows the subsidence of modules and their sanding up, deviations from the vertical axis, and changes in the height of the surface part

only occur within the inter-groin pocket blocked by the structure. At this stage, based on the results of the experiment, the organisers admit that a mistake was made in the location of the structure: with its short length, it was too far from the shore. This experience will have to be taken into account when building similar structures in the future.

The modules are preferably orientated so that the additional horizontal pipe at the base is on the shore side, providing support against wave action and preventing overturning. In this installation, the modules were orientated the other way round.

Conclusions

Five 12-metre modules were installed on the northern shore of the Sambia Peninsula (Baltic Sea, Kaliningrad Oblast') during the "Grebenka" breakwater (a breakwater of through construction, or wave-dampening permeable wall) natural experiment. The technology of module assembly on shore, their transport and submersion to the bottom was worked out. For a year and a half (03 October 2021–30 April 2023) the investigated structures were exposed to wave and ice loads.

The preparation of the breakwater site is important for the safety of structures exposed to wave action. Initially it was assumed that no bottom preparation would be required. However, the influence of coastal currents in the vicinity of the underwater berm in the absence of bottom preparation resulted in the breakwater subsidence into the sand.

Some of the modules changed their position after the experiment, which means that despite the use of concrete to weight the structure, the effects of the waves and currents were sufficient to shear the structures. One solution to this problem is to weight the structure or, as discussed above, to prepare the bottom more thoroughly.

One of the modules failed to withstand the load and split at the base (possible cause: underfilling of the cofferdams in the base with concrete). In order to clarify the details of this fact, it is necessary to examine the elements of the damaged module.

All vertical wave-dampening piled rows remained intact, indicating that the proposed structure is sufficiently resistant to wave and ice loads. The vertical pipe-piles forming the wave-dampening piled rows with cantilevered sealing at the base and free upper ends did not break off or corrode.

The large number of algae and other organic objects observed on the surface of glass-basalt-plastic indicates the friendliness of this material to the biotic component of the environment.

The experiment proved to be very useful for further improvement of the structure taking into account both negative and positive results achieved. It should be emphasised that this work is a rare example of testing a life-size structure in the very conditions, in which it can be used further after modification.

REFERENCES

1. Burnashov, E.M., Chubarenko, B.V., Cherkasov, S.S. and Karmanov, K.V., 2022. Shore Protection System for Coastal Region: Experience of the Kaliningrad Oblast. In: B. V. Chubarenko, ed., 2022. *Proceedings of All-Russian Conference with International Participation "XXIX Coastal Conference: Field-Based and Theoretical Research in Shore Use Practice"*. Kaliningrad, April 18–24, 2022. Kaliningrad: Izd-vo BFU im. I. Kanta, pp. 17–19 (in Russian).
2. Chubarenko, B., Domnin, D., Simon, F.-G., Scholz, P., Leitsin, V. Tovpinets, A., Karmanov, K. and Esiukova, E., 2023. Change over Time in the Mechanical Properties of Geosynthetics Used in Coastal Protection in the South-Eastern Baltic. *Journal of Marine Science and Engineering*, 11(1), 113. https://doi.org/10.3390/jmse11010113
3. Domnin, D. and Burnashov, E., 2021. Geographical Information Dataset "Geosynthetics in Coastal Protection of the South-East Baltic". *Data in Brief*, 40, 107693. https://doi.org/10.1016/j.dib.2021.107693
4. Leitsin, V.N., Tovpinets, A.O., Chubarenko, B.V., Domnin, D.A., Esiukova, E.E. and Burnashov, E.M., 2020. Approach to Evaluating the Change of Properties of the Geosynthetic Material Used to Stabilize the Marine Landscape Slopes. In: IOP, 2020. IOP Conference Series: Materials Science and Engineering. III International Scientific and Practical Conference "Advanced Building Materials and Technologies 2020", 26–29 May 2020, Kaliningrad. Kaliningrad. Vol. 911, 012004. https://doi.org/10.1088/1757-899X/911/1/012004
5. Dalinkevich, A.A., Gumargalieva, K.Z., Soukhanov, A.V. and Marakhocsky, S.S., 2010. Modern Basalt Fibers and Polymeric Composites on Their Basis. *Composite Materials Constructions*, (3), pp. 37–54 (in Russian).
6. Leont'yev, I.O., 2007. Changes in the Shoreline Caused by Coastal Structures. *Oceanology*, 47(6), pp. 877–883. https://doi.org/10.1134/S0001437007060124
7. Makarov, K., Tlyavlina, G., Tlyavlin, R. and Shelushinin, Y., 2019. Interaction of Waves with Slotted Vertical Walls. *The Hydrotechnika*, (3), pp. 32–36 (in Russian).
8. Bass, O.V., Vasutkin, E.S. and Efremov, B.I., 2021. Approach to Reducing Shore Erosion Based on Application of Composite Pile Breakwater "Comb". *Construction Economic and Environmental Management*, (3), pp. 124–133. https://doi.org/10.37279/2519-4453-2021-3-124-133 (in Russian).
9. Ostrowski, R. and Stella, M., 2016. Sediment Transport Beyond the Surf Zone Under Waves and Currents of the Non-Tidal Sea: Lubiatowo (Poland) Case Study. *Archives of Hydro-Engineering and Environmental Mechanics*, 63(1), pp. 63–77. https://doi.org/10.1515/heem-2016-0005
10. Leont'yev, I.O., 2012. Predicting Shoreline Evolution on a Centennial Scale Using the Example of the Vistula (Baltic) Spit. *Oceanology*, 52(5), pp. 700–709. https://doi.org/10.1134/S0001437012050104
11. Chubarenko, B.V., Sokolov, A.N. and Dikii, D.I., 2023. Variability of the Coastal Currents, Waves and Wind Surge Along the Shore of the South-Eastern Baltic (Kaliningrad Oblast, Russian Federation). *Regional Studies in Marine Science*, 57, 102762. https://doi.org/10.1016/j.rsma.2022.102762
12. Krylenko, M. and Krylenko, V., 2020. Features of Performing High-Precision Survey of the Abrasion Coast Relief by UAV. *Bulletin of Science and Practice*, 6(2), pp. 10–19. https:/doi.org/10.33619/2414-2948/51/01

13. Ivlieva, O.V., Bespalova, L.A., Glinka, V.V., Serdyuk, L.V. and Chmykhov, A.A., 2021. The Use of Unmanned Aerial Vehicles to Assess the Intensity of Manifestation of Dangerous Coastal Processes in the Water Protection Zone of Tsimlyansk Reservoir. *Bulletin of Higher Educational Institutions. North Caucasus Region. Natural Science*, (2), pp. 56–65. https:/doi.org/10.18522/1026-2237-2021-2-56-65 (in Russian).

14. Ilyasov, R.M. and Kolesnikov, R.A., 2022. The Practice of Using Unmanned Aerial Vehicles in Monitoring Water Bodies and Their Water Protection Zones. *Scientific Bulletin of the Yamal-Nenets Autonomous District*, (3), pp. 97–110. https:/doi.org/10.26110/ARCTIC.2022.116.3.006 (in Russian).

Submitted 18.04.2024; accepted after review 21.05.2024;
revised 17.06.2024; published 25.09.2024

About the authors:

Dmitry I. Dikii, Junior Research Associate, Shirshov Institute of Oceanology of Russian Academy of Sciences (36 Nakhimovskiy Ave., Moscow, 117997, Russian Federation), Ph.D. (Tech.), **ORCID ID: 0000-0002-8819-8423**, **Scopus Author ID: 56998707400**, *dimandikiy@mail.ru*

Vladimir I. Efremov, Executive Director, LLC Trading House Basalt Pipes (29, Bldg 4, Petrovsko-Razumovsky Drive, Moscow, 127287, Russian Federation), *zbt@bk.ru*

Boris V. Chubarenko, Leading Research Associate, Head of the Laboratory of Coastal Systems, Shirshov Institute of Oceanology of Russian Academy of Sciences (36 Nakhimovskiy Ave., Moscow, 117997, Russian Federation), Ph.D. (Phys.-Math.), **ORCID ID: 0000-0001-7988-1717**, **Scopus Author ID: 6507102508**, *chuboris@mail.ru*

Dmitry A. Domnin, Senior Research Associate, Shirshov Institute of Oceanology of Russian Academy of Sciences (36 Nakhimovskiy Ave., Moscow, 117997, Russian Federation), Ph.D. (Geogr.), **ORCID ID: 0000-0001-8627-2055**, **Scopus Author ID: 9250345600**, **SPIN-код: 1174-4997,** *dimanisha@gmail.com*

Ruslan B. Zakirov, Research Associate, Shirshov Institute of Oceanology of Russian Academy of Sciences (36 Nakhimovskiy Ave., Moscow, 117997, Russian Federation), Ph.D. (Geogr.), **Scopus Author ID: 57222497041**, *zakirov.ruslan.kaliningrad@yandex.ru*

Evgeny M. Burnashov, Deputy Director for Monitoring and Security of Hydraulic Facilities, GBU KO Baltberegozashhita (1 Khutorskaya Str., Kaliningrad Oblast, Svetlogorsk, 238560, Russian Federation), Ph.D. (Geogr.), **Scopus Author ID: 41261235800**, *burnashov_neo@mail.ru*

Konstantin V. Karmanov, Graduate Student, Kaliningrad State Technical University (1 Sovetsky Drive, Kaliningrad, 236000, Russian Federation), **Scopus Author ID: 55377991800**, *konstantin.karmanoff@yandex.ru*

Oleg V. Bass, Associate Professor, Institute of High Technology, Immanuel Kant Baltic Federal University (14 Aleksandra Nevskogo Str., Kaliningrad, 236041, Russian Federation), Ph.D. (Geogr.), **Scopus Author ID: 57219593321**, *o.bass@mail.ru*

Contribution of the authors:

Dmitry I. Dikii – material collecting and grouping, preparing the first draft of the article, finalising the text

Vladimir I. Efremov – development of the breakwater design, supervision of the installation and participation therein, photographic documentation of the breakwater state, partial funding of the works, drawing of conclusions and recommendations on the design

Boris V. Chubarenko – planning and drafting the first draft of the article, analysis of all the results and drawing general conclusions, final editing of the article text

Dmitry A. Domnin – conduction of aerial visual surveys, underwater video surveys, analysis of the results

Ruslan B. Zakirov – georeferencing of satellite images, analysing changes in module locations, preparation of relevant illustrations

Evgeny M. Burnashov – analysis of the results and contribution to the overall conclusions

Konstantin V. Karmanov – conduction of aerial visual surveys, analysis of the obtained data

Oleg V. Bass – participation in the breakwater installation, participation in drawing of conclusions on the breakwater

All the authors have read and approved the final manuscript.

Original article

Modeling of Artificial Beach Morphodynamics in the Koktebel Village Coastal Zone (Crimea) under the Storm Wave Impact

L. V. Kharitonova *, D. I. Lazorenko, D. V. Alekseev, V. V. Fomin

Marine Hydrophysical Institute of RAS, Sevastopol, Russia
* *e-mail: l.kharitonova@mhi-ras.ru*

Abstract
Artificial beaches are one of the most effective methods of protecting shores and hydraulic structures under shortage of natural beach-forming material. This work investigates the influence of extreme storms on the erosion zone width of an artificial pebble beach located in front of a vertical concrete seawall in the village of Koktebel (Feodosia, Crimea). The storm power index in the central part of Koktebel Bay was calculated on the basis of wind wave reanalysis data for 1979–2020 obtained using the SWAN spectral model and ERA-Interim and ERA5 surface wind fields. We identified 146 storm situations with duration of at least 12 hours. Three most extreme storms were analysed: in terms of power index (660 $m^2 \cdot h$), the storm of 26–29 January 1988; in terms of mean significant wave height (3.6 m), the storm of 10–11 November 2007; and in terms of duration (95 h), the storm of 25–29 September 2017. The profile deformations of the artificial pebble beach attached to a vertical concrete seawall were calculated for the first and second storms using a one-dimensional version of the XBeach (eXtreme Beach behavior) numerical model. It was shown, that under the impact of storm waves, the coast steepness near the coastline changes gradually and material from the beach nearshore part slid down the underwater slope leading to a local depth decrease near the shore. It was found, that the underwater erosion zone width of the beach was three times greater than the surface one. The most significant deformations of the beach profile occurred during the first 6 hours of storm action, and then the rate of beach deformation decreased. It was obtained that the coastline in the area of interest could retreat up to 10 m under the impact of an extreme storm. The study revealed that ≥ 20 m wide pebble beaches (a mean particle size of 30 mm) would fully absorb the wave energy of extreme storms and provide adequate protection for the coastal zone of Koktebel Bay.

Keywords: beach, coast protection structures, wind waves, extreme storm, XBeach, Crimea, Koktebel

Acknowledgments: The work was carried out within the framework of the theme of state assignment of FSBSI FRC MHI FNNN-2024-0016.

For citation: Kharitonova, L.V., Lazorenko, D.I., Alekseev, D.V. and Fomin, V.V., 2024. Modeling of Artificial Beach Morphodynamics in the Koktebel Village Coastal Zone (Crimea) under the Storm Wave Impact. *Ecological Safety of Coastal and Shelf Zones of Sea*, (3), pp. 93–109.

Моделирование морфодинамики искусственного пляжа в береговой зоне пгт Коктебель (Крым) под воздействием штормового волнения

Л. В. Харитонова *, Д. И. Лазоренко, Д. В. Алексеев, В. В. Фомин

Морской гидрофизический институт РАН, Севастополь, Россия
* *e-mail: l.kharitonova@mhi-ras.ru*

Аннотация
Искусственные пляжи являются одним из наиболее эффективных методов защиты берегов и гидротехнических сооружений в условиях дефицита естественного пляжеобразующего материала. В статье на примере района берега пгт Коктебель (г. Феодосия, Крым) исследуется изменение ширины зон размыва искусственного галечного пляжа, расположенного перед отвесной бетонной гидротехнической стенкой, под воздействием экстремальных штормов. На основе данных реанализа ветрового волнения, полученных с использованием спектральной модели *SWAN* и полей приземного ветра *ERA-Interim* и *ERA*5 за 1979–2020 гг., проведены расчеты индекса мощности шторма в центральной части бухты Коктебель. Выделено 146 штормовых ситуаций с продолжительностью не менее 12 ч. Проанализировано три наиболее экстремальных шторма: по индексу мощности (660 м^2·ч) – шторм 26–29 января 1988 г.; по средней высоте значительных волн (3.6 м) – шторм 10–11 ноября 2007 г.; по длительности (95 ч) – шторм 25–29 сентября 2017 г. Для первого и второго штормов на основе одномерного варианта численной модели *XBeach* (*eXtreme Beach behavior*) рассчитаны штормовые деформации профиля искусственного, прислоненного к отвесной бетонной стенке галечного пляжа. Показано, что под воздействием штормового волнения крутизна берега в районе уреза постепенно меняется и происходит сползание материала с приурезовой части пляжа вниз по подводному склону. Это приводит к локальному уменьшению глубины у берега. Установлено, что ширина зоны размыва подводной части пляжа в три раза больше надводной. Наиболее значительные деформации профиля пляжа происходят в первые 6 часов действия штормов, далее скорость деформации снижается. Отступание береговой линии под воздействием экстремального шторма для исследуемого района может достигать 10 м. При средней крупности пляжеобразующего материала 30 мм для береговой зоны бухты Коктебель пляжи шириной 20 м и более могут полностью гасить энергию волнения экстремальных штормов и в достаточной мере выполнять защитные функции.

Ключевые слова: пляж, берегозащитные сооружения, ветровое волнение, экстремальный шторм, XBeach, Крым, Коктебель

Благодарности: работа выполнена в рамках темы государственного задания ФГБУН ФИЦ МГИ FNNN-2024-0016.

Для цитирования: Моделирование морфодинамики искусственного пляжа в береговой зоне пгт Коктебель (Крым) под воздействием штормового волнения / Л. В. Харитонова и [др.] // Экологическая безопасность прибрежной и шельфовой зон моря. 2024. № 3. С. 93–109. EDN OILBDL.

Introduction

Since ancient times, the economic activity of mankind has been inextricably linked with the development of the coasts of seas and oceans. In most cases, the Crimean coastline is used in an integrated manner for urban, port and resort construction [1]. Therefore, the requirements for coast protection are the following: coast protection structures should be effective and well integrated into natural processes. Both artificial free beaches and those with beach-retaining structures fulfil such requirements. According to [2], on the Black Sea coast, a wave-absorbing beach should have a width of about 25 m to dampen waves that may occur once in 25 years. Under shortage of beach material, effective and long-term operation of coast protection structures is mainly based on timely and sufficient beach nourishment. When the width of beaches is reduced, not only their wave-absorbing function, but also their recreational opportunities decrease. Thus, recreational beaches should be at least 35 m wide. An important factor for comfortable recreation on the beach is the material forming it. Artificial wave-absorbing pebble and crushed stone beaches have the greatest efficiency and creation and operation of such beaches is 2–3 times cheaper than the creation of sandy beaches from the economic point of view (less volumes of initial filling, abrasion and entrainment of beach-forming material) [2]. The optimum material size for recreational purposes is 30–40 mm.

Currently, a common problem for the Crimean coastline is the significant wear and damage of coast protection structures, the service life of which is close to the limit (50 years) [3]. A significant part of them is in an emergency condition as they were not properly maintained: no beach nourishment has been made, storm-damaged structures were not repaired. From 2014 to the present day, a significant number of coast protection complexes have been reconstructed in the Republic of Crimea under the Federal Target Program. No master plan for coast protection has been implemented in the region. In accordance with Point 5.8 of Regulations 277.1325800.2016 [1)], additional scientific research is required for its development. In this regard, it is an urgent task to study the dynamics of beaches of different areas of the peninsula under the influence of real extreme storm situations with the help of mathematical modeling methods.

One of the modern freely available models for the study of coastal zone reshaping by hydrodynamic processes is the two-dimensional XBeach (eXtreme Beach behavior) model [2)] [4, 5]. Regional modeling studies of coastal zone dynamics

---

[1)] JSC TsNIITS, 2016. *Book of Rules СП 277.13258000.2016. Coastal protection constructions. Design rules*. Moscow, 91 p. (in Russian).

[2)] Roelvink, D.J.A., van Dongeren, A., McCall, R.T., Hoonhout B., van Rooijen, A., van Geer, P., de Vet, L., Nederhoff, K. and Quataert, E., 2015. *XBeach Technical Reference: Kingsday Release. Model Description and Reference Guide to Functionalities*. Delft: Deltares, 141 p. doi:10.13140/RG.2.1.4025.6244

for the Black Sea coasts have been carried out for the Bulgarian [6, 7] and Western Crimea coasts [8–15]. The application of the model to the problems of design and construction of protective hydraulic structures is described in [15].

The purpose of this work is to study the influence of extreme storms on the erosion zone width of an artificial pebble beach located in front of a vertical concrete seawall in the village of Koktebel on the basis of numerical modeling.

Characteristics of area under study

The anthropogenic load varies for different parts of the Crimean coastline. Thus, the eastern coast has been affected by economic activity to the least extent [16]. However, the coastal zone has been transformed to a significant extent in local areas, such as the popular resort village of Koktebel.

The village is located on the Black Sea coast of Koktebel Bay bounded by Cape Planerny from the south-west and Cape Lagerny from the east (Fig. 1). The coastline of the bay is about 7 km long. The bay is shallow: depths of 5 m are noted at a distance of about 200-300 m from the coast and those of about 10–15 m – at the outer boundary of the bay. Winds coming from the land side (sector 0°–90°) are most frequent (~39 %), and the maximum frequency of strong winds (more than 15 m/s) corresponds to the northeastern direction. From the sea side, the most wave-prone sector for the study area is 90°–180°. More than 50 % of all storms enter the study area from the east (90°) and east-southeast (112.5°), with the highest storm waves with heights greater than 2.5 m entering the bay from the east-southeast direction. A study of the bay wind climate based on a reanalysis of wind waves for the present climate period 1979–2020 is given in [17]. The analysis of extreme wave characteristics showed that the duration of storms with significant wave heights greater than 1.57 m varied from 5.6 to 34.3 days, with their average value of 16.4 days. The duration of storms averaged by months varies from 0.6 to 9.8 days. The longest storms (more than 7 days) occur from November to March. The minimum duration of storms (less than 1 day) is observed in May–August.

A detailed description of the anthropogenic impact on the Koktebel Bay coastal zone over the last 100 years is given in [18]. Since the 1950s, the active transformation of the coast began. Industrial extraction of sand and gravel mixtures, construction of a complex of coast protection structures (their refinement and reconstruction) over a significant length of the area led to degradation of natural sand, gravel and pebble beaches which had been 20–30 m wide before that. Blocking of cliffs and regulation of watercourses have led to the fact that at present the natural supply of Koktebel Bay beaches is provided by the abrasion of undeveloped cliffs in the western and eastern parts of the bay and the intake of biogenic material from the underwater coastal slope. Since almost half of the coastal zone is occupied by man-made shores (about 3 km), beaches are largely composed of imported material [18].

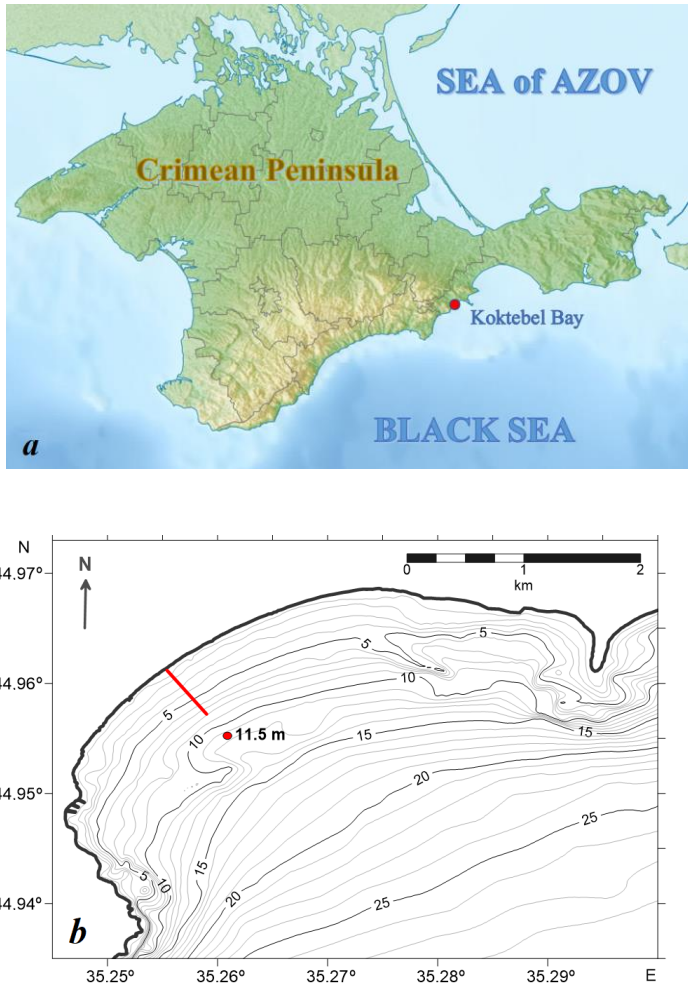

Fig. 1. Location of the area under study (*a*); bathymetric map of Koktebel Bay (*b*) (reference point with depth of 11.5 m for SWAN-ERA statistical analysis; red line represents profile of the modeled coastal zone)

In [19], a study of the current granulometric composition of sediments in the Koktebel coastal zone is presented. It is found that the granulometric composition of the sediment is quite varied: coarse-grained pebble and gravel material predominates in the nearshore zone with an admixture of coarse- and fine-grained sandy material (about 15 %); the central part of the beaches consists mainly of coarse gravel (27 %) and coarse sand (26 %) with inclusions of fine gravel (18 %) and medium sand (14 %); coarse gravel predominates (about 60 %) in the rear zone of the beaches.

Reconstruction of the complex of coast protection structures of Koktebel settlement was last carried out in the late 1980s when embankments were built, an artificial beach was created and a reserve crushed stone filling was made on the westernmost section of the coast. This scheme of coast protection structures functioned effectively. However, the area of the reserve filling was developed at the beginning of the 21st century, which resulted in active degradation of beaches and made it necessary to reconstruct the complex of coast protection structures [18]. Reconstruction of the embankment and restoration of the Koktebel Bay beaches with a total length of 1850 m are currently in progress (the period of works is 2023 – end of 2024). The project takes into account the results of this work.

Materials and methods

Data from retrospective wind wave calculations for 1979–2020 from the model data array (hereinafter referred to as the SWAN-ERA array) were used to calculate storm deformations of the beach profile. The reanalysis was obtained using SWAN (Simulating Waves Nearshore) numerical spectral model [20] on an unstructured computational grid with densification in the Black Sea coastal zone [21]. Atmospheric forcing of the model was provided by data from ERA-Interim and ERA5 global atmospheric reanalyses [3)].

A node of the calculation grid located in the centre of Koktebel Bay at an isobath of ~11.5 m was selected from the SWAN-ERA array (Fig. 1, *b*). Long-term series of parameters with a time discreteness of 1 h were formed for this point, including: wind speed and direction at a height of 10 m; significant wave height h_s; mean wave period $\bar{\tau}$; mean wave direction θ; peak wave period τ_p. The calculated operational wave characteristics for Koktebel Bay are presented in [17]. For further calculations, storms were identified from the SWAN-ERA array and the SPI (storm power index) was calculated.

Condition [22] was used as a criterion to distinguish storms

$$h_s \geq \bar{h}_s + 2 \cdot \sigma, \quad (1)$$

where h_s is significant wave height at a fixed moment of time, m; $\bar{h}_s$ = 0.61 m is long-term average of h_s for this series; σ = 0.48 m is standard deviation of the h_s series. We obtain that the minimum threshold value of significant wave height is h_{st} = 1.57 m. Thus, a storm is an event defined as a period of time during which h_s exceeds the minimum threshold value of h_{st} for a sufficiently long time.

The SPI was calculated with formula [22, p. 5]

$$SPI = h_d^2 \cdot T_p, \quad (2)$$

where h_d is average value of h_s for the storm period, m; T_d is storm duration, h.

[3)] Available at: https://www.ecmwf.int/en/forecasts [Accessed: 20 August 2024].

The coastal zone profile for modeling was selected to correspond to the central part of the Koktebel village embankment (Fig. 1, *b*). A profile of the coastal slope was constructed based on the survey data of the nearshore water area of the bay. In the beach area, the original profile was rearranged according to the parameters of the dynamic equilibrium profile of the pebble beach with a mean particle size of homogeneous pebble material D_{50} equal to 30 mm, which corresponds to the most comfortable beach recreation.

Based on the data on the wave regime in Koktebel Bay [17], the parameters of the transverse profile of the above-water and underwater parts of the beach were calculated according to the regulatory methodology set out in Regulations 277.13258000.2016 [1)] which define the procedure for the arrangement of coast protection structures on the seashore of the Russian Federation. The calculations were carried out for the third wave breaking, the wave height at the line of the first breaking of 1 % probability was 2.55 m and it was 1.45 m at 30 % probability. According to data from the Feodosia Marine Hydrometeorological Station, in the Baltic Sea System (BS), the sea level of 1% probability of the highest annual values is H1% = 0.28 m BS; mean sea level is H50% = −0.2 m BS. Fig. 2, *a* shows the obtained dynamic equilibrium profile of the beach.

On the coast, the model profile is bounded by a steep concrete embankment seawall which was given as a non-erodible object with a height mark of 4 m. Further, the initial profile was changed in the nearshore part: the width of the artificial pebble beach was assumed to be equal to 10 (F10), 20 (F20), 30 (F30) and 40 m (F40) in front of the embankment seawall (Fig. 2, *b*). Since the width of the estimated dynamic equilibrium profile is about 24 m, the beach profile was linearly extended at the 2.73 m height mark for a width of more than 20 m.

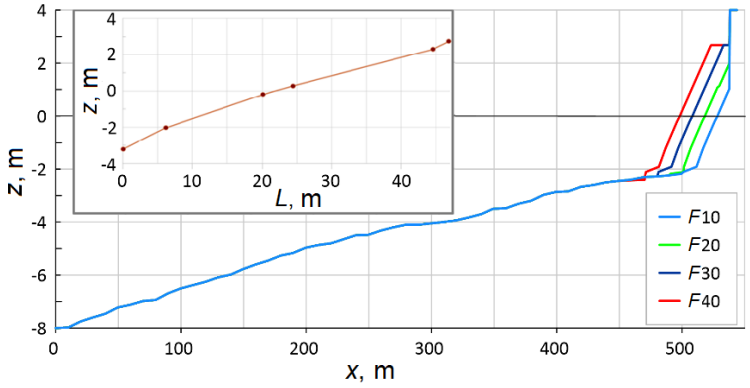

Fig. 2. Modeling profiles at the width of the designed beach F10 = 10 m, F20 = 20 m, F30 = 30 m and F40 = 40 m in the central part of the embankment in the village of Koktebel. The inset shows the estimated dynamic equilibrium profile for a mean particle size of 30 mm

A one-dimensional version of the XBeach numerical model was used to simulate storm deformation of beach and underwater coastal slope profiles. The source code of the model is in the public domain [4]. The model uses a local coordinate system in which axis x is orientated in the coastal direction perpendicular to the coastline.

The storm waves at the seaward boundary of the computational domain ($x = 0$) were given with JONSWAP [2] spectrum which is defined by angular wave dispersion index s = 10, significant wave height h_s and peak wave period τ_p.

The spatial resolution in the XBeach model was 0.5 m and the computational domain length was ~550 m. The model time integration was performed with a step $\Delta t = 0.025$ s. During the time integration, the beach profiles $z(x, t)$ were produced with a discreteness of 1 h. The beach profile deformation at time t was estimated as

$$\Delta z(x,t) = z(x,t) - z(x,0), \quad (3)$$

where $z(x, 0)$ is beach profile at $t = 0$.

Discussion of results

SPI calculation for the Koktebel Bay central part made it possible to identify 146 storms with duration of at least 12 h from SWAN-ERA data for 1979–2020. The selected storms exhibit SPI values that range between 62 and 660 m²·h, with average duration of the active phase of storms T = 26 h. During the developed phase of the storm, significant wave height h_s varies from 2.3 to 3.6 m, with an average value of 2.6 m. Table 1 presents the characteristics of 25 strongest storms according to storm power index ranked in descending order of its value.

Figs. 3–5 show significant wave height and mean wave direction for three different storms which are extreme by storm index, mean h_s and active phase duration.

The first storm situation, designated as S1, commenced on 10 November 2007 and was constituted by a deep, rapidly moving autumn cyclone (Fig. 3). The active phase of the storm lasted 25 h. The prevailing winds were of southeastern and southern directions. The mean significant wave height (h_s) for the active phase of the storm was 3.6 m (the maximum value for all identified storms); period (τ_p) was 9.6 s. At the same time, the SPI storm index was only 320 m²·h (Table 1).

The second (S2) (Fig. 4) and third (S3) (Fig. 5) storm situations commenced on 26 January 1988 and 25 September 2017, respectively. The storms in question were caused by the occurrence of intense prolonged low-moving anticyclonic anomalies characterised by winds originating from the east-southeast (112.5°). Storm S2, having the maximum value of the SPI power index equal to 660 m²·h, is characterised by the following parameter values for the active phase: h_s = 2.9 m; τ_p = 9.4 s; T = 72 h. Storm S3 exhibited the longest active phase duration of all identified storms, spanning a total of 95 h, the power index was 625 m²·h, with a mean significant wave height of 2.6 m.

[4] Available at: http://oss.deltares.nl/web/xbeach [Accessed: 20 August 2024].

Table 1. Characteristics of intense storms in the central part of Koktebel Bay according to the SWAN-ERA wave reanalysis data for 1979–2020

Storm start date, yy. mm. dd	Storm duration, h	Average value, h_s, m	Storm Power Index, $m^2 \cdot h$
1988.01.30	77	2.9	660
2017.09.25	95	2.6	625
1979.02.18	83	2.7	623
1993.11.22	87	2.7	615
2005.02.03	94	2.5	570
2012.01.25	67	2.9	560
2014.10.25	58	2.8	465
2012.02.06	40	3.4	460
1997.12.15	55	2.9	450
1983.09.19	56	2.7	398
1998.01.22	50	2.8	378
1988.03.01	53	2.6	360
1993.11.29	50	2.7	360
1981.02.28	44	2.8	338
2007.11.10	25	3.6	320
1987.10.27	44	2.7	312
1993.01.02	45	2.6	310
1994.10.21	38	2.9	308
2020.02.10	30	3.1	286
1979.12.25	39	2.7	274
2002.12.01	32	2.9	263
1993.11.10	38	2.6	256
1980.01.03	32	2.8	254
2008.11.22	28	3.0	252
2001.11.24	24	3.2	249

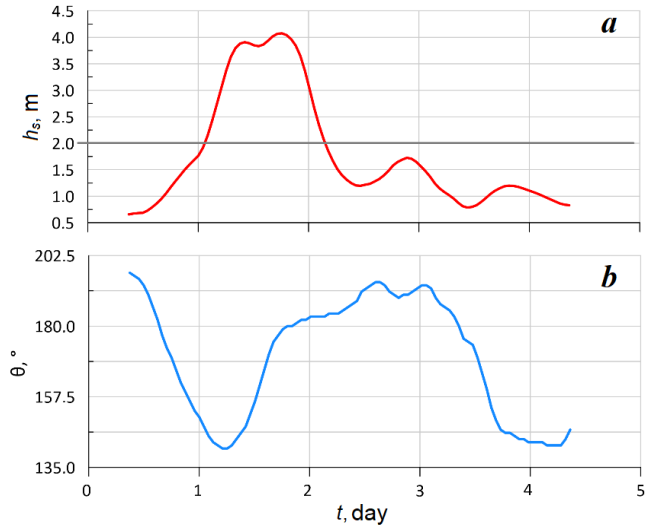

Fig. 3. Significant wave heights (*a*) and mean wave direction (*b*) in the central part of Koktebel Bay for storm (S1) which is extreme by significant wave height value (h_s = 3.6 m, T = 25 h, SPI = 320 m^2·h) according to SWAN-ERA data

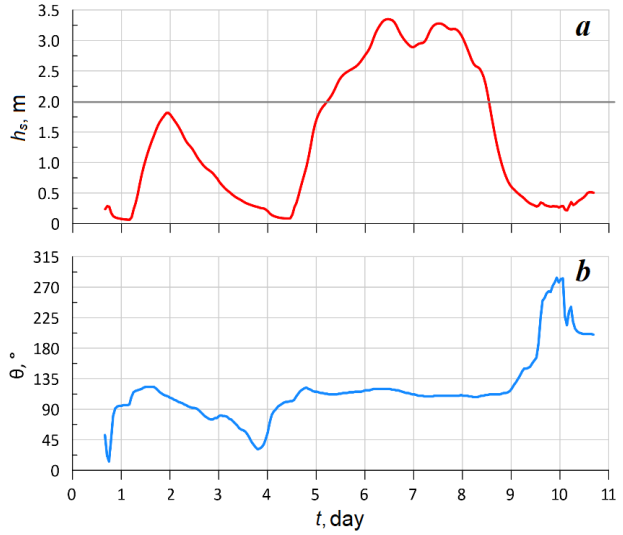

Fig. 4. Significant wave heights (*a*) and mean wave direction (*b*) in the central part of Koktebel Bay for storm (S2) which is extreme by storm index (SPI = 660 m^2·h, h_s = 2.9 m, T = 77 h) according to SWAN-ERA data

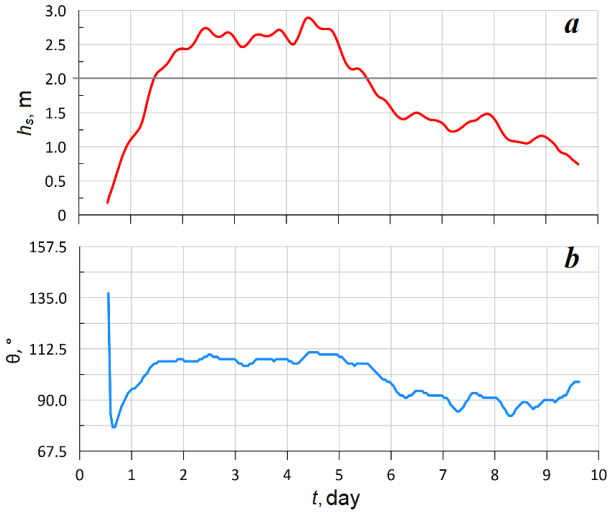

Fig. 5. Significant wave heights (*a*) and mean wave direction (*b*) in the central part of Koktebel Bay for storm (S3) which is extreme by duration (T = 95 hours, h_s = 2.6 m, SPI = 625 m^2·h) according to SWAN-ERA data

Figs. 6, 7 show the modeling results of the artificial pebble beach deformation profile for their four options during S1 and S2 storms having maximum values of height and power index.

A detailed examination of the graphical data allows us to make the following observations. Under the impact of storm waves, the coast steepness near the coastline changes gradually and pebble material from the beach nearshore part slides down the underwater slope leading to a local depth decrease near the shore. In the upper part of the beach profile, the process of erosion occurs, which results in the retreat of the coastline. The extent of the bottom deformation zone from the coastline is significantly greater than that of the erosion zone of the above-water part of the beach. The most significant deformations of the beach profile occur during the initial stages of the storm. Subsequently, the deformation rate declines due to the increase in wave energy dissipation on the underwater ledge formed by waves.

In order to quantify the extent of coastal zone deformations induced by storms, the following calculations were performed for each of four profile options: L_C – erosion zone width of the coast; L_S – extent of the bottom deformation zone from the coastline towards the sea. The starting point for determining the L_C and L_S parameters was the position of the coastline at the initial moment of time. The outer boundary of the bottom deformation zone was identified by locating the coordinate of the initial point out at sea, at which the bottom deformation reached a value of 0.1 m in absolute terms.

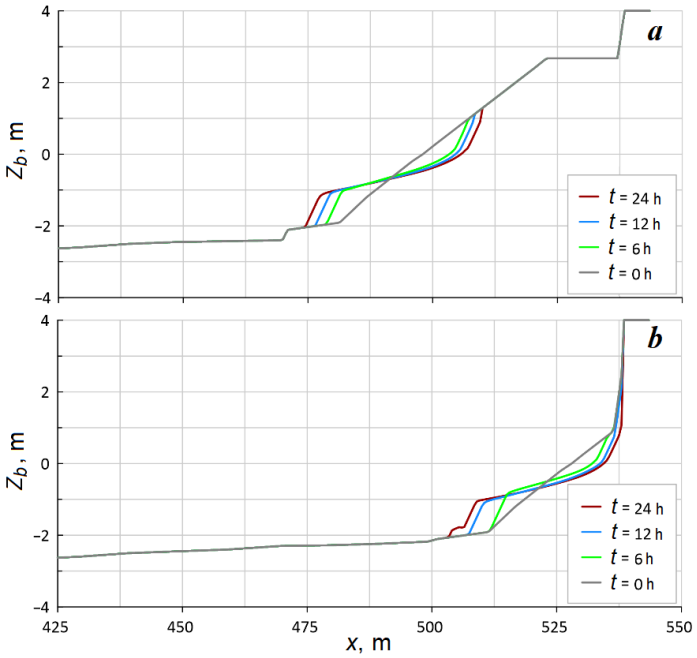

Fig. 6. Calculated beach profile F40 (*a*) and F10 (*b*) for four points of time during S1 storm

Tables 2, 3 present the results of the L_C and L_S parameter calculations. The data indicate that the most significant changes in L_C and L_S occur during the initial six hours of a storm. Therefore, the rate of shoreline retreat can reach 3.9–5.3 m even in a relatively brief storm. Following a period of storm activity lasting 24 hours, the L_C values for the S1 storm were observed to range between 6.4 and 8.3 m, while those for the S2 storm ranged between 6.1 and 6.7 m. At the end of the S2 storm (t = 72 h), the L_C values attained a maximum range of 9.1–10.0 m. The extent of the underwater erosion zones is three times greater than that of the erosion zones of the above-water part of the beach for all profile types.

The most critical situation occurs at the end of the S2 storm for a profile with a beach width of 10 m (F10): the value of L_C = 10 m at t = 72 h. Storm waves erode the beach completely down to the base of the protection seawall, which can be clearly seen in Fig. 7, *b*. At the same time, the calculated bottom deformation zone also reaches maximum values, with L_S = 26.5 m. This phenomenon can be attributed to the augmented backflow that occurs when waves reflect off a concrete seawall and pulls the material to greater depths. A profile with a beach width of 20 m (F20) will result in a shoreline retreat of 9.7 m at the end of the S2 storm, thus leaving an above-water beach width of 10.3 m.

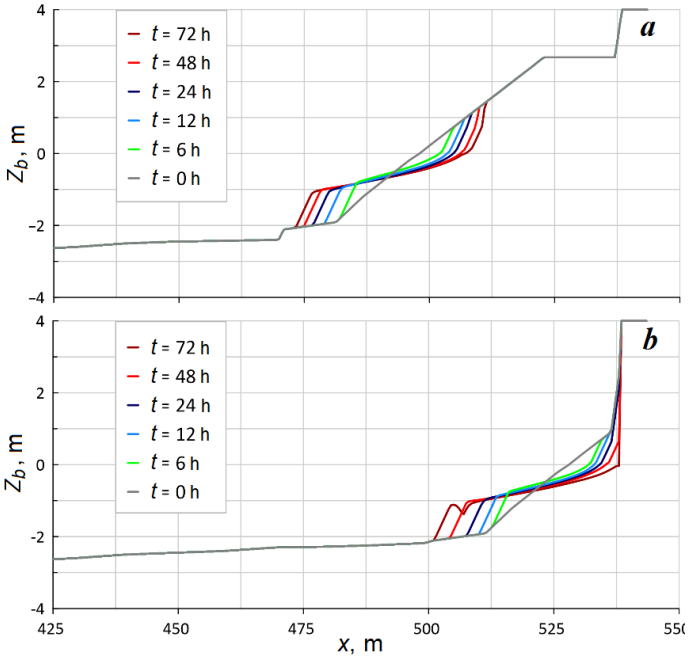

Fig. 7. Calculated beach profile F40 (*a*) and F10 (*b*) for six points of time during S2 storm

Table 2. Erosion zone width of the above-water part of beach L_C (m) at different durations of S1 and S2 storms

Beach profile	S1			S2				
	Storm duration, h							
	6	12	24	6	12	24	48	72
F40	5.3	6.5	7.6	4.0	5.5	6.7	8.2	9.1
F30	4.1	5.8	7.3	3.9	5.2	6.5	8.1	9.7
F20	5.0	6.9	8.3	4.0	5.5	7.2	8.8	9.7
F10	4.1	5.7	6.4	3.9	5.0	6.61	7.3	10.0
Averaged	4.6	6.2	7.4	4.0	5.3	6.6	8.1	9.6

Table 3. Width of bottom deformation zone L_S (m) from the coastline at different durations of S1 and S2 storms

Beach profile	S1			S2				
	Storm duration, h							
	6	12	24	6	12	24	48	72
F40	18.5	21.0	23.0	15.0	18.5	20.5	22.5	24.0
F30	16.5	19.0	23.0	14.0	17.5	20.5	23.5	25.5
F20	18.0	20.5	23.0	15.0	18.0	20.0	22.5	24.0
F10	15.5	20.0	24.0	14.5	17.5	20.0	23.0	26.5
Averaged	17.1	20.1	23.3	14.6	17.9	20.3	22.9	25.0

In the more intense but less prolonged S1 storm, no erosion of the F10 profile to the foundation of the protection seawall is observed. After the storm, the beach width is ~3.5 m, and even a relatively minor swell will cause the embankment seawall to be bombarded with pebbles and to collapse as soon as possible.

The calculations conducted for the S2 storm demonstrated that the profile deformations remained insignificant even after 48 hours of storm impact. The results for a longer, weaker storm (S3) yielded comparable outcomes and are not included in the paper. Accordingly, calculations for a longer, weaker storm were not conducted.

Thus, the results of the numerical experiments suggest that at mean particle size of the beach-forming material D_{50} = 30 mm, the construction of artificial beach profiles with a width of 20 m or more can serve to mitigate the impact of storm surges, thereby providing an effective means of protection from extreme wave action.

Conclusion

The storm power index (SPI) was calculated for the central part of Koktebel Bay based on the wave reanalysis data for 1979–2020. A total of 146 storms with a minimum duration of 12 h were also identified. Three most extreme storms were analyzed. The storm of 10–11 November 2007 had the maximum value of significant wave height (h_s = 3.6 m). The storm of 26–29 January 1988 was the most powerful (SPI = 660 $m^2 \cdot h$) in the 41-year period under review. The storm situation of 25–29 September 2017 was also identified as the longest on record (T = 95 h).

For real extreme storms, the deformation profile of the artificial pebble beach located in front of the steep seawall of the embankment was calculated. The width of the beach was 10, 20, 30 and 40 m. It was shown that under the impact of storm waves,

the coast steepness near the coastline changed gradually and material from the beach nearshore part slid down the underwater slope leading to a local depth decrease near the shore.

In the upper part of the beach profile, erosion occurs, resulting in the retreat of the coastline. The length of the erosion zone of the underwater coastal slope in the nearshore zone is three times the width of the above-water beach erosion. The most significant deformations of the beach profile occur during the first 6 hours of storms. Further, the beach deformation rate decreases due to the increase in wave energy dissipation on the underwater ledge formed by waves. The erosion of the above-water part of the beach can reach 10 m.

In light of the findings from the numerical experiments, it can be concluded that at mean particle size of the beach-forming material D_{50} = 30 mm, a beach 10 m wide or less in front of a cliff or breakwater cannot absorb the energy of storm waves. Even a brief storm would result in significant erosion of the beach and active erosion of the breakwater seawall by pebble bombardment. It is improbable that the beach at this location would be restored naturally, as the reflection of waves from the surface of the seawall would tend to pull beach-forming material down to depth and carry it away by the longshore flow.

The study revealed that ≥ 20 m wide pebble beaches would fully absorb the wave energy of extreme storms and provide adequate protection. Nevertheless, when designing a beach with recreational value, it is recommended that the width of the beach exceed 30 m.

References

1. Shuisky, Yu.D., 2022. *Anthropogenous Relief of Coastal Zone of a Seas (the Black and Azov Seas for Example)*. Odessa: Fenix, 102 p. (in Russian).
2. Shakhin, V.M., Ribka, V.G. and Yaroslavtsev, N.A., 2001. A Modern Condition of a Coastal Zone and Coastal-Protection Structures of the Black and Azov Seas within the Limits of Krasnodar Region. In: N. A. Aibulatov, ed., 2001. *The Mankind and the Coastal Zone of the World Ocean in XXI Century*. Moscow: GEOS, pp. 423–429 (in Russian).
3. Goryachkin, Yu.N. and Markov, A.A., 2009. Effectless Analysis of Reconstruction of Crimean Coastal Protection Structures. *The Hydrotechnika*, (3), pp. 2–9. https://doi.org/10.55326/22278400_2023_3_2 (in Russian).
4. Roelvink, D., Reniers, A., van Dongeren, A., van Thiel de Vries, J., McCall, R. and Lescinski, J., 2009. Modelling Storm Impacts on Beaches, Dunes and Barrier Islands. *Coastal Engineering*, 56(11–12), pp. 1133–1152. https://doi.org/10.1016/j.coastaleng.2009.08.006
5. Bolle, A., Mercelis, P., Roelvink, D., Haerens, P. and Trouw, K., 2011. Application and Validation of Xbeach for Three Different Field Sites. *Coastal Engineering Proceedings*, 1(32), sediment 40. https://doi.org/10.9753/icce.v32.sediment.40
6. Kuznetsova, O.A. and Saprykina, Ya.V., 2017. Intra-Annual Storm Deformations of Sandy Beach by an Example of Kamchia-Shkorpilovtsi Coast (Black Sea, Bulgaria). *Processes in Geomedia*, (1), pp. 435–444 (in Russian).

7. Kuznetsova, O.A. and Saprykina, Ya.V., 2019. Modeling the Dynamics of a Sand Beach Governed by the Wave and Underwater Bar Interaction. *Geomorfologiya*, (3), pp. 57–67. https://doi.org/10.31857/S0435-42812019357-67 (in Russian).

8. Kharitonova, L.V., Ivancha, E.V. and Alekseev, D.V., 2015. Effect of Storm Surges and Wind Waves on Morphodynamic Processes in the Bakalskaya Spit Region. *Physical Oceanography*, (1), pp. 73–84. https://doi.org/10.22449/1573-160X-2015-1-73-84

9. Korzinin, D.V., 2015. Features of Formation Equilibrium Profile Underwater Coastal Slope (Accumulative Coast of the West Crimea As Example). *Ecological Safety of Coastal and Shelf Zones of Sea*, (1), pp. 29–33 (in Russian).

10. Gurov, K.I., Fomin, V.V. and Lazorenko, D.I., 2016. Mathematical Modeling of the Redistribution of Sand Fractions According to a Underwater Coastal Slope Under the Influence of the Wind Waves. *Ecological Safety of Coastal and Shelf Zones of Sea*, (3), pp. 65–71 (in Russian).

11. Fomin, V.V., Gurov, K.I., Udovik, V.F. and Konovalov, S.K., 2016. Dynamics of the Nearshore Zone of Kalamitskiy Gulf (Black Sea) under Influence of Wind Waves. In: International EMECS Center, 2016. *Proceedings of XXVI International Coastal Conference «Managing Risks to Coastal Regions and Communities in a Changing world»*. St. Petersburg, August 22–27, 2016. Academus Publishing, 2016. P. 1–1. https://doi.org/10.31519/conferencearticle_5b1b948b20d587.32401065

12. Gurov, K.I., Udovik, V.F. and Fomin, V.V., 2019. Modeling of the Coastal Zone Relief and Granulometric Composition Changes of Sediments in the Region of the Bogaily Lake Bay-Bar (the Western Crimea) during Storm. *Physical Oceanography*, 26(2), pp. 170–180. https://doi.org/10.22449/1573-160X-2019-2-170-180

13. Gurov, K.I., Fomin, V.V., Alekseev, D.V. and Ivancha, E.V., 2019. Sediments Granulometric Composition Dynamics in the Kalamitsky Gulf. In: MEDCOAST, 2019. *14th MEDCOAST Congress on Coastal and Marine Sciences, Engineering, Management and Conservation, MEDCOAST 2019.* Marmaris, 2019. Vol. 2, pp. 597–606.

14. Gurov, K.I. and Fomin, V.V., 2021. Influence of Storm Conditions on Changes in the Granulometric Composition of Bottom Sediments in the Coastal Zone of the Western Crimea. *Ecological Safety of Coastal and Shelf Zones of Sea*, (2), pp. 30–46. https://doi.org/10.22449/2413-5577-2021-2-30-46 (in Russian).

15. Fomin, V.V. and Goryachkin, Yu.N., 2022. Accounting for the Local Wave and Morphodynamic Processes in Coastal Hydraulic Engineering. *Physical Oceanography*, 29(3), pp. 271–290. doi:10.22449/1573-160X-2022-3-271-290

16. Goryachkin, Yu.N. and Efremova, T.V., 2022. Anthropogenic Impact on the Lithodynamics of the Black Sea Coastal Zone of the Crimean Peninsula. *Ecological Safety of Coastal and Shelf Zones of Sea*, (1), pp. 6–30. https://doi.org/10.22449/2413-5577-2022-1-6-30

17. Kharitonova, L.V., Fomin, V.V. and Alekseev, D.V., 2024. Wave Climate of Koktebel Bay (Crimea) of the Black Sea. In: T. Chaplina, ed., 2024. *Processes in GeoMedia—Volume VIII*. Springer Geology. Springer, 12 p. https://doi.org/10.1007/978-981-97-6627-7_28

18. Goryachkin, Yu.N., 2024. Anthropogenic Impact on the Coastal Zone of Koktebel Bay (Black Sea) over the Last 100 Years. *Ecological Safety of Coastal and Shelf Zones of Sea*, (2), pp. 6–22.

19. Gurov, K.I., 2023. Granulometric Composition of Sediments in the Coastal Zone of Koktebel Bay (Crimea). *Ecological Safety of Coastal and Shelf Zones of Sea*, (4), pp. 34–45.

20. Booij, N., Ris, R.C. and Holthuijsen, L.H., 1999. A Third-Generation Wave Model for Coastal Regions: 1. Model Description and Validation. *Journal of Geophysical Research: Oceans*, 104(C4), pp. 7649–7666. https://doi.org/10.1029/98JC02622

21. Divinsky, B.V., Fomin, V.V., Kosyan, R.D. and Ratner, Y.D., 2020. Extreme Wind Waves in the Black Sea. *Oceanologia*, 62(1), pp. 23–30. https://doi.org/10.1016/j.oceano.2019.06.003

22. Amarouche, K. and Akpınar, A., 2021. Increasing Trend on Storm Wave Intensity in the Western Mediterranean. *Climate*, 9(1), 11. https://doi.org/10.3390/cli9010011

Submitted 19.04.2024; accepted after review 27.05.2024;
revised 17.06.2024; published 25.09.2024

About the authors:

Lyudmila V. Kharitonova, Senior Research Associate, Marine Hydrophysical Institute of RAS (2 Kapitanskaya St., Sevastopol, 299011, Russian Federation), Ph.D. (Geogr.), **ORCID ID: 0000-0003-0705-0812, ResearcherID: Y-17802018**, *l.kharitonova@mhi-ras.ru*

Dmitry I. Lazorenko, Research Associate, Marine Hydrophysical Institute of RAS (2 Kapitanskaya St., Sevastopol, 299011, Russian Federation), Ph.D. (Tech.), **ORCID ID: 0000-0001-7524-565X, ResearcherID: J-1925-2015**, *d.lazorenko@mhi-ras.ru*

Dmitry V. Alekseev, Scientific Secretary, Marine Hydrophysical Institute of RAS (2 Kapitanskaya St., Sevastopol, 299011, Russian Federation), Ph.D. (Phys.-Math.), **ORCID ID: 0000-0003-4006-0967, ResearcherID: I-3548-2017**, *d.alekseev@mhi-ras.ru*

Vladimir V. Fomin, Chief Research Associate, Marine Hydrophysical Institute of RAS (2 Kapitanskaya St., Sevastopol, 299011, Russian Federation), Dr.Sci. (Phys.-Math.), **ORCID: 0000-0002-9070-4460, ResearcherID: H-8185-2015**, *v.fomin@mhi-ras.ru*

Contribution of the authors:

Lyudmila V. Kharitonova – literature review on the study problem, preparation of input parameters for numerical modelling, description of the study results, article text and graphic materials preparation

Dmitry I. Lazorenko – preparation of input parameters for numerical modelling, article preparation

Dmitry V. Alekseev – processing of the numerical modelling results, article preparation

Vladimir V. Fomin – problem statement, numerical experiments, processing and analysis of modelling results, preparation of the text of the article and graphic materials

All the authors have read and approved the final manuscript.

Original article

Synoptic Water Temperature Variations in Martynova Bay (Black Sea) in 2000–2020 and the Factors Defining Them

P. D. Lomakin [1] *, **M. A. Popov** [2]

[1] *Marine Hydrophysical Institute of RAS, Sevastopol, Russia*

[2] *A. O. Kovalevsky Institute of Biology of the Southern Seas of RAS, Sevastopol, Russia*

* *e-mail: p_lomakin@mail.ru*

Abstract

The paper analyses a sample of daily coastal observations to reveal patterns of water temperature temporal variability in Martynova Bay for 2000–2020. In the time course of water temperature, a response (in the form of positive and negative extremes) to synoptic processes in the atmosphere and sea was tracked. In the cold season, three groups of such extrema were identified. These are clearly expressed maximums in November determined by the transfer of warm air mass from the Transcaucasia to the Black Sea; minimums in December–February due to Arctic invasions; and less significant highs in February–March caused by the foehn wind effect. In the warm half of the year, two groups of extremes were identified in the time course of water temperature. These are maxima caused by overheated air masses, which spread to the Black Sea from the Sal steppes in June–August, and minimums in June–September associated with the influence of the Black Sea upwelling. It is shown that in the bays of the northern coast of the Heraclean Peninsula, fluctuations in water temperature caused by surge winds were insignificant. Their range did not exceed 1 °C, and the duration of the cycle, as a rule, was no more than one day.

Keywords: water temperature, anomalies, Arctic invasion, foehn, upwelling, surge phenomena, bays of Sevastopol, Crimea

Acknowledgements: The work was performed under state assignment of MHI RAS on topic FNNN-2024-0016 “Studies of spatial and temporal variability of oceanological processes in the coastal, near-shore and shelf zones of the Black Sea influenced by natural and anthropogenic factors on the basis of in situ measurements and numerical modelling” (code “Coastal studies”) and state assignment of IBSS on topic “Research of control mechanisms for production processes in biotechnological complexes with the aim of developing scientific foundations for obtaining biologically active substances and technical products of marine genesis”, state registration no. 121030300149-0

For citation: Lomakin, P.D. and Popov, M.A., 2024. Synoptic Water Temperature Variations in Martynova Bay (Black Sea) in 2000–2020 and the Factors Defining Them. *Ecological Safety of Coastal and Shelf Zones of Sea*, (3), pp. 110–122.

Синоптические вариации температуры воды в Мартыновой бухте (Черное море) в 2000–2020 годы и определявшие их факторы

П. Д. Ломакин [1] *, **М. А. Попов** [2]

[1] *Морской гидрофизический институт РАН, Севастополь, Россия*

[2] *Институт биологии южных морей им. А. О. Ковалевского РАН, Севастополь, Россия*

* *e-mail: p_lomakin@mail.ru*

Аннотация

На основе анализа выборки ежесуточных прибрежных наблюдений раскрыты закономерности временной изменчивости температуры воды в Мартыновой бухте с 2000 по 2020 г. Во временном ходе температуры воды отслежен отклик (в виде положительных и отрицательных экстремумов) на синоптические процессы в атмосфере и море. В холодное время года выявлено три группы таких экстремумов: отчетливо выраженные максимумы в ноябре, определявшиеся выносом на Черное море теплой воздушной массы из Закавказья; минимумы в декабре – феврале, обусловленные арктическими вторжениями; и менее значимые максимумы в феврале – марте как следствие фёнового эффекта. В теплое полугодие во временном ходе температуры воды выделены две группы экстремумов: максимумы, обусловленные перегретыми воздушными массами, которые распространялись на Черное море из района Сальских степей в июне – августе, и минимумы в июне – сентябре, связанные с влиянием черноморского апвеллинга. Показано, что в бухтах северного берега Гераклейского полуострова колебания температуры воды, вызываемые сгонно-нагонными ветрами, незначительны. Их размах не превышает 1 °С, а длительность цикла, как правило, не более 1 сут.

Ключевые слова: температура воды, аномалии, арктическое вторжение, фён, апвеллинг, сгонно-нагонные явления, бухты Севастополя, Крым

Благодарности: работа выполнена в рамках государственного задания ФИЦ МГИ по теме № FNNN-2024-0016 «Исследование пространственно-временной изменчивости океанологических процессов в береговой, прибрежной и шельфовых зонах Черного моря под воздействием природных и антропогенных факторов на основе контактных измерений и математического моделирования» (шифр «Прибрежные исследования») и государственного задания ФИЦ ИнБЮМ по теме «Исследование механизмов управления продукционными процессами в биотехнологических комплексах с целью разработки научных основ получения биологически активных веществ и технических продуктов морского генезиса», № гос. регистрации 121030300149-0.

Для цитирования: *Ломакин П. Д., Попов М. А.* Синоптические вариации температуры воды в Мартыновой бухте (Черное море) в 2000–2020 годы и определявшие их факторы // Экологическая безопасность прибрежной и шельфовой зон моря. 2024. № 3. С. 110–122. EDN MYQGGD.

Introduction

Martynova Bay is located in the south-west of Sevastopol Bay, at its mouth. Until the 1970s, it was not part of Sevastopol Bay. At present, the bay is separated from the open sea by the southern breakwater. Its maximum depth is 17 m at the end of the breakwater. The meridional length and width at the entrance is about 480 m. Water exchange with the open sea is limited. Irrespective of wind direction and strength, smooth waves prevail in Martynova Bay. In the open part of the sea behind the southern breakwater, there is an oyster and mussel farm of LLC NIO Mariculture. In this water area, Institute of Biology of the Southern Seas (IBSS) regularly monitors water temperature (Fig. 1).

Time series of observations of aquatic environment parameters in coastal waters are extremely important for the improvement of knowledge in various fields of the marine science. The combination of coastal temporal observations with observations in open waters, which, as a rule, are presented as spatial distributions, allows revealing the regularities of temporal variability of the fields of oceanological variables in the oceans and seas [1, 2].

The results of the analysis of observations in the bay under study has applied significance because of their representativeness both for the entire Black Sea area and for the sea area off South-West Crimea, including bays and open areas of the Sevastopol seashore.

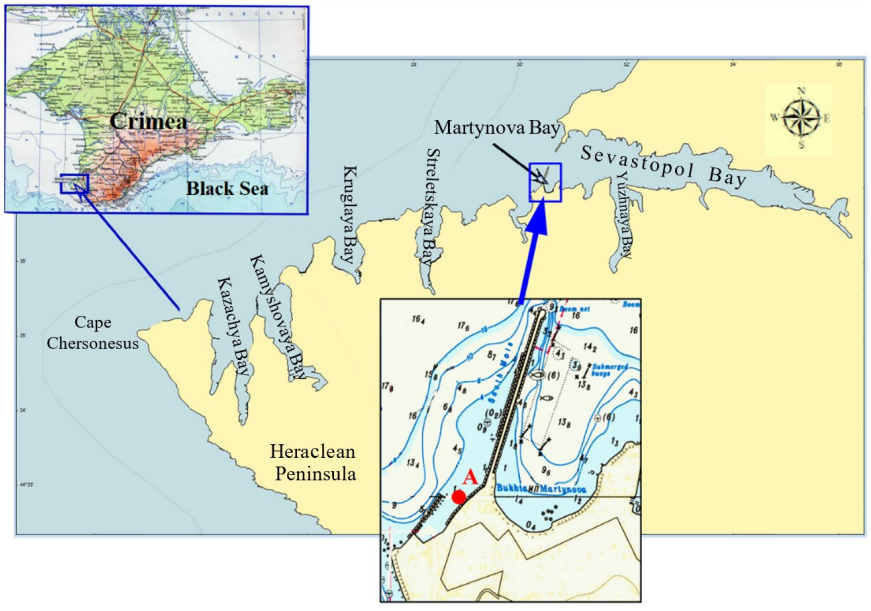

Fig. 1. Geographical position of Martynova Bay (A is the point of water temperature observations)

The aim of the work is to reveal the regularities of synoptic variability of water temperature in Martynova Bay for the time interval from 2000 to 2020 based on the analysis of coastal observations, as well as to identify the factors determining the corresponding types of fluctuations.

Source data and study methods

We analysed a sample of daily (conducted at 12:00 (GMT +3)) coastal water temperature observations from 2000 to 2020, which were taken in Martynova Bay near the oyster and mussel farm of LLC NIO Mariculture (point A in Fig. 1).

Information on the atmospheric synoptic situation in the Azov-Black Sea basin was obtained by analysing synoptic maps from the archive of Wetterzentrale Hydromet Centre (Germany) (URL: http://old.wetterzentrale.de/topkarten/fsreaeur.html).

Synoptic weather data for Sevastopol were taken from the Weather website of the marine meteorological station Chersonesos Lighthouse (URL: http://rp5.am/Погода_на_Херсонесском_маяке).

For ease of analysis, the entire initial set of actual water temperature observations was divided into two parts, referring to cold (November–April) and warm (May–October) half-years. The data was then averaged on a ten-day basis. Further, for each half-year in the coordinate system "current day, current year" and "current ten-day period, current year", temporal temperature sweeps were constructed (Figs. 2, 3), which were used to assess the response of the considered variable to synoptic processes in the atmosphere and in the sea, as well as to local regional processes.

The averaged schemes were calculated to filter out the noise and assess the significance of the extremes detected in the actual time sweeps. Only significant extremes that appeared in the mean ten-day sweeps were considered in detail.

Discussion of results

The temporal sweeps of both the actual and mean ten-day water temperature show positive and negative local extremes indicating processes of different time scales in the atmosphere and sea that determined the variability of the considered parameter of the aquatic environment (Figs. 2, 3).

In the cold season, three groups of such extremes were identified: pronounced maxima in November, minima in December–February and less significant maxima in February–March.

In November, in the temporal sweep of the actual water temperature, the maximum was observed in 15 cases (years) out of 21, whereas in the sweep of mean ten-day temperature, this extreme was quite clearly manifested only 12 times: in 2000, 2004, 2005, 2007–2010, 2012, 2015, 2018–2020 (Fig. 2).

In these years, the atmospheric synoptic situation was analysed for November using archived synoptic maps, which showed the following. The weather over the Black Sea was determined by the influence of the southern southwestern periphery of the Siberian High (Transcaucasia), which determined the heat transfer from the warmed continent (Fig. 4).

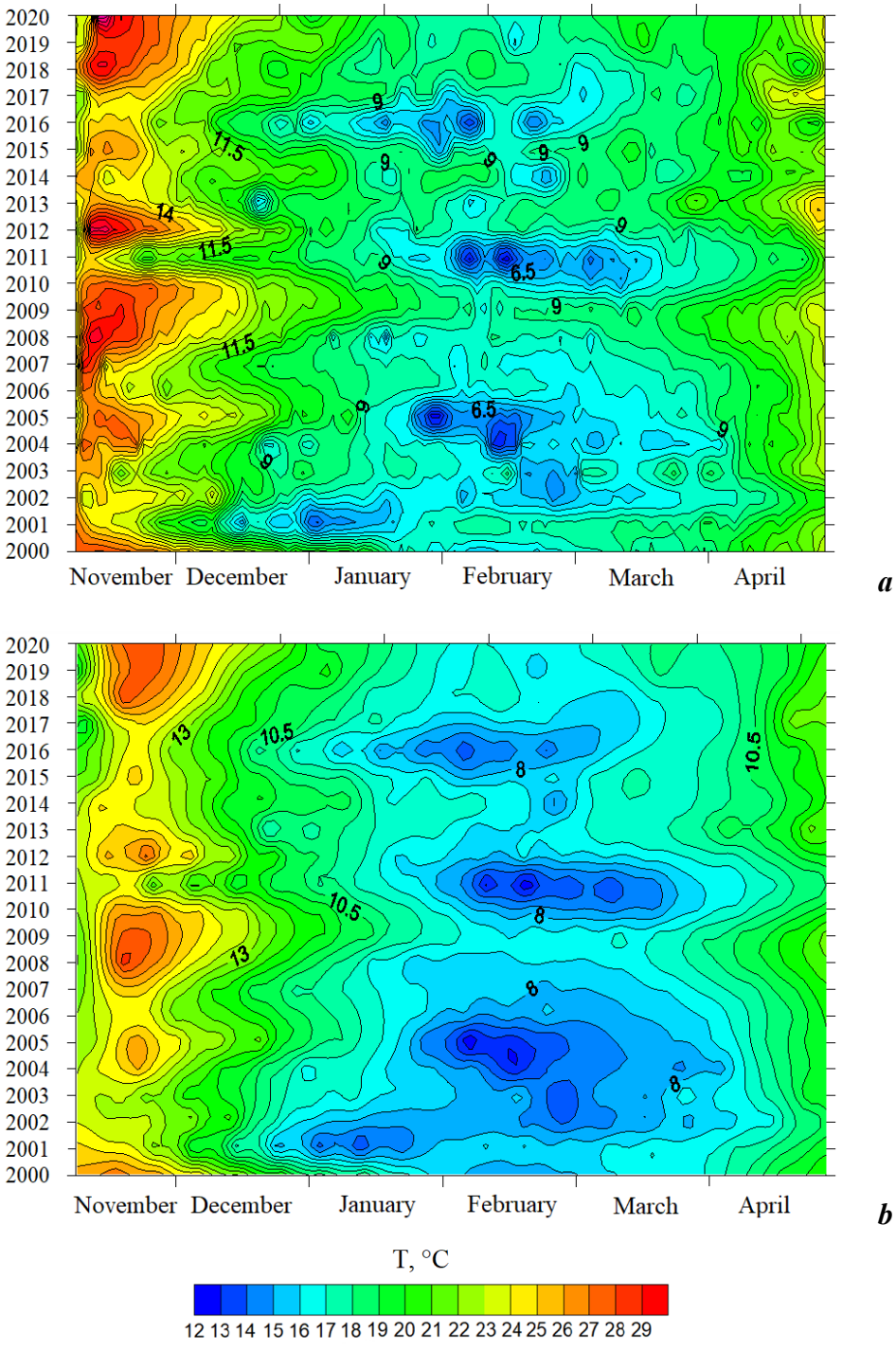

Fig. 2. Time variations of water temperature in Martynova Bay during the cold half of the year for 2000–2020: daily (*a*), average ten-day (*b*)

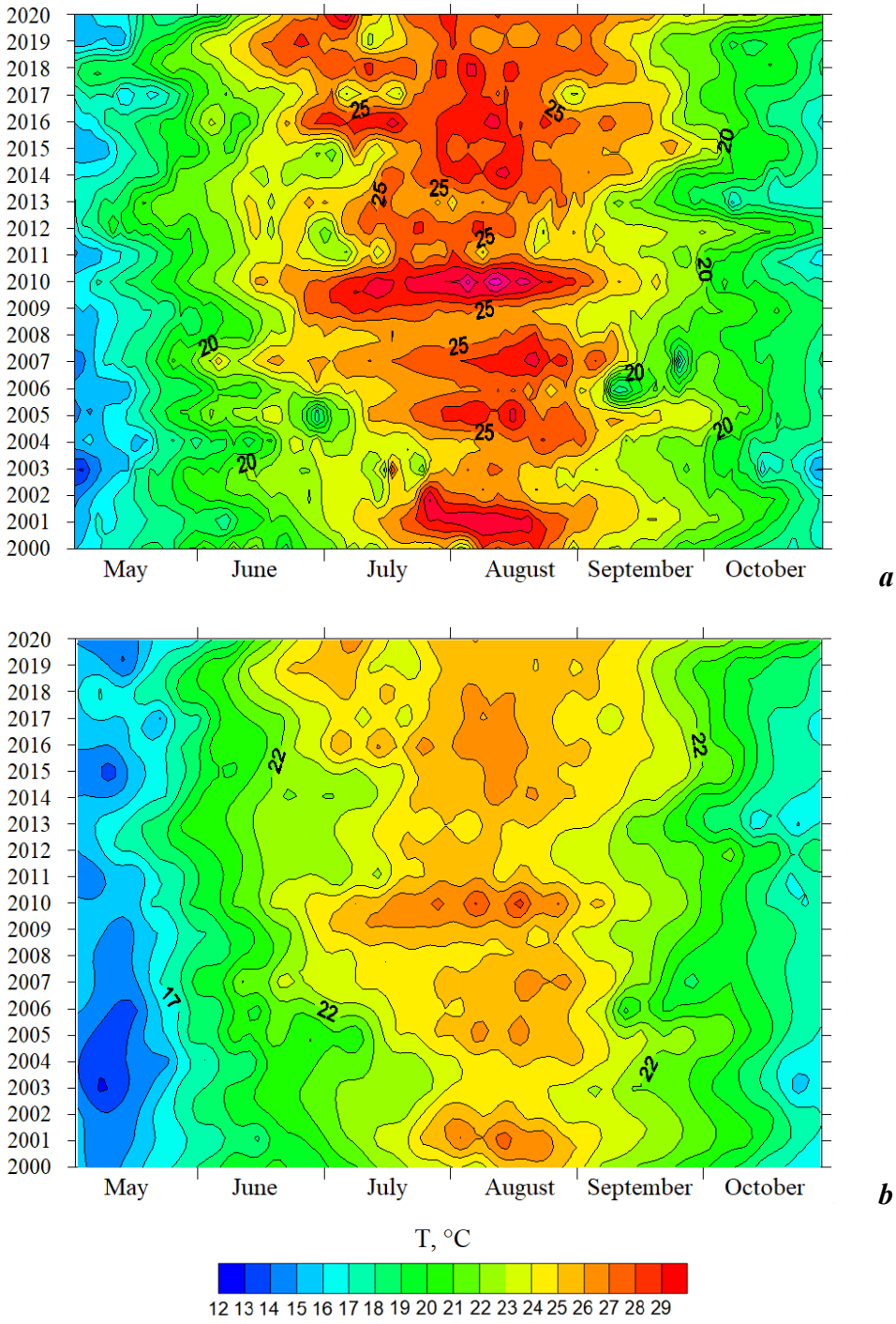

Fig. 3. Time variations of water temperature in Martynova Bay during the warm half of the year for 2000–2020: daily (*a*), average ten-day (*b*)

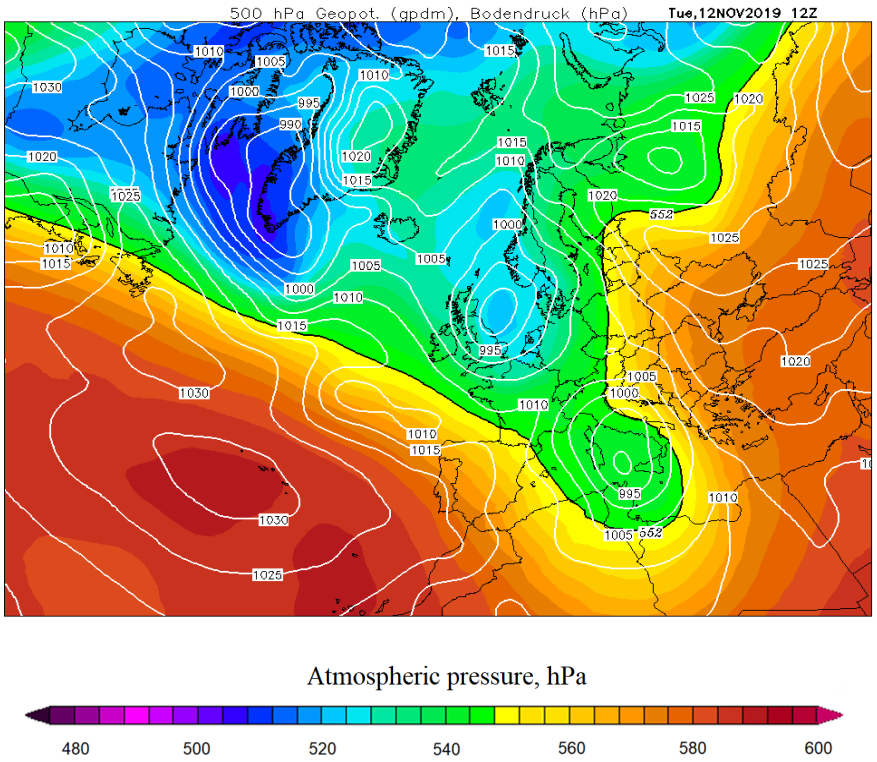

Fig. 4. Synoptic situation illustrating the transfer of heat from Transcaucasia to the Black Sea in the circulation system of the southern south-western periphery of the Siberian High, map on 12 November 2019, 12:00 GMT

During this atmospheric natural anticyclonic synoptic period lasting from 1 to 2 ten-day periods, the air in Sevastopol warmed up to 15–20°C and the water temperature in Martynova Bay increased by 0.6–1.7 °C against seasonal cooling and reached 15.1–17.4°C.

In similar situations, there is a noticeable warming of shallow top parts of Sevastopol bays, where vertical stratification of the temperature field also forms. At the boundary with the central parts of the bays, pronounced frontal temperature sections appear. In the morning, at the maximum difference of water and air temperature (up to 10 °C), steam fog can be observed over the top parts of the bays.

Another significant atmospheric natural synoptic process that contributed to the extreme cooling of coastal waters during the cold half-year is determined by the Arctic invasions of cold air masses. The synoptic situation typical of the Arctic invasion was determined by the rear part of a trough meridionally orientated

from the Kara Sea to the Black Sea (Fig. 5). The most powerful inflows of Arctic cold observed in December–February were accompanied by a significant (down to –17...–15 °C) drop in air temperature in Sevastopol, and the water temperature in Martynova Bay dropped to minimum values (4–6 °C).

In the time course of the actual water temperature, local minima associated with Arctic invasions were observed in 9 cases (years) out of 21 (see Fig. 2, *a*). In the sweep of the mean ten-day temperature for the cold half-year, the most significant extremes appeared 8 times: in 2001, 2003–2005, 2011, 2014–2016 (Fig. 2, *b*).

The insignificant increase in water temperature observed in February–March was due to a local meteorological phenomenon – the foehn effect.

In Sevastopol, foehn is usually observed in February with southeastern transfer in the atmosphere. In this case, a dry warm wind from the spurs of the Crimean

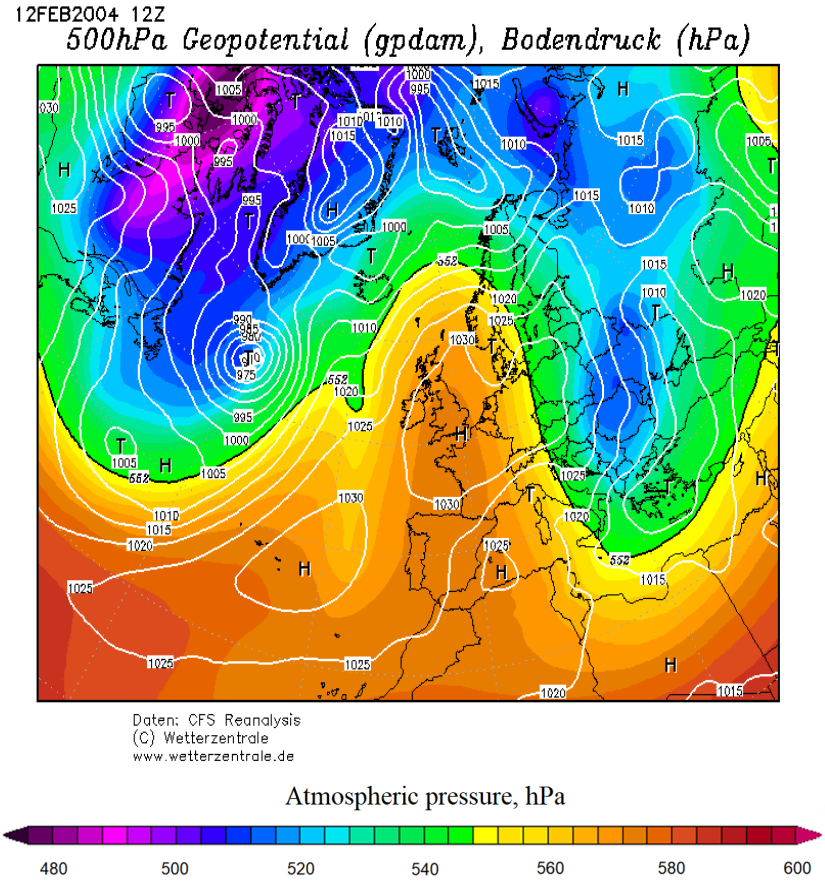

Fig. 5. Synoptic situation during the polar invasion of the Black Sea, map on 12 February 2004, 12:00 GMT

Mountains contributes to the inflow of warm air and setting in of dry clear weather with air temperatures in the Sevastopol region up to 20 °C and higher.

Foehn, as a local phenomenon lasting up to ten days, does not lead to a fairly significant increase in water temperature. According to the analysed data, the water temperature increase caused by the foehn effect is generally no more than 0.5 °C; in some cases, it can be 0.6–0.8 °C.

Foehns are a rather frequently observed phenomenon at the end of winter. In the field of actual water temperature, they were recorded almost annually except for four years with the lowest winter temperature: 2004, 2005, 2011, 2016 (Fig. 2, *a*).

The most intense foehns, which caused water warming in Martynova Bay by 0.6–0.8 °C, are quite rare and were observed only in 2015 and 2018–2020 (Fig. 2, *b*).

For the Sevastopol region, the foehn effect is extremely important in terms of ecology. A sharp increase in air temperature at the end of winter causes intensive snow melting in the catchments of Crimean rivers, which are traditionally considered polluted [3]. The water flow rate in the rivers almost instantly increases to values that are by an order of magnitude higher than average. At the same time, a huge number of pollutants enters the bays and open areas of the sea. These phenomena for the Balaklava Bay area are considered in detail in the book [4].

For the warm season, the time course of water temperature revealed two groups of extremes: distinct maxima in June–August and minima in June–September (see Fig. 3).

High actual water temperatures (26–28 °C) were observed in 2005, 2007, 2012, 2014–2017. The water in the analysed bay warmed up to the maximum (up to 28–30°C) in 2001 and 2010 (Fig. 3, a). In 2001, 2010, 2014–2017, the temperature maxima (27–28°C) were manifested in the mean ten-day sweep (Fig. 3, *b*).

The above cases were caused by extremely high air temperatures (up to 33–37 °C). In July–August, overheated air masses spread to the Azov–Black Sea basin by the northeastern wind from the Sal steppes, where the average summer air temperature reaches 35–45 °C [5]. At the same time, the synoptic situation was determined by the eastern southeastern periphery of the Azores High (Fig. 6).

In June–September, cyclic changes in water temperature were observed on the time scale from several days to 2–3 ten-day periods. These changes, accompanied by a significant decrease in water temperature, were caused by the coastal Black Sea upwelling. The coastal Black Sea upwelling, the most significant mechanism providing the water exchange between the shelf and deep-sea zones, is relatively well studied for the deep-water areas around the perimeter of the Black Sea. The nature of this phenomenon is attributed to the influence of atmospheric circulation over the Azov–Black Sea basin [6–8].

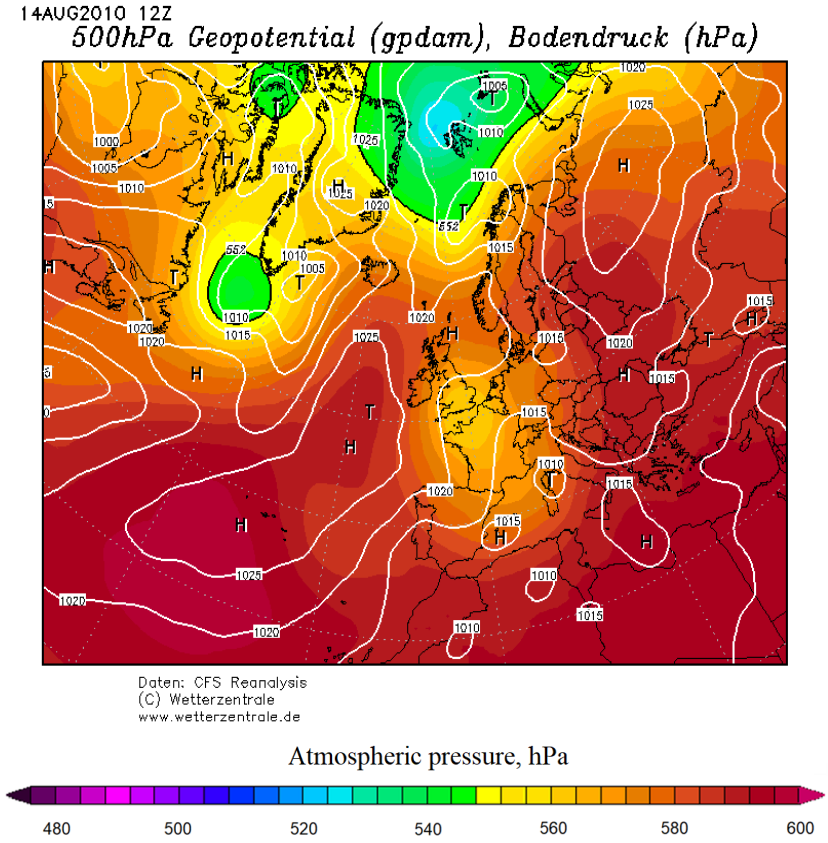

F i g . 6 . Synoptic situation in conditions of superheated air outflow to the Black Sea from the Sal steppes, map on 14 August 2010, 12:00 GMT

The features of the coastal Black Sea upwelling in Martynova Bay and on the Sevastopol seashore were analysed in the article [9] and are briefly listed below. The most powerful upwelling was observed in June 2001, June–July 2005, September 2006, September 2007, July–August 2011, July–August 2013, July–August 2015, July and September 2017, July 2019, July 2020 (Fig. 5). A total of 42 upwelling events with a temperature range of 2–7°C were recorded from 2000 to 2020. Their duration varied from 4 to 32 days.

The most frequent upwellings in Martynova Bay were recorded in June–July. The most intensive ones were recorded in June. The same pattern is typical of upwelling in the area of the depth gradient off the western coast of Crimea [7]. Upwellings with a cycle duration of 4–8 days had the highest frequency of occurrence (31 %). Upwellings with a cycle of 20–32 days were observed much less frequently. Their total frequency of occurrence was 11 %.

The typical properties of the hydrological regime of Sevastopol bays include surge phenomena [10]. The analysed dataset does not allow us to consider such phenomena due to the discreteness of observations.

Observations of water temperature, which were conducted in the Sevastopol marine fishing port in Kamyshovaya Bay and on the beach in Kruglaya Bay (Omega) with a discreteness of 6 h, showed that water temperature fluctuations caused by water surge winds were insignificant. Their magnitude did not exceed 1 °C and the cycle duration was generally not more than 1 day.

This effect can be explained by the morphometric features and location of the bays on the northern coast of the Heraclean Peninsula as well as by the wind regime of the Sevastopol region. The axial lines of the bays – from Kazachya Bay to Yuzhnaya Bay (see Fig. 1) – are oriented along the meridian, and the bays themselves face northwards with their open parts. The winds of the northern quarter cause an upsurge, while the winds of the southern quarter cause a downsurge.

A special property of the breeze circulation in the Sevastopol region is that the daytime northwesterly breeze as well as the nighttime northeasterly one have a significant northerly component, which often prevails over the gradient wind in the warm season. Therefore, during the warm half of the year, the northern coast of the Heraclean Peninsula with its bays is mainly affected by the upsurge winds. Southern quarter downsurge winds, which cause a decrease in water temperature, are rare. Moreover, they have a very limited acceleration within each of the bays, and the adjacent water area of the Sevastopol seashore has a relatively shallow depth.

The above mentioned allows us to suppose that near the northern shore of the Heraclean Peninsula and in the corresponding bays, the wind-induced water temperature fluctuations are insignificant and their range is not more than 1 °C.

Conclusion

Based on the analysis of a sample of daily coastal observations, the regularities of temporal variability of surface water temperature in Martynova Bay from 2000 to 2020 were considered, and the factors causing this variability were analysed.

In the time course of water temperature, both actual and average ten-day temperature, the response (in the form of positive and negative extremes) to synoptic processes in the atmosphere and in the sea was traced.

During the cold season, three groups of such extrema were identified: distinct maxima in November, minima in December–February and less significant maxima in February–March.

The increase in water temperature in November by 0.6–1.7 °C against a seasonal cooling was determined by the transfer of warm air masses from the Transcaucasia to the Black Sea in the circulation system of the southern south-western periphery of the Siberian maximum. A drop in water temperature to a minimum of 4–6 °C in December–February was provided by Arctic intrusions. The foehns in February–March were accompanied with water warming in Martynova Bay by about 0.5 °C.

During the warm half of the year, two groups of extrema were identified in the time course of water temperature: maxima in June–August and minima in June–September.

Extremely high water temperatures of 28–30 °C were caused by overheated air masses that travelled to the Black Sea from the Sal steppes, where the average summer air temperature reaches 45 °C. The synoptic situation over the Black Sea was determined by the eastern south-eastern periphery of the Azores High.

The cyclical changes of water temperature observed in June–September on a time scale from several days to 2–3 ten-day periods, which were accompanied with its decrease by 2–7 °C, were determined by the Black Sea upwelling.

In the bays of the northern coast of the Heraclean Peninsula, the water temperature fluctuations caused by water surge winds were insignificant. Their magnitude did not exceed 1 °C and the cycle duration was usually not more than 1 day.

References

1. De Steur, L., Sumata, H., Divine, D.V., Granskog, M.A. and Pavlova, O., 2023. Upper Ocean Warming and Sea Ice Reduction in the East Greenland Current from 2003 to 2019. *Communications Earth and Environment*, 4, 261. https://doi.org/10.1038/s43247-023-00913-3
2. Boss, E., Waite, A.M., Karstensen, J., Trull, T., Muller-Karger, F., Sosik, H.M., Uitz, J., Acinas, S.G., Fennel K. [et al.], 2022. Recommendations for Plankton Measurements on OceanSITES Moorings with Relevance to Other Observing Sites. *Frontiers in Marine Science*, 9, 929436. https://doi.org/10.3389/fmars.2022.929436
3. Gruzinov, V.M., Dyakov, N.N., Mezenceva, I.V., Malchenko, Y.A., Zhohova, N.V. and Korshenko, A.N., 2019. Sources of Coastal Water Pollution near Sevastopol. *Oceanology*, 59(4), pp. 523–532. https://doi.org/10.1134/S0001437019040076
4. Lomakin, P.D. and Popov, M.A., 2013. *Oceanological Characteristic and Estimation of the Water Pollution in the Balaklava Bay*. Sevastopol: ECOSI-Gifrofizika, 220 p. (in Russian).
5. Panov, V.D., Lurye, P.M. and Larionov, Yu.A., 2006. [*Climate of the Rostov Region: Yesterday, Today, Tomorrow*]. Rostov-on-Don: Donskoy Izdatelsky Dom, 488 p. (in Russian).
6. Ginzburg, A.I., Kostianoy, A.G., Soloviev, D.M. and Stanichny, S.V., 2000. Coastal Upwelling in the North-West Black Sea. *Earth Observation and Remote Sensing*, 15(6), pp. 933–948.
7. Borovskaja, R.V., Lomakin, P.D., Panov, B.N. and Spiridonova, E.O., 2008. Structure and Interannual Variability of Characteristics of Inshore Black Sea Upwelling on Basis of Satellite Monitoring Data. *Issledovanie Zemli iz Kosmosa*, (2), pp. 26–36 (in Russian).
8. Lomakin, P.D., 2018. Upwelling in the Kerch Strait and the Adjacent Waters of the Black Sea Based on the Contact and Satellite Data. *Physical Oceanography*, 25(2), pp. 114–123. https://doi.org/10.22449/1573-160X-2018-2-114-123
9. Lomakin, P.D. and Popov, M.A., 2021. Large-Scale Upwelling in the Sevastopol Seaside Area and its Influence on the Structure and Quality of Water. *Ecological Safety of Coastal and Shelf Zones of Sea*, (4), pp. 39–50. https://doi.org/10.22449/2413-5577-2021-4-39-50 (in Russian).
10. Ivanov, V.A., Ovsyany, E.I., Repetin, L.N., Romanov, A.S. and Ignatyeva, O.G., 2006. *Hydrological and Hydrochemical Regime of the Sebastopol Bay and its Changing under Influence of Climatic and Anthropogenic Factors*. Sevastopol: MHI NAS of Ukraine, 90 p. (in Russian).

Submitted 12.01.2024; accepted after review 4.05.2024;
revised 17.06.2024; published 25.09.2024

About the authors:

Pavel D. Lomakin, Leading Research Associate, Marine Hydrophysical Institute of RAS (2 Kapitanskaya St., Sevastopol, 299011, Russian Federation), Dr.Sci. (Geogr.), Professor, **ResearcherID: V-7761-2017, Scopus Author ID: 6701439810, IstinaResearcherID: 18321047**, *p_lomakin@mail.ru*

Mark A. Popov, Senior Research Associate, A. O. Kovalevsky Institute of Biology of the Southern Seas of RAS (2 Nakhimov Av., Sevastopol, 299011, Russian Federation), Ph.D. (Geogr.), **ORCID ID: 0000-0003-0220-1298, Scopus AuthorID: 57197871255**, *mark.a.popov@mail.ru*

Contribution of the authors:

Pavel D. Lomakin – setting the study goals and objectives, analysis of the obtained results, their interpretation, discussion of the results, writing the article

Mark A. Popov – construction of graphs, maps, qualitative analysis of the results and their interpretation, quantitative processing and description of the study results, discussion of the results, editing the article

All the authors have read and approved the final manuscript.

Original article

Trace Elements in the Components of the Aquatic Ecosystem of the North Crimean Canal and Irrigated Farmland

V. Yu. Proskurnin, N. Yu. Mirzoeva, O. D. Chuzhikova *, M. O. Vakhrushev

A. O. Kovalevsky Institute of Biology of the Southern Seas of RAS, Sevastopol, Russia
* *e-mail: olga88.chp@ya.ru*

Abstract
For 2022–2023, the concentrations of trace elements (Be, V, Fe, Co, Ni, Cu, Zn, As, Se, Mo, Cd, Sb, Tl, Pb, Ag) were determined in the aquatic ecosystem of the North Crimean Canal, adjacent irrigated soils and cultivated irrigated agricultural crops. The content of all studied elements was determined in their acidic concentrates and mineralizates in accordance with State Standard of Russia 56219-2014 by mass spectrometry with inductively coupled plasma on a PlasmaQuant MS Elite mass spectrometer (AnalytikJena, Germany) on the basis of the collective use center "Spectrometry and Chromatography", A.O. Kovalevsky Institute of Biology of the Southern Seas of RAS. The concentrations of heavy metals and trace elements in the aquatic ecosystem of the North Crimean Canal allowed safe use of the Dnieper water both for drinking and for other economic needs of Crimea. The maximum relative increase in the heavy metals pool due to irrigation of fields with the Dnieper water was for Mo (up to 0.1 %), Zn, Sb and Pb (no more than 0.04 %), which cannot affect the ecological state of the irrigated lands. In soils, a systematic excess of the maximum permissible concentrations was observed for Cd (up to 230 %) both in rice and wheat fields as well as in virgin lands. In rice and wheat crops, the maximum permissible levels for grain and grain fodder for Fe, Ni, Cd, As were exceeded. In the wheat ear, maximum permissible levels were exceeded for Fe (by 24 %), Ni (by 110 %) and As (by 70 %). Maximum permissible concentrations in rice grain were exceeded for Cu (by 29 %), Cd (by 150 %) and Pb (by 438 %), and in wheat grain – for Cd (by 360 %) and Pb (by 300 %). It was revealed that insignificant amounts of trace elements brought with the Dnieper water through the North Crimean Canal cannot have a noticeable effect on the irrigated farmland of Crimea. The detected excesses of maximum permissible concentrations and maximum permissible levels of trace elements in soils and agricultural crops are probably due to the activities of industrial enterprises in the north of the peninsula.

Keywords: North Crimean Canal, heavy metals in soil, heavy metals in plants, heavy metals in water, irrigated soils, agricultural plants, heavy metal pollution

Acknowledgments: The work was carried out within the framework of the Russian Science Foundation Grant, Project No. 23-26-00128: "The role of the North Crimean Canal irrigation system in the processes of transfer of long-lived radionuclides of Chernobyl origin, heavy metals, as well as hydrocarbons with Dnieper water to irrigated farmland of the Crimea".

For citation: Proskurnin, V.Yu., Mirzoeva, N.Yu., Chuzhikova, O.D. and Vakhrushev, M.O., 2024. Trace Elements in the Components of the Aquatic Ecosystem of the North Crimean Canal and Irrigated Farmland. *Ecological Safety of Coastal and Shelf Zones of Sea*, (3), pp. 123–138.

Микроэлементы в компонентах водной экосистемы Северо-Крымского канала и орошаемых сельхозугодий

В. Ю. Проскурнин, Н. Ю. Мирзоева, О. Д. Чужикова *, М. О. Вахрушев

Институт биологии южных морей имени А. О. Ковалевского РАН, Севастополь, Россия

* *e-mail: olga88.chp@ya.ru*

Аннотация

В 2022–2023 гг. в водной экосистеме Северо-Крымского канала, орошаемых почвах вдоль него и выращиваемых поливных сельскохозяйственных культурах были определены концентрации микроэлементов Be, V, Fe, Co, Ni, Cu, Zn, As, Se, Mo, Cd, Sb, Tl, Pb, Ag. Содержание всех изучаемых элементов определяли в их кислотных концентратах и минерализатах в соответствии с ГОСТ Р 56219-2014 методом масс-спектрометрии с индуктивно-связанной плазмой на масс-спектрометре PlasmaQuant MS Elite (AnalytikJena, Германия) на базе НО ЦКП «Спектрометрия и хроматография» ФИЦ ИнБЮМ. Концентрации тяжелых металлов и микроэлементов в водной экосистеме Северо-Крымского канала были безопасны для использования днепровской воды в качестве питьевой, а также для других хозяйственных нужд Крыма. Максимальное относительное увеличение пула микроэлементов вследствие орошения полей днепровской водой было определено для Mo (до 0.1 %), а также для Zn, Sb и Pb (не более 0.04 %), что не может существенно влиять на экологическое состояние орошаемых земель. В почвах как рисовых и пшеничных полей, так и целинных земель наблюдалось систематическое превышение предельно допустимой концентрации Cd для почв сельхозугодий (до 230 %). В культурах риса и пшеницы обнаружено превышение максимально допустимых уровней содержания Fe, Ni, Cd, As для зерна и зернофуража. В колосе пшеницы максимально допустимые уровни Fe были превышены на 24 %, Ni – на 110 %, As – на 70 %. В зерне риса были превышены предельно допустимые концентрации для продуктов питания Cu (на 29 %), Cd (на 150 %) и Pb (на 438 %), а в зерне пшеницы – Cd (на 360 %) и Pb (на 300 %). Выявлено, что незначительные количества микроэлементов, приносимые с днепровской водой по Северо-Крымскому каналу, не могут оказать ощутимого эффекта на орошаемые сельхозугодья Крыма. Обнаруженные превышения предельно допустимых концентраций и максимально допустимых уровней микроэлементов в почвах и сельскохозяйственных культурах обусловлены, вероятно, деятельностью промышленных предприятий на севере полуострова.

Ключевые слова: Северо-Крымский канал, тяжелые металлы в почве, тяжелые металлы в растениях, тяжелые металлы в воде, орошаемые почвы, сельскохозяйственные растения, загрязнение тяжелыми металлами

Благодарности: работа выполнена в рамках гранта РНФ, проект № 23-26-00128: «Роль оросительной системы Северо-Крымского канала в процессах переноса долгоживущих радионуклидов чернобыльского происхождения, тяжелых металлов, а также углеводородов с днепровской водой на поливные сельхозугодья Крыма».

Для цитирования: Микроэлементы в компонентах водной экосистемы Северо-Крымского канала и орошаемых сельхозугодий / В. Ю. Проскурнин [и др.] // Экологическая безопасность прибрежной и шельфовой зон моря. 2024. № 3. С. 123– 138. EDN MHWSYU.

Introduction

The North Crimean Canal (NCC) was constructed and brought into operation in 1971 with the objective of providing a sustainable water supply to Southern Ukraine and Crimea. The arid climate of the Crimean peninsula presents significant challenges to agricultural production. Consequently, the operation of the NCC system is of great strategic importance for the water supply of the vast agricultural lands in the northern and north-western parts of the peninsula [1)] [1]. Among the agricultural crops grown on the peninsula, rice and wheat are of particular importance [2, 3]. In 2022, after an eight-year break in the regular operation of the canal, the supply of the Dnieper water to Crimea via the NCC was resumed [4]. One of the most important indicators of the quality of used water is the content of heavy metals (HM) and other trace elements in it. It is advisable to monitor this indicator both in soils irrigated with this water and in agricultural crops grown on them [5, 6]. In order to ascertain the potential adverse effects of the Dnieper water supplied by the NCC on the quality of irrigated agricultural crops cultivated on the peninsula, it is essential to gain an understanding of the patterns of HM redistribution within the following system: water – irrigated soils – irrigated agricultural crops.

The objectives of the study are as follows:

a) determination of the current quality of the Dnieper water supplied along the NCC with respect to trace elements (Be, V, Fe, Co, Ni, Cu, Zn, As, Se, Mo, Cd, Sb, Tl, Pb, Ag), including heavy metals;

b) quantification of the levels of transfer of these elements from water to irrigated soils located along the NCC and agricultural crops grown on them;

c) comparison of the obtained results with the sanitary norms established in the Russian Federation regarding the content of HM and other trace elements in the studied objects.

This study is the first of its kind to examine the objectives set and the number of elements studied in the sampled objects in the NCC area and in the adjacent irrigated farmland. Consequently, it is a pioneering piece of research.

Material and methods

To determine trace elements, including HM, water and suspended matter samples were taken directly from the NCC bed and diversion canals. Soil samples of fields irrigated with water from the NCC as well as rice and wheat grown on them

---

[1)] Sokolov, A.A., 1964. [*Hydrography of the USSR (Land Waters)*]. Leningrad: Gidrometeoizdat, 535 p. (in Russian).

were taken in the areas of the villages of Krepkoe and Ilyinka and the city of Dzhankoy (the village of Pobednoe), (Fig. 1, Table 1). Samples were collected between April 2022 and May 2023, and the concentration of 15 trace elements (Be, V, Fe, Co, Ni, Cu, Zn, As, Se, Mo, Ag, Cd, Sb, Tl, Pb) was determined. The dissolved forms of the determined elements were extracted from water by their extraction concentration as diethyldithiocarbamates using carbon tetrachloride,

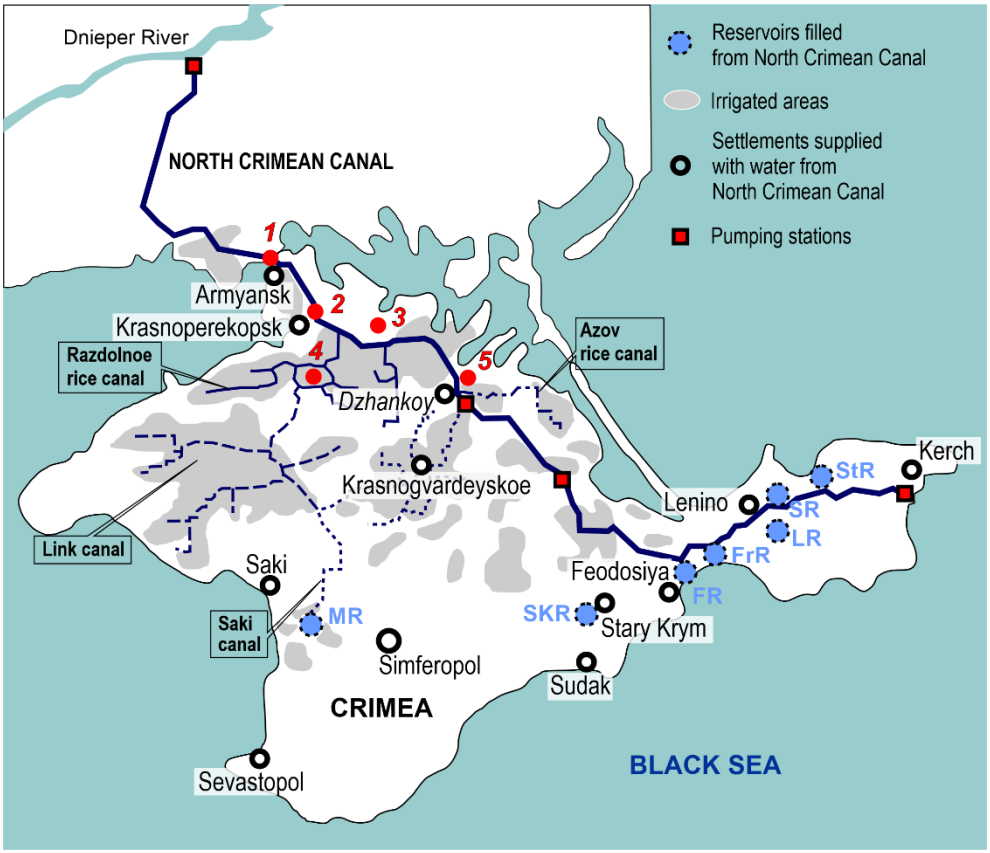

F i g . 1 . Scheme map of sampling in the area of the North Crimean Canal (2022–2023). Sampling stations: *1* – main bed of the NCC, Armyansk area; *2* – main bed of the NCC, Krasnoperekopsk area; *3* – the village of Krepkoe, Krasnoperekopsk area; *4* – branch of the NCC, the village of Ilyinka, Krasnoperekopsk area; *5* – the village of Pobednoe, Dzhankoy area). Water reservoirs: MR – Mezhgornoe, SKR – Starokrymskoe, FR – Feodosiyskoe, FrR – Frontovoe, LR – Leninskoe, SR – Samarlinskoe, StR – Stantsionnoe (Kerchenskoe)

Table 1. Coordinates of sampling stations

Study area	Sampling coordinates (N, E)
1. NCC main bed (Armyansk area)	46°07.208', 33°41.426'
2. NCC main bed (Krasnoperekopsk area)	45°57.261', 33°49.184'
3. The village of Krepkoe (Krasnoperekopsk area):	
wheat field	45°55.419', 33°54.223'
paddy fields	45°56.097', 33°55.029'
4. NCC branch (Krasnoperekopsk area), the village of Ilyinka	45°50.067', 33°45.600'
5. NCC main bed, the village of Pobednoe (Dzhankoy area), irrigated field	45°45.500', 34°26.230'

in accordance with Regulatory Document 52.10.243-92. The determined elements were extracted from solid samples (soils, suspended matter, stems and grains of rice and wheat) by acid mineralization followed by filtration in accordance with Federal Environmental Regulations 16.2.2:2.3.71-2011. The content of all studied elements was determined in their acidic concentrates and mineralizates in accordance with State Standard of Russia 56219-2014 by mass spectrometry with inductively coupled plasma on a PlasmaQuant MS Elite mass spectrometer (AnalytikJena, Germany) on the basis of the collective use center "Spectrometry and Chromatography" A.O. Kovalevsky Institute of Biology of the Southern Seas of RAS. The mass spectrometer was calibrated using standard solution "Calibration Multielement Standard IV-28, HNO_3/HF, 125 mL" (Inorganic Ventures) by plotting a calibration straight line across solutions with dilution degrees of the standard covering the full range of element concentrations to be determined. The measurement procedure included at least seven repetitions for each measured element in each sample. The measurement time of each m/z ratio was determined by the intensity of the detector response to the presence of a particular element in solution and ranged from 0.01 to 0.1 s. The relative error of measurement was determined for all measured elements, with a maximum value of 10 % observed.

To assess water quality, the obtained values of element concentrations were compared with the maximum permissible concentrations (MPC) established by Sanitary Regulations and Standards 1.2.3.3685-21 [2)] for domestic and drinking water use (MPC_{DD}). It should be noted that such MPCs are also applied to waters used for irrigation. As the local population catches and consumes the fish that inhabit the canal, the obtained values were also compared with MPC recommended for waters of water bodies for fishery purposes [3)] (MPC_{fish}). The values of element concentrations determined in soils were compared with MPC (MPC_{soil}) (or approximately permissible concentrations (APC_{soil})) values established for agricultural soils [2)]. In addition, since farming in Crimea is primarily based on chestnut soils with pH > 5.5, the MPC_{soil} (APC_{soil}) values for clay and loam soils with pH > 5.5 were used where applicable. The transfer of elements with the NCC waters to irrigated fields was estimated based on the average norm of specific mass of arable horizon of soil 3000 $t \cdot ha^{-1}$ (in accordance with Sanitary Regulations and Standards 2.1.7.573-96) and maximum water consumption rates for irrigation of fields with spring grain crops in Rostov Oblast as similar in soil type and climatic features to the Crimean peninsula, up to 4140 $m^3 \cdot ha^{-1} \cdot year^{-1}$ (in accordance with State Standard of Russia 58331.3-2019). Agricultural crop quality was assessed according to the temporary maximum permissible levels (MPL) for grain and grain fodder for farm animals [4)] and MPC for cereals as a human foodstuff (MPC_{food}) (Sanitary Regulations and Standards 2.3.2.560-96). Regularities of trace elements accumulation by agricultural crops from soils were characterized by conversion factors (F_c) calculated as the ratio of the concentration of the element in the crop (part of the crop) C_{crop} to the concentration of the element in the soil under this crop C_{soil}.

Results and discussion

Table 2 shows the results of measurements of trace elements concentrations in the Dnieper water of the NCC used for irrigation, in irrigated soils and crops.

Fig. 2 shows the assessment of the NCC water quality in relation to trace elements content in 2022–2023.

[2)] Popova, A.Yu., 2021. Sanitary Regulations and Standards СанПиН 1.2.3.3685-21 *Hygienic Norms and Requirements to Ensure Safety and/or Harmlessness of Habitat Factors for Humans (as Amended for 30 December 2022)*. Moscow, 469 p. (in Russian).

[3)] *On the Approval of Water Quality Standards for Water Bodies of Commercial Fishing Importance, Including Standards for Maximum Permissible Concentrations of Harmful Substances in the Waters of Water Bodies of Commercial Fishing Importance*: Order of the Ministry of Agriculture of Russia dated December 13, 2016, No. 552 (in Russian)

[4)] Tretyakov, A.D. and Zaichenko, A.I., 1987. *Temporary maximum permissible level (MPL) of the content of some chemical elements and gossypol in feed for farm animals and feed additives (approved by the Main Veterinary Department of the State Agro-Industrial Committee of the USSR on 7 August 1987)*. Moscow.

Table 2. Concentrations of trace elements in the water ($\mu g \cdot L^{-1}$), in the soil and in the agricultural crops ($mg \cdot kg^{-1}$ D.W.)

Element	Water		Soil	Agricultural crops
	Dissolved form	Total concentration		
Pb	0.05–0.19	0.70–1.96	8.63–70.82	0.86–7.68
Cd	0.02–0.37	0.10–0.61	0.56–6.64	0.07–1.00
Zn	6.42–113.83	8.51–117.38	63.47–122.07	3.70–26.79
Cu	0.64–2.29	1.16–3.01	20.02–59.43	1.24–12.87
Fe	0.63–2.83	36.69–230.71	$10.2 \cdot 10^3$–$42.7 \cdot 10^3$	33–2941
Co	0.02–0.06	0.04–0.14	11.33–15.42	0.02–0.89
Ni	0.76–1.39	1.24–2.26	38.22–51.65	0.39–4.21
Mo	0.02–0.21	0.34–0.65	0.45–2.85	0.03–1.33
Sb	0.008–0.015	0.014–0.023	0.03–0.22	<0.01–0.03
As	0.01–0.20	0.06–0.27	4.91–10.91	<0.10–0.85
V	0.16–0.61	0.33–0.96	43.94–76.39	<0.10–5.40
Tl	<0.001–0.005	0.001–0.006	0.11–0.27	<0.001–0.017
Se	<0.03–0.19	<0.03–0.19	0.75–3.29	<0.30–0.32
Ag	<0.001	<0.001–0.11	0.12–0.32	<0.01
Be	<0.01	<0.01–0.01	0.80–1.30	<0.001–0.086

It should be noted that RF normative documents [2), 3), 5), 6)] regulate the content of dissolved forms of elements only. On the basis of the analysis of the data obtained, it was found that the concentrations of trace elements in the water (both in their dissolved and total (suspended) forms) did not exceed MPC_{DD} [2), 5), 6)] throughout the period of the studies.

With regard to MPC_{fish} [3)], a single exceedance of twice the standard for zinc concentration in the water (dissolved form) was observed in March 2023 under low level conditions prior to the start of water supply.

---

5) Kurlyandsky, B.A. and Sidorov, K.K., eds., 2003. *Hygienic standard ГН 2.1.5.1315-03. Maximum permissible concentrations of chemical substances in the water of water bodies of household and cultural and domestic water use: approved by the Decree of the Head State Sanitary Doctor of the Russian Federation from 30 April 2003 no. 79*. Moscow: Neftyanik, 152 p. (in Russian).

6) Mazaev, V.T., 2002. *Sanitary Regulations and Standards SANPIN 2.1.4.1074-01. Drinking Water. Hygienic Requirements for Water Quality of Centralised Drinking Water Supply Systems. Quality Control (Approved by the Chief State Sanitary Doctor of the Russian Federation on 26 September 2001, no. 24)*. Moscow, 103 p.

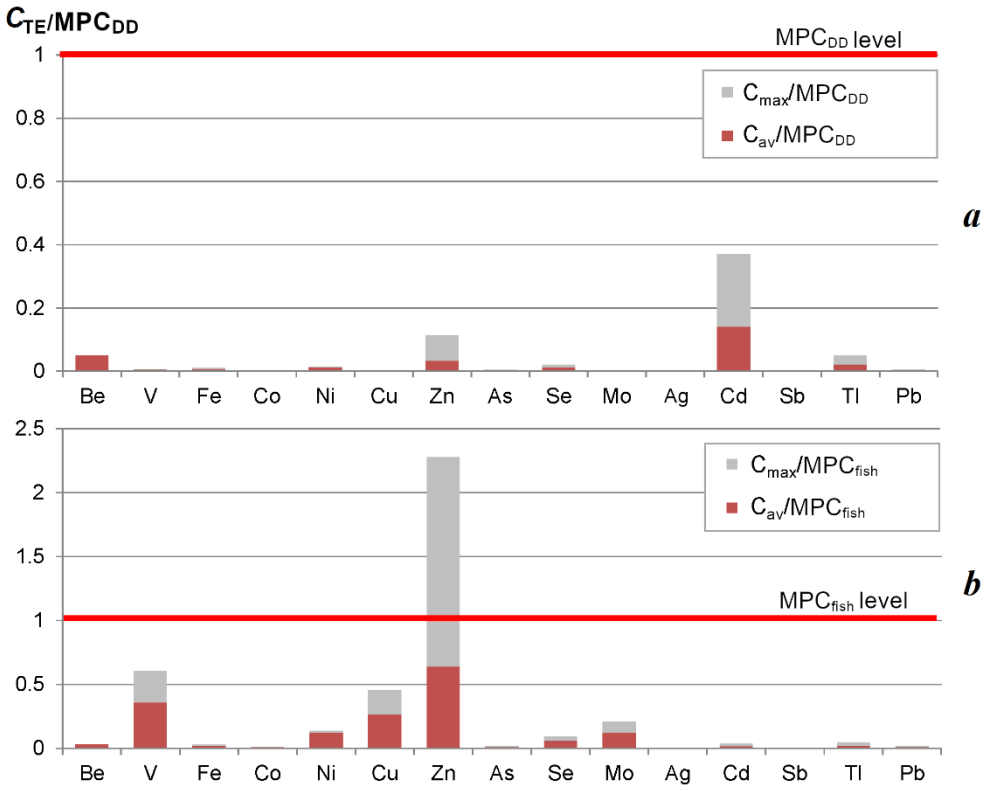

Fig. 2. Ratio of average (C_{av}) and maximum (C_{max}) concentrations of dissolved forms of trace elements (TE) in the North Crimean Canal water to MPC_{DD} (*a*) and MPC_{fish} (*b*) in 2022–2023

It was determined that the maximum concentration factors (C_f) of elements by suspensions were observed for Fe – $n \cdot 10^7$, slightly lower values of C_f were observed for As, Mo, Cd and Pb – $n \cdot (10^5 \div 10^6)$, the values of C_f did not exceed $n \cdot 10^5$ for V, Co, Ni, Cu, Se, Sb and Tl, and the values of this coefficient were minimal for Zn and varied in the range of $n \cdot (10^3 \div 10^4)$. Such high values of C_f determine the most efficient sedimentation self-purification of the NCC waters from Fe, As, Mo, Cd and Pb, to a lesser extent from V, Co, Ni, Cu, Se, Sb and Tl and the least efficient from Zn.

Concentrations of dissolved forms of Be and Ag were below their detection limits: for Be – 0.01 μg·L^{-1}, Ag – 0.001 μg·L^{-1}. Fig. 2 shows the ratios of the detection limits to the corresponding MPC values for these elements.

Fig. 3 shows the assessment of the quality of arable soils of agricultural lands and adjacent virgin land plots in the north of Crimea with regard to the content of trace elements in them.

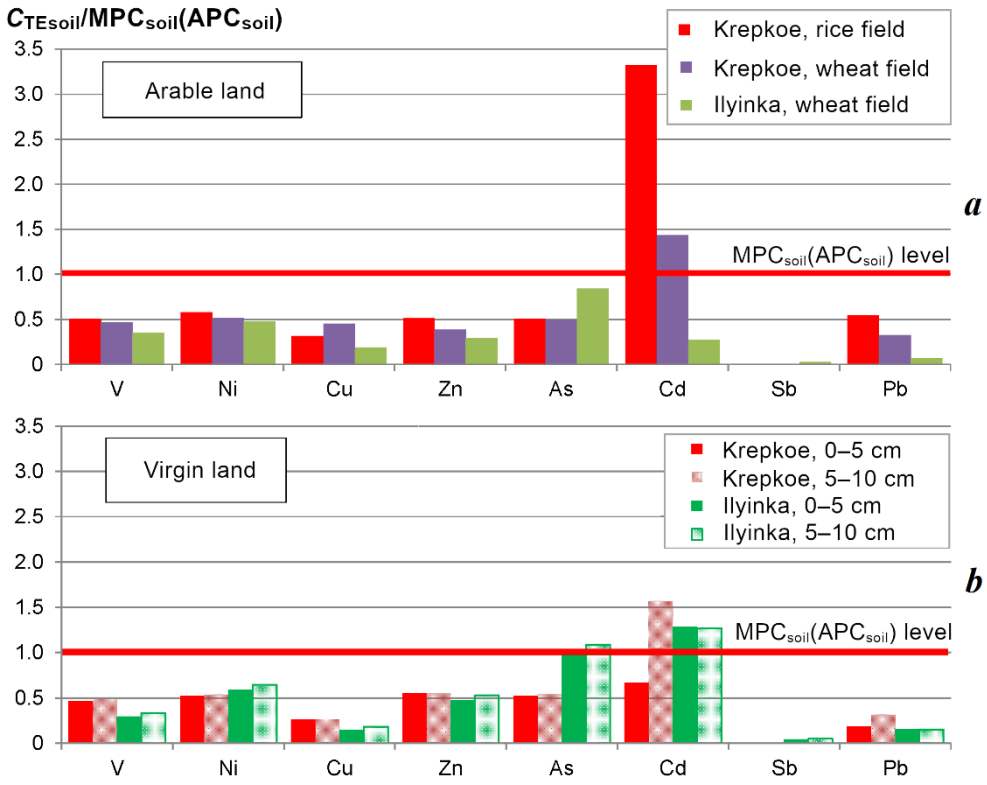

Fig. 3. Ratio of trace elements (TE) concentrations (C_{TE}) in soils of arable (*a*) and virgin (*b*) land plots in the north of Crimea to the maximum (MPC_{soil}) and approximately (APC_{soil}) permissible concentrations of TE in soils in 2022–2023

A systematic excess of MPC_{soil} was observed for Cd – up to 230 % – both in rice and wheat fields (the village of Krepkoe, Fig. 1, Table 1) as well as in virgin lands (the village of Krepkoe, the village of Ilyinka, Fig. 1, Table 1). The vertical distribution of Cd in arable soils indicated an increase in its concentration with the depth of the bedding layer. Maximum exceedance of MPC_{soil} for Cd in the rice field in this area appeared to be due to homogenisation of surface soil layers by mechanical processing. Minor exceedance of MPC_{soil} for As was observed only in virgin soil adjacent to the rice field near the village of Ilyinka (Fig. 1, Table 1), with no exceedances observed in the arable soil itself.

Fig. 4 shows the results of calculation of ranges of specific pools of trace elements in arable soils of the studied fields and of elements supply with the NCC waters used for irrigation.

The results of calculations (Fig. 4) show that the maximum values of metal supply to irrigated soil with irrigation water are expected for Fe – 0.43÷0.95 kg·ha^{-1} (0.001 % of the pool) and Zn – 0.05÷0.11 kg·ha^{-1} (0.03 % of the pool).

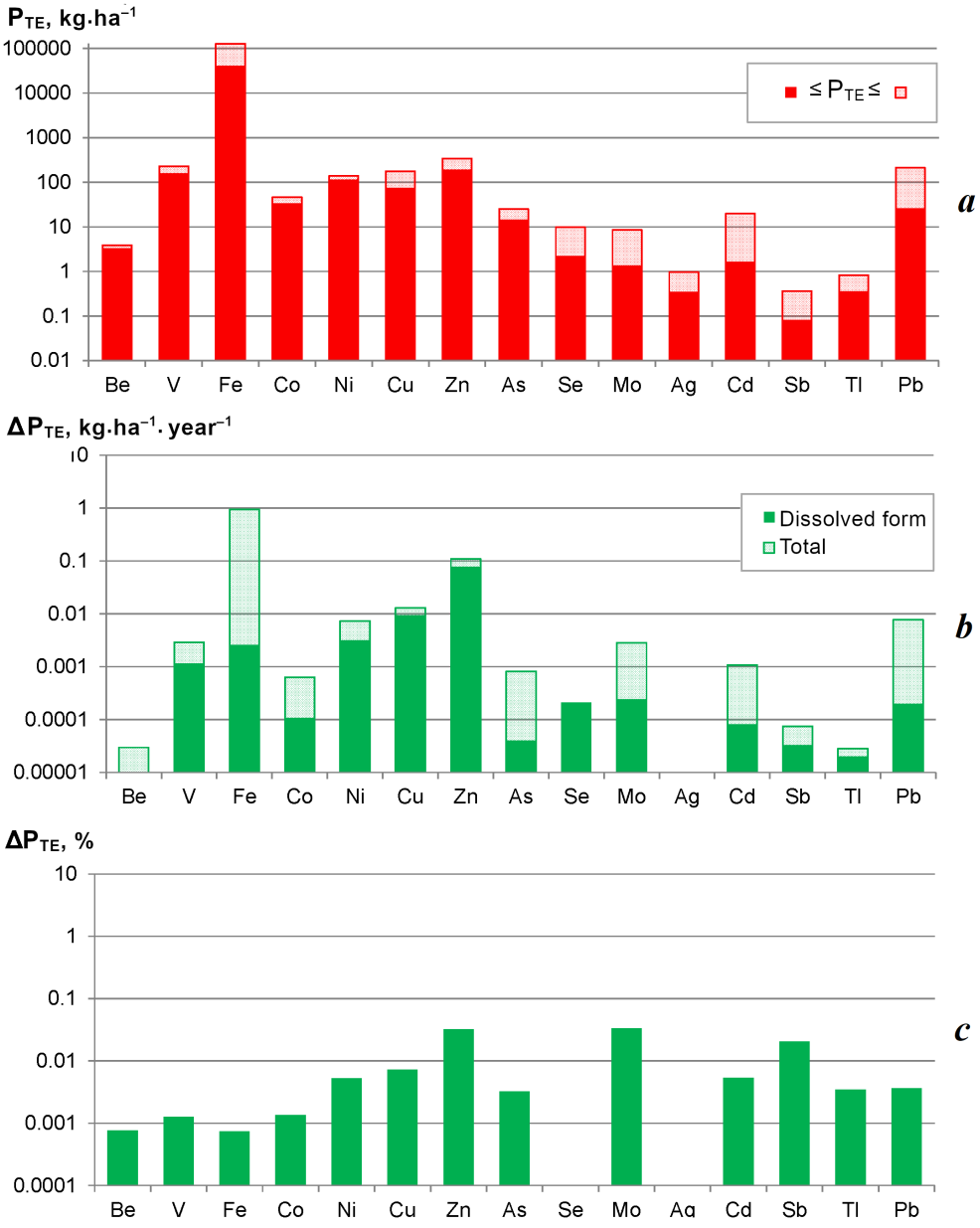

Fig. 4. Ranges of specific pools of microelements (*a*) in arable soils of Crimea (P_{TE}) and assessment of the absolute (*b*) and relative (*c*) changes in these pools (ΔP_{TE}) due to the supply with the North Crimean Canal waters used for irrigation

At the same time, the maximum relative increase in the pool of trace elements due to irrigation is expected for Mo (up to 0.1 %), Zn, Sb and Pb (not more than 0.04 %), which, obviously, will not affect the ecological state of the irrigated lands.

Calculations of conversion factors (F_c) of elements from irrigated soils to rice and wheat crops grown on them show that with respect to many elements their concentration in grain in relation to the stem of the studied crops is observed. To quantify this concentration, magnification coefficients (C_m) were calculated as the ratio of the concentration of trace elements in the grain to the concentration in the plant stem. Figs. 5 and 6 show the results of such calculations.

It was demonstrated (see Figs. 5 and 6) that, of the trace elements (Fe, Ni, Co, Cu, Zn, Mo, Sb, Cd and Pb) reliably measured in rice cultivation, all elements except Cd exhibited a greater accumulation in the grain than in the stems. In contrast, the accumulation of Cd in wheat grain was found to be significantly higher than that of other elements, while Sb and Mo were more concentrated in plant stems. This discrepancy highlights the distinctive physiological characteristics of rice and wheat crops.

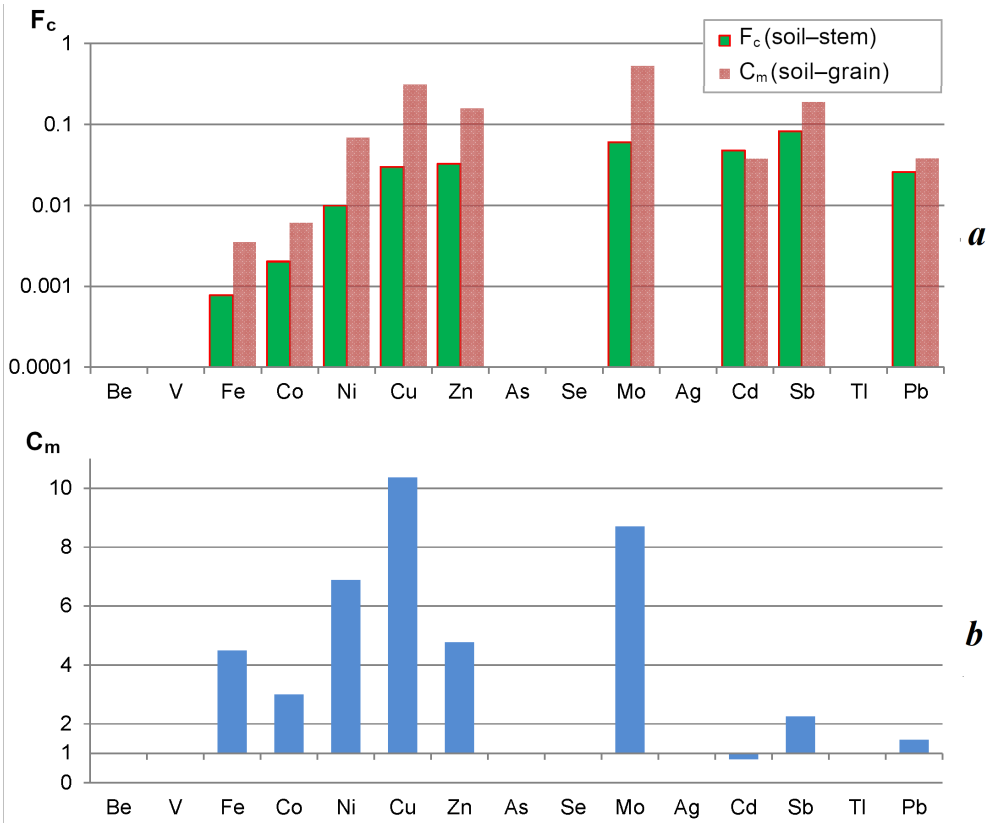

Fig. 5. Coefficients F_c (conversion factor) (*a*) and C_m (magnification coefficient) (*b*) of the trace elements for rice crops in the village of Krepkoe

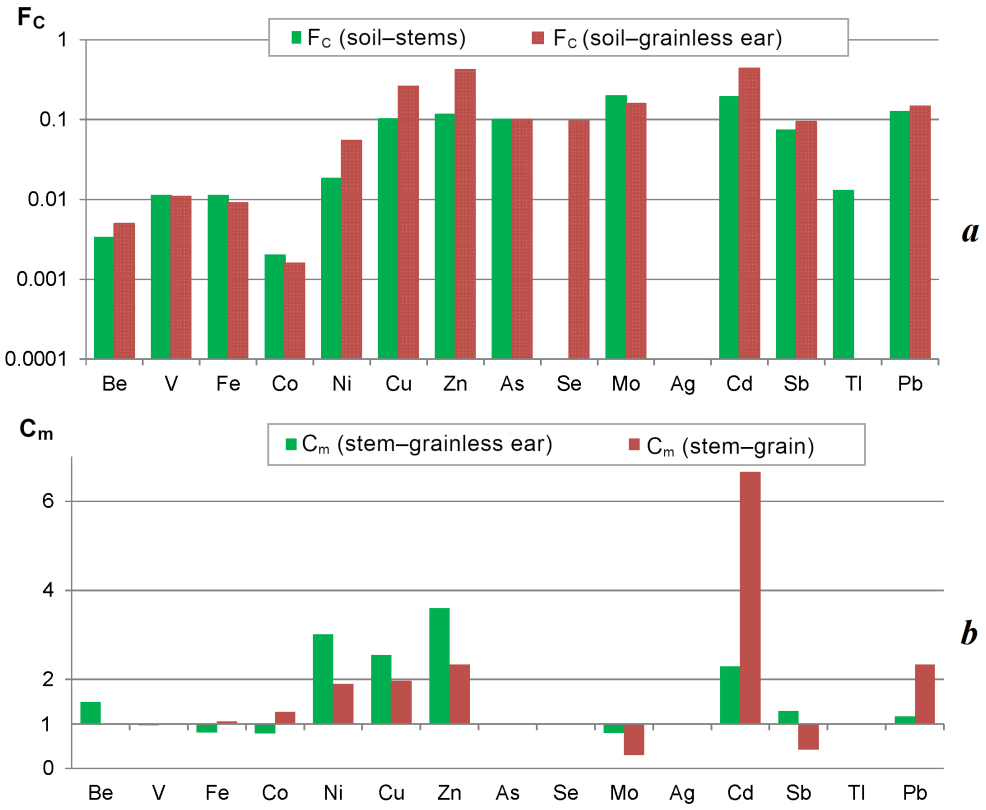

Fig. 6. Coefficients F_c (conversion factor) (*b*) and C_m (magnification coefficient) (*b*) of the microelements for wheat crop in the village of Ilyinka (Krasnoperekopsk area) and the village of Pobednoye (Dzhankoy area)

Fig. 7 shows the results of quality assessment of the studied crops with respect to their trace elements content.

In a rice crop from the village of Krepkoe, maximum permissible levels for Fe content in grain and grain fodder as animal feed were exceeded in grain by 49 % and for Ni – by 214 %, while Cd concentrations in rice stems reached maximum permissible levels [4].

In a wheat crop from the village of Ilyinka, maximum permissible levels for Fe were exceeded in ear by 24 %, for Ni – by 110 %, for As – by 70 %, and in wheat stems, Fe and As content exceeded maximum permissible levels by 52 and 68 %, respectively. MPC_{food} [7, 8] in rice grain were exceeded for Cu by 29 %, for Cd – by

[7] Trukhachev, V.I., Tolokonnikov, V.P. and Lysenko, I.O., 2005. [*Food as an Environmental Factor: A Textbook for the Discipline of Biology and Bioecology*]. Stavropol: AGRUS, 182 p. (in Russian).

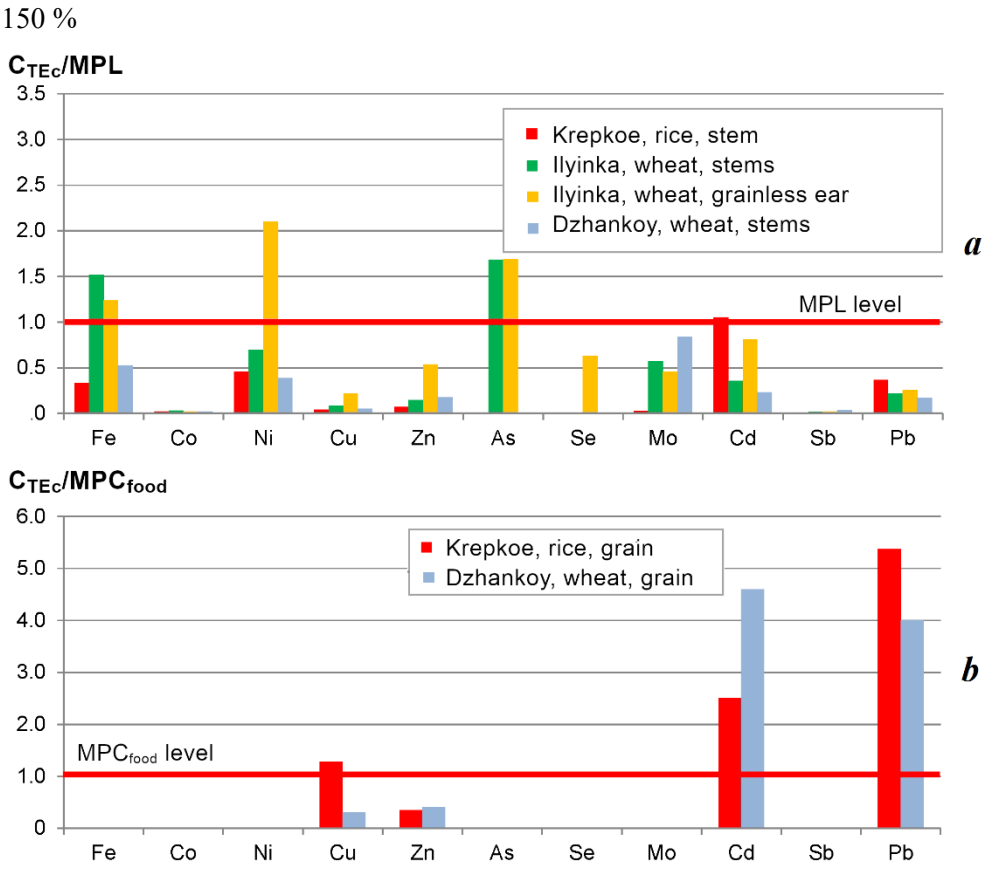

Fig. 7. Ratio of trace elements concentrations in rice and wheat crops (C_{TEc}) to MPL (maximum permissible levels for grain and grain fodder for livestock feed) (*a*) and MPC_{food} (MPC for grains and cereals as human food products) (*b*)

and for Pb – by 438 %, and in wheat grain from a field near Dzhankoy, the Cd content exceeded MPC_{food} by 360 %, Pb – by 300 %.

The findings of the study indicated that during the 2022–2023 period, the Dnieper water in the NCC met the standards set forth by the Russian Federation for the concentration of trace elements in water intended for household use, drinking and irrigation. Exceedances of MPC_{soil} for Cd and As were detected in both arable and virgin soils, which, as noted earlier, is due to the activities of industrial enterprises, including chemical industry, located in the north of the peninsula [13, 14]. Exceedance of maximum permissible levels of some trace elements

[8] State Committee for Sanitary Supervision and Disease Control, 1997. *SANPIN 2.3.2.560-96. [2.3.2 Food Raw Materials and Food Products. Hygienic Requirements to Quality and Safety of Food Raw Materials and Food Products]*. Moscow: Goskomepidnadzor Rossii, 269 p. (in Russian).

in agricultural crops was also observed, which is connected with transfer of these elements from soils and their concentration by plants.

Conclusion

In 2022–2023, during the period of the NCC operation from the moment of resumption of the Dnieper water inflow through the canal system (March 2022, after eight years of its absence since 2014) and until the termination of water supply to the canal ecosystem (after the destruction of Kakhovka Hydroelectric Power Plant in June 2023), studies were conducted to determine the concentrations, migration and distribution of trace elements (Be, V, Fe, Co, Ni, Cu, Zn, As, Se, Mo, Cd, Sb, Tl, Pb, Ag), including HM, in the NCC water, irrigated soils and growing irrigated crops.

It was determined that the concentrations of HM and microelements in the aquatic ecosystem of the NCC allowed safe use of the Dnieper water both for drinking and for other economic needs of Crimea.

The concentrating capacity of suspended matter in the NCC water was determined, expressed by concentration factors (C_f), the values of which varied in the range from $n \cdot 10^7$ (for Fe) to $n \cdot 10^3$ (for Zn). Such high values of C_f of the investigated elements cause effective sedimentation self-purification of the NCC waters from HM and other pollutants.

Systematic exceedances of MPC_{soil} for Cd up to 230 % were observed both in rice and wheat fields and in virgin soils. Exceedances of MPC_{food} for Cu (by 29 %), Cd (by 150 %) and Pb (by 438 %) were noted in rice grain and MPC_{food} for Cd (by 360 %) and Pb (by 300 %) – in wheat grain from a field near Dzhankoy. The revealed exceedances of MPC and maximum permissible levels of trace elements in soils and crops are probably caused by the activities of industrial enterprises in the north of the peninsula.

The results of calculations of trace elements and HM pools supply to irrigated soils showed that even maximum values of metals supply with irrigation water (they do not exceed 0.001 % of the pool for Fe) would not affect the ecological state of irrigated lands. In other words, insignificant amounts of trace elements brought with the Dnieper water through the NCC cannot have a noticeable effect on the irrigated farmland of Crimea. At the same time, estimation of trace elements content in agricultural crop grain and grain fodder requires additional monitoring studies.

The results obtained can be used to devise strategies for the prevention of chemical contamination of irrigated agricultural lands in Crimea, thereby addressing the challenges of sustainable development in the Crimean region and the Black Sea regions of Russia as a whole.

REFERENCES

1. Shevchenko, M.A., ed., 1989. [*Hydrology and Hydrochemistry of the Dnieper River and its Reservoirs*]. Kiev: Naukova Dumka, 216 p. (in Russian).
2. Koba, V.P. and Sakhno, T.M., 2020. Soil Fertility and Yielding Capacity of Grain and Leguminous Crops in the Crimea. *ArgoEcoInfo*, (2) (in Russian).
3. Rodin, I.K. and Klepova, I.K., 2023. [Distribution of Cultivated Areas of Agricultural Crops in the Republic of Crimea after 2014]. In: RSAU, 2023. *Proceedings of VII In-*

ternational Scientific and Practical Conference: The Ecological State of the Natural Environment and the Scientific and Practical Aspects of Modern Agricultural Technologies. Ryazan, 6 April 2023. Ryazan: Ryazan State Agrotechnological University Named after P. A. Kostychev, pp. 351–354 (in Russian).

4. Mirzoeva, N., Tereshchenko, N. and Korotkov, A., 2022. Artificial Radionuclides in the System: Water, Irrigated Soils, and Agricultural Plants of the Crimea Region. *Land*, 11(9), 1539. https://doi.org/10.3390/land11091539
5. Ulesov, A.S., Tsedrik, E.S., Stich, A.A. and Gutsalova, A.A., 2020. [The Problem of Increasing Levels of Heavy Metals in Crop Irrigation Water]. In: RSAU, 2020. *International Scientific-Practical Conference to the Memory of Corresponding Member of RAAS and KAS, Academician of MAEL and RAVN Bochkarev Y. V. 'Integrated Approach to Scientific and Technical Support of Agriculture'*. Ryazan, 9 December 2020. Part II. Ryazan: RGATU, pp. 340–343 (in Russian).
6. Chernykh, N.A., The Cuong Ngo, Tran Quoc Hoan, Baeva, Yu.I. and Grachev, V.A., 2018. The Regularities of Heavy Metals and Arsenic Accumulation in the Vegetation of Riverside Depending on the Level of Technogenic Load. *Journal of Pharmaceutical Sciences and Research*, 10(4), pp. 800–804. Available at: https://www.jpsr.pharmainfo.in/documents/Volumes/vol10Issue04/jpsr10041823.pdf [Accessed: 8 September 2024].
7. Perevolotskaya, T.V. and Anisimov, V.S., 2017. Regularities of Migratory Processes of Heavy Metals in the System "Soil – Agricultural Plant" on the Example of the Coefficient of Accumulation of Cu, Zn, Pb, Cd in Grain Crops (Grain of Wheat and Barley). *Problemy Sovremennoy Nauki i Obrazovaniya*, (10), pp. 27–32 (in Russian).
8. Koretskaya, A.S., Andreeva, G.Yu. and Nikonova, G.N., 2023. The Content of Heavy Metals in the Soil-Grain System. *Bulletin of Michurinsk State Agrarian University*, (4), pp. 96–100 (in Russian).
9. Lukyanova, E.S. and Fedotov, V.A., 2024. Features of Accumulation of Heavy Metals in Soil and Grain Crops. *Trace Elements in Medicine*, 25(2), pp. 54–55 (in Russian). http://doi.org/10.19112/2413-6174-2024-25-2-23
10. Bashmakov, D.I. and Lukatkin, A.S., 2009. [*Ecological and Physiological Aspects of Accumulation and Distribution of Heavy Metals in Higher Plants*]. Saransk: MRSU, 236 p. (in Russian).
11. Krupnova, T.G., Rakova, O.V., Popkova, M.A. and Gavrilkina, S.V., 2023. Distribution of Some Heavy Metals in Winter Wheat at Different Stages of its Development. *Bulletin of the South Ural State University. Series "Chemistry"*, 15(3), pp. 148–158. EDN UNIELM. https://doi.org/10.14529/chem230308
12. Inisheva, V.D., Kurbanova, V.Yu., Fedorova, E.A., Shapovalova, A.A., Shapovalova, A.A., Naronova, A.A., 2018. Adsorption Properties of Rice in Relation to Salts of Heavy Metals. In: USMU, 2018. *Proceedings of III International Scientific and Practice Conference of Young Scientists and Students "Issues of Modern Medical Science and Health Care" III Forum of Medical and Pharmaceutical High Schools in Russia "For Qualitative Education". Ekaterinburg, 03–05 April 2018*. Ekaterinburg: USMU, pp. 592–595 (in Russian).
13. Evstafeva, E.V., Bogdanova, A.M., Minkina, T.M., Sushkova, S.N., Baranovskaya, N.V., Mandzhieva, S.S. and Antonenko, E.M., 2018. Heavy Metal Content in Soils of Residential Territories of Crimea Republic. *Bulletin of the Tomsk Polytechnic University. Geo Assets Engineering*, 329(10), pp. 19–29. https://doi.org/10.18799/24131830/2018/10/2101 (in Russian).
14. Lisetskii, F.N., Marinina, O.A., Poletaev, A.O. and Zelenskaya, E.Ya., 2020. Comparative evaluation of pollution by heavy metals of ploughed and fallow land

at various duration of agropedogenesis. *Journal of Agriculture and Environment*, (3). https://doi.org/10.23649/jae.2020.3.15.2

Submitted 29.02.2024; accepted after review 25.03.2024;
revised 17.06.2024; published 25.09.2024

About the authors:

Vladislav Yu. Proskurnin, Junior Research Associate, A. O. Kovalevsky Institute of Biology of the Southern Seas of RAS (2 Nakhimov Av., Sevastopol, 299011, Russian Federation), **ORCID ID: 0000-0002-2176-9228, Scopus Author ID: 55653290000, Researcher ID: H-4611-2018**, *v_proskurnin@ibss-ras.ru*

Natalya Yu. Mirzoeva, Leading Research Associate, Head of the RchBD, A. O. Kovalevsky Institute of Biology of the Southern Seas of RAS (2 Nakhimov Av., Sevastopol, 299011, Russian Federation), Ph.D. (Biol.), **ORCID ID: 0000-0002-8538-2436; Scopus Author ID: 55623414000; Researcher ID: Q-9393-2016**, *natmirz@mail.ru*

Olga D. Chuzhikova, Junior Research Associate, A. O. Kovalevsky Institute of Biology of the Southern Seas of RAS (2 Nakhimov Av., Sevastopol, 299011, Russian Federation), **ORCID ID: 0000-0002-4518- 2624, Scopus AuthorID: 57205198922, Researcher ID: X-4583-2019,** *olga88.chp@ya.ru*

Maxim O. Vakhrushev, Leading Engineer, Graduate Student, A. O. Kovalevsky Institute of Biology of the Southern Seas of RAS (2 Nakhimov Av., Sevastopol, 299011, Russian Federation), *140393@inbox.ru*

Contribution of the authors:

Vladislav Yu. Proskurnin – setting goals and objectives, performing chemical analysis and measuring concentrations to determine microelements, including HMs, analytical data processing, writing the manuscript

Natalya Yu. Mirzoeva – setting goals, objectives, analyzing the results obtained, discussing the results, writing the article

Olga D. Chuzhikova – sample preparation and chemical analysis to determine the concentrations of heavy metals and microelements, drafting the article

Maxim O. Vakhrushev – participation in expeditions, sampling and preparation of samples, participation in chemical analysis to determine the concentrations of heavy metals and trace elements in the objects under study

All the authors have read and approved the final version of the manuscript.

Original article

Hydrochemical State of the Waters of the Salgir and Biyuk-Karasu Rivers (Crimean Peninsula) in Summer 2023

N. P. Kovrigina *, D. S. Borisova, S. V. Ovechko, V. I. Ryabushko

A.O. Kovalevsky Institute of Biology of Southern Seas of RAS, Sevastopol, Russia
**e-mail: npkovrigina@yandex.ru*

Abstract
The paper studies hydrochemical characteristics of waters of the Salgir and Biyuk-Karasu Rivers in summer, when the anthropogenic load is increased. Data were obtained on dissolved oxygen concentration, five-day biochemical oxygen demand (BOD_5), alkaline permanganate oxidizability, concentrations of silicate, mineral and organic forms of nitrogen and phosphorus. The samples were collected in July, August and September 2023 in Simferopol and in the Krasnogvardeisk, Nizhnegorsk and Belogorsk regions in the Republic of Crimea. The analyses were performed according to the generally accepted methods. Compliance of the obtained results on hydrochemical indicators with water quality regulations was assessed. A high level of oxygen content was noted at all stations. BOD_5 values varied from 0.98 to 3.34 mg/L (the village of Molochnoye) and exceeded the limit for fisheries by up to 1.6 times. The oxidizability values exceeded the maximum allowable value by 2 to 4 times. The concentrations of the mineral forms of nitrogen did not exceed maximum allowable concentrations, except for nitrite concentration (maximum exceedance by 2.8 times). The phosphate concentration exceeded the maximum permissible concentrations near the villages of Novogrigoryevka and Molochnoye (maximum by up to 5.6). The study results allow determining the areas of Molochnoye and Novogrigoryevka as most polluted.

Keywords: hydrochemical characteristics, nutrients, anthropogenic load, water quality, Salgir river, Crimea

Acknowledgments: The work was supported within the governmental research assignment of Research Center for Freshwater and Saltwater Hydrobiology no. 102320600002-2-1.6.17 “Study of features of the structure and dynamics in freshwater ecosystems of the Northern Black Sea region” and partially within the governmental research assignment of IBSS of RAS 1023032700554-2-1.6.16 (FNNZ-2024-0032) “Integrated study of mechanisms of functioning of marine biotechnological complexes for the purpose of obtaining biologically active substances from hydrobionts”.

For citation: Kovrigina, N.P., Borisova, D.S., Ovechko, S.V. and Ryabushko, V.I., 2024. Hydrochemical State of the Waters of the Salgir and Biyuk-Karasu Rivers (Crimean Peninsula) in Summer 2023. *Ecological Safety of Coastal and Shelf Zones of Sea*, (3), pp. 139–148.

Гидрохимическое состояние вод рек Салгир и Биюк-Карасу (полуостров Крым) в летний сезон 2023 года

Н. П. Ковригина *, Д. С. Борисова, С. В. Овечко, В. И. Рябушко

ФИЦ «Институт биологии южных морей имени А.О. Ковалевского РАН», Севастополь, Россия

* *e-mail: npkovrigina@yandex.ru*

Аннотация

Приведены гидрохимические характеристики вод рек Салгир и Биюк-Карасу в летний период при возрастающей антропогенной нагрузке. Получены данные о содержании растворенного кислорода, биохимическом потреблении кислорода на пятые сутки, перманганатной окисляемости в щелочной среде, концентрации кремния, минеральных и органических форм азота и фосфора. Пробы отобраны в июле, августе и сентябре 2023 г. в Симферопольском, Красногвардейском, Нижнегорском и Белогорском районах Республики Крым. Анализы выполнены согласно общепринятой методике. Оценено соответствие полученных результатов по гидрохимическим показателям нормативным требованиям к качеству вод. Отмечен высокий уровень содержания кислорода на всех участках; биохимическое потребление кислорода на пятые сутки изменялось от 0.98 до 3.34 мг/л (с. Молочное) и превышало норматив для водных объектов рыбохозяйственного значения максимум в 1.6 раза, значения окисляемости превышали предельно допустимые показатели в 2–4 раза. Концентрации минеральных форм азота не превышали предельно допустимую концентрацию, кроме нитритов (максимальное превышение в 2.8 раза). Зафиксировано также превышение предельно допустимой концентрации фосфатов в районах с. Новогригорьевка и с. Молочного (максимум в 5.6 раза). Результаты исследований позволяют выделить наиболее загрязненные районы, такие как с. Молочное и с. Новогригорьевка.

Ключевые слова: гидрохимические показатели, биогенные вещества, качество вод, антропогенная нагрузка, река Салгир, Крым

Благодарности: работа выполнена по темам НИЦ ПСГ 102320600002-2-1.6.17 «Изучение особенностей структуры и динамики пресноводных экосистем Северного Причерноморья» и ФИЦ ИнБЮМ 1023032700554-2-1.6.16 (FNNZ-2024-0032) «Комплексное исследование механизмов функционирования морских биотехнологических комплексов с целью получения биологически активных веществ из гидробионтов».

Для цитирования: Гидрохимическое состояние вод рек Салгир и Биюк-Карасу (полуостров Крым) в летний сезон 2023 года / Н. П. Ковригина [и др.] // Экологическая безопасность прибрежной и шельфовой зон моря. 2024. № 3. С. 139–148. EDN SZZDMX.

Introduction

The Salgir River represents the largest water system of the Crimean Peninsula flowing into Sivash Bay of the Sea of Azov during periods of high water. The scientific research of the Salgir River and its basin was initiated in the late 19th century [1)].

[1)] Golovkinskiy, N.A., 1893. [*Springs of Chatyrdag and Babugan*]. Simferopol: Tip. Spiro, 35 p. (in Russian).

The results of expeditionary studies of the Salgir River and its tributary Biyuk-Karasu are described in work [2)]. In 1961, information about the Salgir River basin was presented in the work of M.E. Miller [1] in connection with the construction of the Simferopol Reservoir and the Salgir irrigation system. The study of the natural landscapes and the use of nature in the Salgir River basin as well as the justification of measures to ensure the quantity and quality of water resources in the basin were carried out by A. M. Vlasova [2]. The study considers the main sources of pollution in the Salgir River basin and identifies the areas of the basin with stable and unstable ecological state. The analysis of the factors of water resources formation in the Salgir River under the conditions of climate change and anthropogenic load is presented in the works of E. A. Pozachenyuk et al. [3].

The greatest contribution to the pollution of the water area of the Salgir and Biyuk-Karasu Rivers is made by industrial and municipal wastewater from the city of Simferopol and its suburbs. This phenomenon can be attributed to a confluence of factors, including the proliferation of industrial facilities, high density of buildings, branched transport networks and municipal infrastructure, among others. The work by N.M. Ivanyutin et al. [4] demonstrates that the primary pollutants identified in the investigation of river runoff, for which exceedances of maximum permissible concentrations (MPC) were observed, are petroleum products, ammonium nitrogen, nitrite, nitrate, phosphate, iron, cadmium, manganese, lead and zinc. Furthermore, the BOD_5 permissible levels were exceeded.

In their study, N. M. Ivanyutin et al. [5] identify the increased withdrawal of water from the river and the discharge of inadequately treated wastewater, in addition to precipitation and snowmelt water runoff, as the primary challenges facing the Salgir River. In addition to the previously mentioned sources, E. Yu. Kuznetsova [6] identifies industrial waste settling and livestock farms as contributors to the pollution of surface water. An increase in the concentration of nitrite, phosphate and ammonium nitrogen in the surface waters of the Salgir River was detected. The gradual increase in nitrite content can be attributed to the conversion of ammonia to nitrite as a result of the nitrification. The MPC of ammonium nitrogen was exceeded. The authors conclude that the ecological condition of the river is unsatisfactory.

In the work of G. A. Kiseleva [7], the monitoring of hydrochemical indicators (dissolved oxygen, BOD_5, etc.) revealed significant changes in the environment and benthic ecosystem. This led to the identification of six areas within the Salgir River, characterised by varying degrees of anthropogenic load. The results demonstrated that the river biocenoses underwent a significant transformation as a consequence of intensive anthropogenic activity. It can be stated now with a reasonable degree of certainty that a number of invertebrate species previously recorded in the Salgir River have disappeared.

In general, the water of the Salgir River is characterised as “polluted” according to the classification of surface water quality in the Russian Federation [3)],

---

[2)] Kocherin, D.I., 1922. [River Run-Off in the Upper Reaches of the Salgir River up to Simferopol (Main Conclusions)]. In: Simferopol, 1922. [*Materials on the Water Management of Crimea*]. Simferopol: 1-ya Gos. Tipo-lit, iss. 2, 8 p. (in Russian).

[3)] Council of Ministers of the Republic of Crimea, 2023. [*Report on State and Protection of Environment of Republic of Crimea in 2022*]. Simferopol: OOO Print, 448 p. (in Russian).

as outlined by L. V. Malakhova et al. [8]. Additionally, the river water in the vicinity of the village of Dvurechnoye exhibits high levels of easily oxidizable organic matter, as indicated by elevated BOD and chemical oxygen demand values [4)]. In the aforementioned works, insufficient attention is paid to the hydrochemical characteristics of water. Consequently, our work classifies the level of water pollution of the Salgir River on the basis of a hydrochemical analysis of the material in question.

The paper analyses new data on the hydrochemical characteristics of waters from the Salgir and Biyuk-Karasu Rivers in summer, when the water area is subjected to an increased anthropogenic load.

Materials and methods

To assess the hydrochemical state of waters of the Salgir River and its most full-flowing tributary, the Biyuk-Karasu River, studies were carried out in July, August and September 2023 in four sections of the Salgir River from its head to its mouth and in three sections of the Biyuk-Karasu River along the main stream to the mouth (Figure).

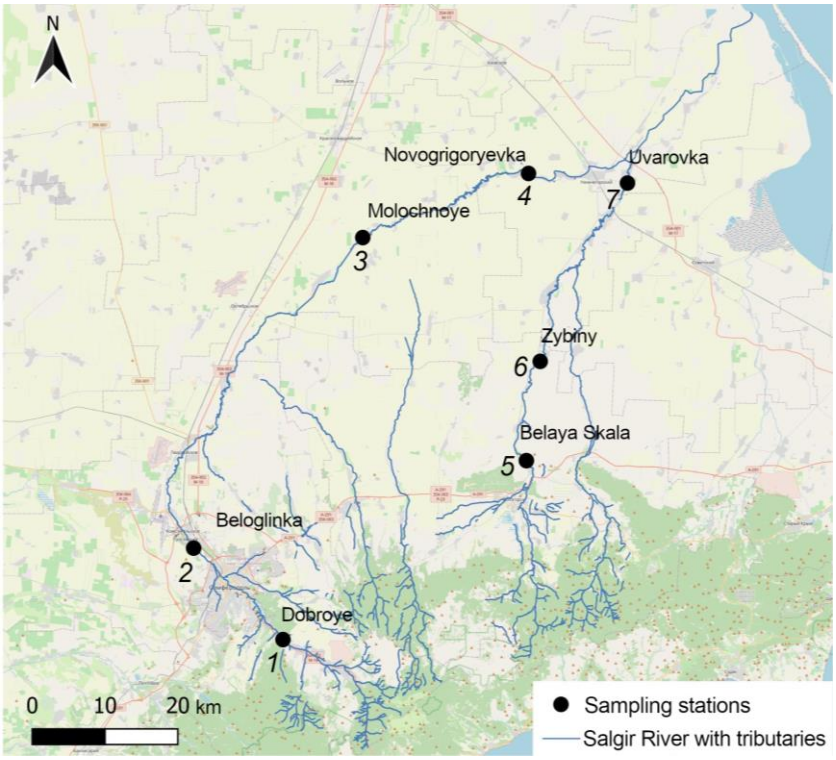

Map of water sampling stations on the Salgir River and its tributary Biyuk-Karasu

[4)] Trofimchuk, M.M., ed., 2021. [*Quality of Surface Waters of the Russian Federation. Information on the Most Polluted Water Bodies of the Russian Federation (Annex to Year-Book for 2020)*]. Rostov-on-Don, 160 p. (in Russian).

On the Salgir River, samples were taken upstream of the Simferopol Reservoir (the village of Dobroye, station *1*) at a station with a presumably low anthropogenic impact, downstream of the city of Simferopol (the village of Beloglinka, station *2*) at a station with a high anthropogenic load, downstream of the river in the developed agricultural area, following an extensive network of fishery ponds (the village of Molochnoye, station *3*), and closer to the mouth, in the area with agricultural land and livestock production (the village of Novogrigoryevka, station *4*). On the Biyuk-Karasu River, samples were taken downstream of Belogorsk (the village of Belaya Skala, station *5*) in the area of orchards, further downstream in the area of grain crops cultivation (the village of Zybiny, station *6*) and closer to the mouth after the settlement where a cattle farm and feed mill are located (the village of Uvarovka, station *7*). Samples were obtained from the surface in triplicate, resulting in a total of 45 samples and 405 hydrochemical analyses.

The following parameters were identified in the samples: dissolved oxygen, five-day biochemical oxygen demand (BOD_5), alkaline permanganate oxidizability, silicate, mineral and organic forms of nitrogen and phosphorus. The analyses were performed according to generally accepted methods [5), 6)]. The oxygen concentration was determined by the Winkler method, while the nutrients were determined photometrically. Phosphates were determined by the Murphy–Riley method; nitrites were quantified photometrically using the Griess method, while nitrates were first reduced to nitrites with copper-plated cadmium. Ammonium nitrogen was determined by the Sagi–Solorzano method, while silicon was quantified by the Koroleff method.

Results and discussion

Dissolved oxygen concentration in the waters of the Salgir and Biyuk-Karasu Rivers (Table) varied from 5.30 (the village of Novogrigoryevka) to 6.57 mL/L (the village of Beloglinka) in July; and from 5.48 (the village of Molochnoye) to 7.12 mL/L (the villages of Dobroye and Beloglinka) in August. The range of variability was 6.09–7.66 mL/L in September. The minimum oxygen content was recorded near the village of Uvarovka and the maximum one was near the village of Novogrigoryevka. In general, the oxygen concentration in the waters of the Salgir River and its tributary Biyuk-Karasu is high; even its minimum content is above the MPC according to the limit for fisheries [7)] by 1.3 mL/L.

Such indicators as BOD_5 and alkaline permanganate oxidizability were used to characterise water pollution of the studied river sections. The first indicator reflects pollution of the environment by non-persistent organic matter, the second one indicates the degree of water pollution by persistent organic matter. BOD_5 values varied from 0.98 (the village of Belaya Skala) to 3.34 mg/L (the village of Molochnoye)

---

5) Sapozhnikov, V.V., ed., 2003. [*Guidelines for the Chemical Analysis of Marine and Freshwater in Environmental Monitoring of Fishery Waters and Prospective Fishing Areas of the World Ocean*]. Moscow: Izd-vo VNIRO, 202 p. (in Russian).

6) HMSO, 1984. *The permanganate index and permanganate value tests for waters and effluents 1983*. London: HMSO, 21 p.

7) *On the Approval of Water Quality Standards for Water Bodies of Commercial Fishing Importance, Including Standards for Maximum Permissible Concentrations of Harmful Substances in the Waters of Water Bodies of Commercial Fishing Importance*: Order of the Ministry of Agriculture of Russia dated December 13, 2016, No. 552 (in Russian)

The main hydrological and hydrochemical parameters of the Salgir and Biyuk-Karasu Rivers in July–September 2023

Sampling date	Station number	*T*, °C	O_2, mL/L	BOD_5, mg/L	Concentration, μg/L					Oxidizability, mg/L
					NO_2^-	NO_3^-	NH_4^+	PO_4^{3-}	Si	
July										
06.07.23	*1*	22.5	6.57	1.67	23.0	964	56.7	15	2186	4.56
06.07.23	*2*	23.0	5.42	1.90	15.7	986	35.2	31	2303	3.88
18.07.23	*3*	23.5	5.37	3.34	49.4	944	54.3	687	4881	5.86
18.07.23	*4*	25.0	5.30	1.63	39.0	962	41.4	612	5708	6.26
26.07.23	*5*	22.0	5.82	0.98	16.2	967	35.7	3	1920	4.16
27.07.23	*6*	23.5	5.70	1.03	10.3	1013	25.2	10	2373	3.58
27.07.23	*7*	26.5	6.50	1.91	3.7	848	39.4	8	2739	5.12
August										
03.08.23	*1*	24.0	7.12	2.42	23.7	3500	336.0	45	3690	7.90
03.08.23	*2*	21.5	7.12	2.35	31.8	7328	63.0	46	4300	8.95
09.08.23	*3*	21.6	5.48	2.26	23.0	6930	31.0	1120	2660	7.27
09.08.23	*4*	25.3	6.71	2.57	6.2	3767	204.0	612	6370	5.63
September										
13.09.23	*5*	18.2	6.09	ND	2.2	2804	18.9	9	1263	ND
14.09.23	*6*	17.3	6.41	ND	21.2	5629	29.9	22	875	ND
20.09.23	*3*	18.0	7.08	ND	44.7	2766	54.1	614	4142	5.85
20.09.23	*4*	19.2	7.66	ND	55.9	2518	45.2	64	8196	3.28

Note: ND – not determined. MAC O_2 – 4.20 μg/L; MAC NO_2^- – 20.0; MAC NO_3^- – 9000 μg/L; NH_4^+ – 390 μg/L. Limit for 5-day biochemical oxygen demand (BOD_5) – 2.1 mg/L; limit for oxidizability – 4.00 mgO/L.

in July. At the same time, the maximum BOD_5 values exceeded the limit (2.1 mgO/L) by 1.6 times. In July, the limit exceedance was observed only once; in August and September, the exceedance was persistent (maximum by 1.3 times). According to the integrated ecological classification of surface water quality [8], the BOD_5 values of the Salgir River waters made it possible to classify them as satisfactorily clean (3rd class of water quality) in July and polluted (4th class) in August and September.

Water oxidizability varied from 3.58 to 20.10 mgO/L. The minimum value was observed in July (the village of Zybiny) and the maximum in September (the village of Molochnoye). The average oxidizability exceeded the MPC (4.0 mgO/L) of the limit for fisheries by 1.6 times in July, by 1.9 times in August and by 4.8 times in September. According to the oxidizability values, waters of the Salgir and Biyuk-Karasu Rivers in July were classified as the 2nd class of quality, corresponding to clean water [8], but in August it was classified as the 3rd class, corresponding to satisfactorily clean waters. In September, the waters were classified to be of the 4th class, indicating a deterioration in quality. Therefore, in terms of oxidizability, a deterioration in the river water quality was observed from July to September, which can be attributed to increased anthropogenic impact and recreational load.

Forms of nitrogen

Water *nitrite nitrogen concentrations* in the waters of the Salgir and Biyuk-Karasu Rivers ranged from 2.2 to 55.9 μg/L; the minimum and maximum values were recorded in September (the villages of Uvarovka and Novogrigoryevka, respectively). Increased NO_2^- concentrations (49.4 and 44.7 μg/L) were observed near the village of Molochnoye in July and September. Exceedance of MPC (20 μg/L) was noted at three out of seven stations in July, at three out of four stations in August, and at three out of four stations in September. The maximum MPC exceedance was by a factor of 2.8. The average value of nitrite concentration equal to 24.4 μg/L exceeded the MPC by 1.2 times.

Nitrate nitrogen concentrations were 1–2 orders of magnitude higher than nitrite nitrogen concentrations and varied over a wide range from 848 to 7328 μg/L. The NO_3^- minimum was observed in July near the village of Uvarovka, and the maximum (0.8 MPC) in August in the vicinity of the village of Beloglinka. Other NO_3^- values were lower and ranged from 0.1 to 0.77 MPC with an average nitrate concentration of 2795 μg/L. It is notable that there was an increase in nitrate concentration from July to September. This can be explained by an increase in the recreational load and anthropogenic impact on the region.

Ammonium nitrogen concentrations were recorded between 19 and 336 μg/L. The minimum NH_4^+ concentration was observed in September near the village of Uvarovka, and the maximum one in August near the village of Dobroye. High ammonium nitrogen content can be impacted by domestic runoff from the village

[8] State Committee on Water Management, 2018. [*Scheme of Integrated Use and Protection of Water Bodies of the Republic Of Crimea, Including Norms of Permissible Impact on Water Bodies, and Water Quality Targets for Water Bodies Located in the Territory of the Republic of Crimea. Book 2: Assessment of the Environmental Condition and Key Problems of River Basins Located in the Territory of the Republic of Crimea*] (in Russian).

of Dobroye; settlements along the Salgir riverbed do not have centralized sewerage systems. All the NH_4^+ concentrations were significantly below the MPC (390 μg/L) according to the fishery regulations. The average NH_4^+ content in the river waters was 72 μg/L, which is 5.4 times lower than MPC.

Organic nitrogen (N_{org}) was determined only in September; its concentrations were high and varied from 2990 to 8110 μg/L. The minimum was recorded near the village of Belaya Skala, and the maximum near the village of Novogrigoryevka. The maximum concentration of nitrite (56 μg/L) and high oxidizability values (18.40 mgO/L) were also recorded there. The presented hydrochemical characteristics show that this area is polluted with organic matter. The average N_{org} content was 5070 μg/L in September.

Mineral phosphorus (PO_4^{3-}) concentrations varied from 3.5 to 1120 μg/L in the waters of the Salgir and Biyuk-Karasu Rivers. The minimum was observed in July (the village of Belaya Skala) and the maximum in August (the village of Molochnoye). In the vicinity of the villages of Molochnoye and Novogrigoryevka, PO_4^{3-} is 1–2 orders of magnitude higher than in other areas. This is likely attributable to the impact of domestic and other anthropogenic sources, as evidenced by the elevated organochlorine concentrations observed in the vicinity of the village of Molochnoye [8]. The average PO_4^{3-} concentration was 260 μg/L in July–September; therefore, the waters under study can be classified as polluted ones [8].

Silicate concentrations had high values and varied in wide ranges from 875 to 8200 μg/L. The minimum and maximum were observed in September near the village of Belaya Skala and the village of Novogrigoryevka, respectively. Increased Si concentrations in the water near the village of Novogrigoryevka are caused by the chemical composition of soils, including aluminosilicates as the main component. In the vicinity of the village of Molochnoye, the concentrations of silicates are about 2 times lower than in the village of Novogrigoryevka. In the other areas, the concentration of Si was almost 4 times lower than the maximum concentrations. The average silicate concentration in July–September was 3574 μg/L.

Conclusions

The analysis of the hydrochemical data obtained in the period between July and September 2023 in the waters of the Salgir and Biyuk-Karasu Rivers has led to the following conclusions:

– the oxygen level in water is high at all river sections;

– the exceedance of BOD_5 and oxidizability limits by a maximum of 1.6 and 4.8 times, respectively, were recorded in the vicinity of the village of Molochnoye. This resulted in the river waters being assigned to the 4th class of water quality in September, down from the 2nd class they were assigned to in July;

– nitrite MPC was exceeded by a factor of 2.5 (the village of Molochnoye). Nitrate concentrations were below MPC and increased from July to September. Ammonium nitrogen concentrations were low and did not exceed MPC;

– high concentrations of phosphates, 1-2 orders of magnitude higher than in other areas, were recorded in the vicinity of the villages of Molochnoye and Novogrigoryevka due to the influence of domestic and household wastewater;

– the results of all hydrochemical analyses of the Salgir River waters indicate that the areas of the villages of Molochnoye and Novogrigoryevka are most polluted.

REFERENCES

1. Miller, M.E., 1961. [The Salgir River Basin and its Economic Use]. In: USSR GS, 1961. *Izvestiya Krymskogo otdela Geograficheskogo obshchestva Soyuza SSR*. Iss. 5, pp. 163–196 (in Russian).
2. Vlasova, A.M., 2011. The Estimation of Ecological State of the Salgir River Basin. *Scientific Notes of Taurida National V. I. Vernadsky University. Series: Geography*, 24(1), pp. 66–71 (in Russian).
3. Pozachenyuk, E.A., Ergina, E.I., Oliferov, A.N., Mikhailov, V.A., Vlasova, A.N., Kudrjan', E.A., Penno, M.V. and Kalinchuk, I.V., 2014. Analysis of Factors of the Salgir River's Water Resources Formation under the Condition of Climate Changing. *Scientific Notes of Tavrida National V.I. Vernadsky University. Geography*, 27(2), pp. 118–138 (in Russian).
4. Ivanyutin, N.M., Podovalova, S.V. and Volkova, N.E., 2020. Research of Spatial-Temporal Transformation of the Qualitative Composition of the River Salgir Waters. *Ecology and Industry of Russia*, 24(3), pp. 65–71. https://doi.org/10.18412/1816-0395-2020-3-65-71 (in Russian).
5. Ivanyutin, N.M., Volkova, N.E. and Zubochenko, A.A., 2022. The Influence of the Simferopol Urban Environment on the Qualitative Indicators of the Salgir River Flow. *Tavricheskiy Vestnik Agrarnoy Nauki*, (4), pp. 82–92 (in Russian).
6. Kuznetsova, E.Yu., 2014. [Results of monitoring studies of chemical pollutants in surface waters of the Salgir River (Republic of Crimea)]. *SCI-ARTICLE.RU*, 14. Available at: https://mail.sci-article.ru/stat.php?i=1414411629 [Accessed: 7 October 2024] (in Russian).
7. Kiseleva, G.A. and Prokopov, G.A., 2003. [Identification of River Sections with Different Degrees of Anthropogenic Transformation (Case of the Salgir River)]. In: V. S. Tarasenko, 2003. [*Sustainable Crimea. Water Resources*]. Simferopol: Tavrida, pp. 139–141 (in Russian).
8. Malakhova, L.V., Karpova, E.P., Belogurova, R.E., Gubanov, V.V., Prokopov, G.A., Chesnokova, I.I., Kurshakov, S.V., Statkevich, S.V., Shavriev, D.G. and Ovechko, S.V., 2023. Organochlorine Xenobiotics in the Salgir River Ecosystem: Content, Distribution, Ecological Risk. *Ecological Safety of Coastal and Shelf Zones of Sea*, (4), pp. 116–133.

Submitted 25.02.2024; accepted after review 28.05.2024;
revised 17.06.2024; published 25.09.2024

About the authors:

Nelya P. Kovrigina, Senior Research Associate, Research Center for Freshwater and Saltwater Hydrobiology, Senior Research Associate, A.O. Kovalevsky Institute of Biology of Southern Seas of RAS (2 Nakhimov Av., Sevastopol, 299011, Russian Federation), Ph.D. (Geogr.), **ORCID ID: 0000-0002-6734-8285, Scopus AuthorID: 6507114864, ResearcherID: AAC-9395-2022**, *npkovrigina@yandex.ru*

Diana S. Borisova, 1st Category Engineer, Research Center for Freshwater and Saltwater Hydrobiology, Leading Engineer, A.O. Kovalevsky Institute of Biology of Southern Seas of RAS (2 Nakhimov Av., Sevastopol, 299011, Russian Federation), **ORCID ID: 0009-0004-0444-1177**, *sergei_diana@mail.ru*

Sergey V. Ovechko, Director, Research Center for Freshwater and Saltwater Hydrobiology (2 Nakhimov Av., Sevastopol, 299011, Russian Federation), **ORCID ID: 0009-0007-1050-9918, ResearcherID: JFJ- 7762-2023**, *hgbs1@yandex.ru*

Vitaly I. Ryabushko, Chief Research Associate, A. O. Kovalevsky Institute of Biology of Southern Seas of RAS (2 Nakhimov Av., Sevastopol, 299011, Russian Federation), Dr.Sci. (Biol.), **ORCID ID: 0000-0001-5052-2024, Scopus AuthorID: 7801673501, ResearcherID: H-4163-2014**, *rabushko2006@yandex.ru*

Contribution of the authors:

Nelya P. Kovrigina – problem statement, work planning, analysis and discussion of the results

Diana S. Borisova – participation in expeditionary sampling, sample processing, obtaining of hydrochemical indicatiors, analysis and discussion of the results, article writing

Sergey V. Ovechko – problem statement, discussion of the results, article editing

Vitaly I. Ryabushko – problem statement, work planning, discussion of the results, final editing

All the authors have read and approved the final version of the manuscript.